Dipl. Manuel Kreimer

Continuous purification and drying of pharmaceuticals with regard to material properties and process stability

DOCTORAL THESIS

to achieve the university degree of

Doktor der technischen Wissenschaften

submitted to

Graz University of Technology

Supervisor

Univ.-Prof. Dipl.-Ing. Dr. techn. Johannes G. Khinast

Institute for Process and Particle Engineering, Technical University, Graz

Research Center Pharmaceutical Engineering GmbH, Graz

Graz, July 2018

i

Manuel Kreimer

Continuous purification and drying of pharmaceuticals with regard to material properties and process stability

Dissertation

First assessor

Univ.-Prof. Dipl.-Ing. Dr.techn. Johannes Khinast
Institute of Process and Particle Engineering
Research Center Pharmaceutical Engineering GmbH
Graz University of Technology

Second assessor

Daniel Lepek, Ph.D.
Associate Professor of Chemical Engineering
The Albert Nerken School of Engineering
The Cooper Union for the Advancement of Science and Art

AFFIDAVIT

I declare that I have authored this thesis independently, that I have not used other than the declared sources / resources, and that I have explicitly indicated all material, which has been quoted either literally or by content from the used sources. The text document uploaded to TUGRAZonline is identical to the present doctoral thesis.

(Ich erkläre an Eides statt, dass ich die vorliegende Arbeit selbstständig verfasst, andere als die angegebenen Quellen/Hilfsmittel nicht benutzt, und die den benutzten Quellen wörtlich und inhaltlich entnommenen Stellen als solche kenntlich gemacht habe. Das im TUGRAZ hochegeladene Textdokument ist identisch mit der vorliegenden Arbeit.)

August, 2018 …………………………………………………………

Dipl.-Ing. Manuel Kreimer

„To develop a complete mind:
Study the science of art;
Study the art of science.
Learn how to see.
Realize that everything
connects to everything else."

Leonardo da Vinci (1452-1519)

Acknowledgements

I am grateful to all people who contributed to this work and supported me during the past few years. Some of them I would like to mention here.

First of all my thanks go to Prof. Johannes Khinast for granting me the opportunity to conduct my PhD thesis at RCPE, for his guidance, motivation and patience. It was always a pleasure to talk about challenges in our work and to create new projects, papers and presentations out of it.

I thank Prof. Daniel Lepek for being the second assessor for this thesis, and his contribution on the extrusion drying publication.

I also want to thank Prof. Günter Brenn, who provided the acoustic levitation equipment and his help during authoring my first publication.

In addition, I thank Isabella Aigner for her help and support in scientific questions. In this context, I also want to thank Manuel Zettl for his help in experimental work and the nice hours we spent together.

Further thanks go to my collaboration partners Markus Krumme (Novartis), Thomas Mannschott (Novartis) and Peter van der Wel (Hosokawa) for the financial and scientific support. I really enjoyed working within our collaboration, because of the numerous fruitful discussions we had in F2F meetings and TC's.

I especially want to thank all the people at RCPE for making this work possible in a friendly and cheerful working environment. In that regard, special thanks go to the following people:

...Julia Kruisz for her patience and help when I had some Matlab issues and the interesting and inspiring conversations we had.

...Johannes Poms and Mathias Wolfgang for being my office colleagues. It was always a pleasure for me to be in the same office with you.

...Eva Faulhammer for her help and support in so many different areas and for the nice lunch breaks.

...Many student employees (Sarah Koller, Daniel Wiegele, etc.), master students (Craig Hauser and Rafael Halb) and bachelor students (Kristian Gavric) for their contribution on this work.

Abstract

Continuous manufacturing of pharmaceuticals has recently gained tremendous interest from different stakeholders like universities, regulatory bodies, equipment vendors and producers because of a large variety of reasons such as flexible production, safer products, smaller ecological footprint, individualized and cost-efficient medicine, etc. However, most processes are still conducted in batch mode, due to established processes from the past and foremost, a lack of well-developed continuous manufacturing equipment. This is especially true for primary manufacturing, where technologies in continuous purification and drying are underdeveloped.

The goal of this thesis is to develop and investigate continuous manufacturing methods for purification and drying of pharmaceutical substances without changing particle properties such as size or shape. Frequently, the particle size is tailored during crystallization and should be maintained in downstream processes. For this reason, a continuous purification process by solvent exchange washing with a static mixer and a continuous drying process by extrusion was developed. The influence of the solvent exchange rate (anti-solvent) during purification on the particle size after drying was analyzed beforehand with small scale studies in an acoustic levitator. Product suspension compositions as present after purification were introduced in small droplets in the acoustic field, to study the drying kinetics and the mechanical properties of the dried particles. It was observed that the suspension composition with variation in the amount of suspended solids, dissolved solids and the liquid mixture, greatly influenced the drying kinetics and mechanical properties of dried microspheres. Stronger agglomerated microspheres were observed by drying of suspensions with more dissolved solids, due to more formation of solid bridges by precipitated material between suspended solids. Moreover, it could be shown that a threshold of dissolved solids exists, where loose microspheres are formed below. Furthermore, the drying time was prolonged for drying of suspensions with higher liquid amounts of lower vapor pressure and more dissolved solids.

Based on the small scale experiments the solvent exchange washing ratios were set for the continuous purification process with a static mixer. Different process settings by variation of suspension compositions and setup configurations (insertion/mixing points, ultrasound application, etc.) were evaluated. The product particle size was mainly influenced by the precipitation rate of dissolved solids during washing: the more solids precipitated, the larger was the increase of the product particle size. Furthermore, the fouling probability and

stability of different equipment configuration was assessed. The most stable process was established for co-axial mixing of feed and anti-solvent before the static mixer with ultrasound application.

Finally, a continuous drying process via extrusion was developed for low throughput ranges (0.5 – 2.0 kg/h) with the goal to preserve the product particle size similar to the raw material. Drying of substances with moisture levels up to 10 wt.% were conducted and product particle properties were analyzed. Successful drying of a crystalline product with very little agglomeration and/or attrition was demonstrated in some process settings. The main drivers for reduction in product particle size were longer residence times and lower moisture levels of the product.

Kurzfassung

Die kontinuierliche Herstellung von pharmazeutischen Produkten wird von verschiedensten Akteuren wie Universitäten, Aufsichtsbehörden, Geräteherstellern und Pharmaunternehmen mit großem Interesse verfolgt. Vielfältige Gründe sprechen für kontinuierliche Prozesse wie flexible Produktion, Produktsicherheit, kleiner ökologischer Fußabdruck, individualisierte und kostengünstigere Medizin, usw. Dennoch werden die meisten Medikamente noch durch Batchprozesse hergestellt, da diese schon seit langer Zeit etabliert sind und wenige ausgereifte Geräte zur kontinuierlichen Herstellung zur Verfügung stehen. Besonders in der Primärherstellung mangelt es an ausgereiften Technologien für die kontinuierliche Reinigung und Trocknung von Wirkstoffen.

Das Ziel der vorliegenden Arbeit ist es, Methoden zur kontinuierlichen Reinigung und Trocknung von pharmazeutischen Substanzen zu entwickeln, ohne dabei die Partikeleigenschaften wie Größe oder Form zu verändern. Die gewünschten Partikeleigenschaften werden häufig während der Kristallisation erzeugt und sollen in nachfolgenden Prozessen nicht verändert werden. Aus diesem Grund wurde ein kontinuierlicher Reinigungsprozess durch Lösungsmittelaustausch mit einem statischen Mischer, sowie ein kontinuierlicher Trocknungsprozess durch Extrusion entwickelt. Um die geeigneten Parameter für die Lösungsmittelaustauschrate zu finden, damit Änderungen der Partikelgröße vermieden werden, wurden Vorversuche der zu prozessierenden Substanzen mit einem akustischen Levitator durchgeführt. In dem akustischen Levitator wurden kleine Tropfen platziert, welche eine ähnliche Zusammensetzung hatten wie die Produktsuspension nach der Reinigung, um die Trocknugnskinetik der Tropfen und die mechanischen Eigenschaften der getrockneten Mikrosphären zu analysieren. Die Trocknungskinetik und die mechanischen Eigenschaften waren maßgeblich von der Zusammensetzung der Suspension aus Feststoffen, gelösten Bestandteilen und Flüssigkeitskomponenten abhängig. Trocknung von Suspensionen mit mehr gelösten Bestandteilen führte zur Bildung von stärker agglomerierten Mikrosphären, durch Bildung von Feststoffbrücken zwischen Primärpartikeln aus ausgefallenem Material. Für die untersuchte Materialkombination wurde auch ein Grenzwert an gelösten Bestandteilen gefunden, unter welchem lose Mikrospähren geformt wurden. Auswertungen der Trocknungskinetiken haben gezeigt, dass die Trocknungszeit für Suspensionen mit höherer Menge an Flüssigkeiten mit geringem Dampfdruck und mehr gelösten Bestandteilen zugenommen hat.

Die Parameter für die kontinuierliche Reinigung wurden basierend auf den Ergebnissen der akustischen Levitatoruntersuchungen definiert. Unterschiedliche Zusammensetzung der Suspensionen, sowie verschieden Setupkonfigurationen (Einbringungs- und Mischpunkt der Flüssigkeiten, Ultraschalleintrag, usw.) wurden untersucht. Die Produktpartikelgröße war hauptsächlich von der Fällungsrate der gelösten Bestandteile abhängig. Umso mehr gelöste Bestandteile ausgefallen sind, desto größer war die Zunahme der Partikelgröße. Des Weiteren wurde die Prozessstabilität bezüglich Materialablagerungen für unterschiedliche Seutpkonfigurationen untersucht. Der stabilste Prozess mit den geringsten Materialablagerungen konnte für koaxiales Mischen von Eingangssupension und Waschflüssigkeit unter Einbringung von Ultraschall erreicht werden.

Abschließend wurde noch ein kontinuierlicher Trocknungsprozess mittels Extrusion für geringe Durchsätze (0,5 - 2.0 kg/h) entwickelt, in welchem die Partikelgröße während der Trocknung nicht verändert werden soll. Substanzen mit einem Feuchtigkeitsgehalt von 10 Gewichtsprozent wurden getrocknet und die Produktpartikelgröße wurde analysiert. In diesen Versuchen wurde eine kristalline Substanz erfolgreich getrocknet, wobei es zu geringer Agglomeration bzw. Abreibung der Partikel gekommen war. Die Verringerung der Partikelgröße war hauptsächlich auf eine längere Verweilzeit im Prozess, sowie geringerer Feuchtigkeitsgehalt der Produkte zurückzuführen.

Table of Contents

Abbreviations

API	Active pharmaceutical ingredient
ASTM	American Society for Testing and Materials
BCS	Biopharmaceutics classification system
CCD	Charge-coupled device
CM	Continuous manufacturing
DSA	Density and sound anemometry
IBC	Intermediate bulk container
ICH	International Conference on Harmonization
Lab	L for lightness, a and b for the color components (green-red and blue-yellow, respectively)
M	Motor mixer
MSM	Metal static mixer
NCE	New chemical entities
PAT	Process analytical technology
PI	Pressure indicator
PSM	Plastic static mixer
PSD	Particle size distribution
RGB	Red-green-blue
RSD	Relative standard deviation
RTD	Residence time distribution
SCS	Side crushing strength
SEM	Scanning electron microscope
SLR	Single-lens reflex
SM	Static mixer
US	Ultrasound

„The important thing is to never stop questioning"

Albert Einstein (1879-1955)

1. Introduction and Motivation

The production of pharmaceutical goods has experienced a high effort to change from traditional batch manufacturing to continuous manufacturing (CM). This new way of manufacturing was first investigated and introduced by academia [1], is supported nowadays by regulatory bodies [2–8] and has been realized and implemented for further development as well as daily production from equipment vendors (GEA, GLATT, Bohle, Bosch, etc.) and manufacturers (Novartis, Pfizer, AstraZeneca, GSK, Bayer, UCB, and many others) [9,10]. A transition from batch to continuous manufacturing offers several advantages in the form of processes with higher production efficiency, lower production costs, more time-efficient, reduced energy consumption and smaller ecological footprint [11]. Batch production is still mainly used nowadays, because the setup costs are initially less expensive and some materials require batch manufacturing due to their composition. One of the biggest advantages of CM over batch manufacturing is the ability of using the same equipment for formulation development, clinical trials and the final production process [12]. Therefore, traditional scale-up issues of batch processes from the development phase to large scale production can be prevented. In a CM environment, larger production rates can be easily realized by longer process times [13], and thereby reducing the scalability efforts to almost zero.

The whole process chain of pharmaceutical goods can be divided into two distinctive areas with primary and secondary manufacturing. Primary manufacturing is related to the production of the active pharmaceutical ingredient (API), involving mostly the consecutive process steps synthesis, crystallization, purification and drying resulting in a powder as intermediate product. Afterwards, secondary manufacturing follows, where the API is transferred to products suitable for administration. For example, the involved process steps to produce a solid dosage are feeding, blending, granulation, drying, feeding, tableting / capsule filling, optional coating and packaging. Therefore, a lot of different process steps are necessary to produce a tablet or capsule. As one can imagine, running the whole production route in a continuous mode is not an easy task. Processes which are already continuous by nature like feeding, extrusion, compression, and milling can be easier implemented in a continuous production line [14]. In such processes, the starting

material is continuously fed and the products are removed simultaneously [15]. In contrast to continuous processes is batch-wise production, where a defined amount of raw material is loaded into the unit operation and discharging occurs asynchronously. Examples are high-shear granulation, drum coating and blending of materials inside a drum or container [14]. A fully continuous manufacturing approach with synthesis, separation, crystallization, drying, formulation and tableting was proposed from Mascia et al. [10].

A very crucial step at the end of primary manufacturing or after wet granulation in secondary manufacturing is drying, which transforms a liquid feedstock into a dry powder. Drying is mainly carried out in batch operation, and therefore development of continuous drying technologies will be a key aspect for further realization of continuous processes [16]. In a continuous drying environment, one of the key aspects is to achieve sufficient drying in a reasonable time frame. Furthermore, in primary manufacturing, the particle morphology (e.g., particle size and shape distribution, etc.) is frequently tailored during crystallization and should be carefully maintained in downstream processes such as purification and drying [17]. The API properties achieved at the end of primary manufacturing are essential parameters in solid dosage formation during secondary manufacturing. For example, blending or tableting performance might be negatively influenced by small particles due to poor flowability, whereas larger particles may result in low dissolution rates, impacting the drug's bioavailability profile [18]. Avoiding changes of the particle properties during drying is a well-known challenge, because several phenomena like agglomerate formation by inter-particle bonding forces, attrition, (re-) crystallization and re-dissolution, may occur simultaneously. Agglomerate formation occurs when wet particles stick together due to inter-particle forces by liquid or solid bridges, van der Waals forces and viscous forces [19]. During drying, the liquid bridge evaporates and the particles move closer to each other, resulting in agglomerate formation. The probability of agglomerate formation is further increased if the liquid bridge contains dissolved components, which precipitate during drying, resulting in the formation of strong solid bridges and agglomerates [20,21]. Contrary to agglomeration, attrition (reduction in particle size) occurs via particles colliding with the equipment or with each other due to shearing [17,22–25], or through induced stresses generated by temperature or pressure differences inside the dryer [26–28]. Both effects are not favorable during drying when the crystallized API properties should be preserved also in the dried state.

The first part of this thesis deals with small scale studies of suspensions in an acoustic levitator, to evaluate the drying performance and the dried particle properties. Pharmaceutical suspensions with different compositions of solvents and dissolved components were prepared, afterwards, small droplets were inserted in the acoustic field of the levitator to observe the drying progression and finally, the dried microspheres were extracted from the acoustic field and the agglomeration strength was measured. In the second part, continuous primary manufacturing methods in purification and drying of pharmaceuticals were developed and characterized. Based on the evaluation of the mechanical properties from the small scale studies, the continuous purification process via solvent exchange washing using a static mixer was designed. Purified particle properties were analyzed and the performance of the solvent exchange washing equipment were evaluated with regard to process stability and fouling probability. Finally, a proof of concept was done for drying of a pharmaceutical substance with cohesive flow behavior in an extruder, where the process characteristics were determined and the dried particle properties (agglomerate formation or attrition) were evaluated.

1.1   Continuous manufacturing of pharmaceuticals

Continuous production originated in the iron industry, where processes such as pig iron production in a blast furnace operate for many years without shutdown. The technical evolution enabled the transformation from batch to continuous processing also in other industries such as petroleum, automotive, consumer goods and food manufacturing [29]. Continuous processes are widely integrated in the industry due to the high product demand, reduced processing costs, consistent product quality as well as higher productivity. For this reason, the pharmaceutical industry also became aware of the advantages of continuous processes, but the implementation is still at a slow pace [30–32]. Successful integration of continuous manufacturing (CM) needs an organized coordination between several industries. The three key attributes for standardized production of pharmaceutical goods are equipment and process analytical tool manufacturers, API and excipient manufacturers, and the finished product manufacturing facilities.

Manufacturing of pharmaceutical compounds can be classified by the mode of operation in relation to the strategy of feeding and removing materials from a single process unit. Based on the feeding and removal strategy, the main differences are made between batch and continuous manufacturing. In batch manufacturing, the materials are charged before processing and are discharged at the end of processing (e.g. batch vacuum

drying). In CM, the materials are simultaneously charged and discharged from the process (e.g. flow reactors) [33]. In between those manufacturing methods slight variations exist in the form of semi-batch (some materials are added simultaneously during processing and the whole batch is discharged at the end), quasi-continuous (material is charged in batches and removed in defined intervals) and semi-continuous manufacturing (the same as CM, but limited for a defined time).

CM is still not commonly used in the pharmaceutical industry, but processes like separation technologies have operated continuously for many decades [34]. Some pharmaceutical unit operations are continuous by nature, such as plug flow reactors, extrusion, roller compaction, tablet compression and capsule filling [35,36]. Nevertheless, these continuous processes were mainly operated in batch mode due to a lack of integrated real-time quality assurance and process control [37]. Therefore, implementation of these tools will support the transfer from batch to continuous manufacturing. In batch manufacturing, the intermediate products are collected in intermediate bulk containers (IBCs) and analyzed off-line in a quality assurance laboratory. Afterwards the intermediates in IBCs are frequently further processed on different locations around the world, which might lead to segregation or instability during the supply chain. The number of globally involved unit operations determines therefore the manufacturing time for batch processing, which may last from several weeks up to years.

On the other hand, using CM drastically reduces the process time to a few hours or days, until a final product is manufactured for the same unit operations as used for batch manufacturing. Material is simultaneously fed and discharged from single unit operations and transferred to the next process, while the manufacturing route is fully monitored and controlled.

1.1.1   Primary and secondary manufacturing

The production of a drug product is usually divided into primary and secondary manufacturing (Figure 1). Primary manufacturing deals with the production of an API while secondary manufacturing deals with the production of a final dosage form [11]. The involved process steps in primary manufacturing are depicted in Figure 2 with synthesis, crystallization, filtration, washing and drying with a dried API as intermediate product. Afterwards production of a drug product continues in secondary manufacturing (Figure 3) with feeding, blending, granulation, drying, milling, tableting / capsule filling, optional coating and packaging. Frequently, in batch manufacturing, primary and secondary

production sites are not located close to each other. Shipping primary manufactured intermediates around the globe to the secondary production site involves major difficulties for the physical and chemical stability of the compounds as well as communication challenges.
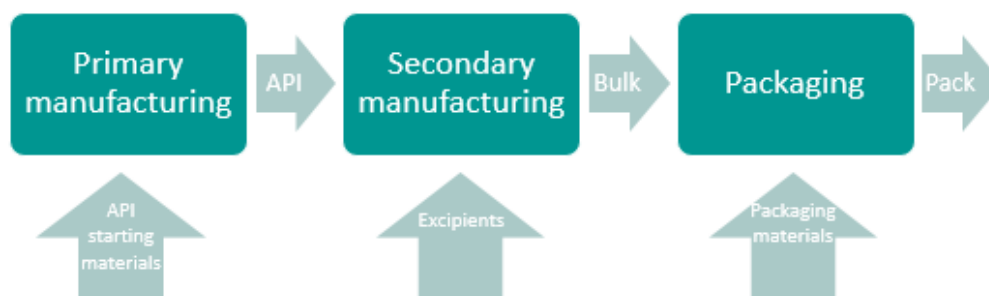
Figure 1. Process chain in manufacturing of pharmaceuticals.

Figure 2. Process steps in primary manufacturing of pharmaceuticals.

Figure 3. Process steps in secondary manufacturing of pharmaceuticals.

Extensive progress has been made in continuous secondary production lines from different suppliers. For example, GEA has developed an integrated tableting production line with the Consigma system [38]. The line consists of feeding, wet granulation, drying, milling, blending and tableting. Several other equipment suppliers as Glatt, Bohle or Bosch extensively work on the realization of continuous process equipment. In addition to research from equipment suppliers, several leading pharmaceutical companies such as Novartis, Pfizer, AstraZeneca, GSK and UCB have launched programs on continuous manufacturing [11]. So far, the first FDA approved continuous manufacturing lines on the market are for Darunavir from Jansen and for Orkambi from Vertex. The continuous

production line for Darunavir consists of the manufacturing steps feeding, milling, blending, compression and coating, and is therefore a direct compaction line in secondary manufacturing [39].

In academia, an end-to-end manufacturing process from synthesis to final dosage form was proposed from Mascia et al at the Novartis-MIT center for continuous manufacturing [10]. End-to-end production is a desired objective in pharmaceutical manufacturing, but it is not always technically and product-wise feasible. For example, continuous mixing, granulation and tableting might be possible, but coating is still done in batch mode. The reason for batch coating might be that tablets need a certain rest time, to avoid cracking of the tablet coating by elastic expansion.

1.1.2   Advantages of continuous manufacturing

Continuous manufacturing of pharmaceuticals offers several advantages to patients, society, pharmaceutical companies and manufacturers [40]. One of the benefits of CM over batch manufacturing is the flexibility of using the same equipment for process development, clinical trials as well as the final production process. Such a line can operate 365 days per year if needed, but usually pharmaceuticals are produced in campaigns lasting from one to several weeks. In the case of immediate needs (e.g., pandemics), companies can react on very short notice and supply the necessary amount of drug products [41].

In a usual batch manufacturing process, several synthesis steps are performed by company A and intermediates are shipped to company B for further production steps. Afterwards, the intermediates are shipped back to company A to manufacture the drug product. Thus, CM is very effective in speeding up the supply chain, because drug products can be produced on demand [2]. The same is true for the development phase, especially the transition from phase II to phase III, due to an increased amount of API material needed. The investment decision for phase III is mostly done before phase II results are available, to avoid significant delays. CM plants can greatly improve this situation, resulting in earlier entering of the market and a longer patent life cycle phase.

Furthermore, CM enables an agile production with reduced scale-up efforts. The usual yearly market volume of APIs is a few kilograms up to a few hundred kilograms. Products with tons per year are exceptions. Typically, CM lines for API production are designed in the range of 0.1-5.0 kg/h. For example, running a CM line for a month will yield in a few thousand kilograms of material, which might be enough for the yearly capacity. Such

production lines make the scale-up issues redundant, because the same equipment can already be used in the development phase. Thus, CM offers a much more agile production without scale-up and with fast reaction times on the demanded production volumes.

Further advantages of CM plants are their small space requirements, which allows decentralized manufacturing in facilities with a floor space of only a few square meters. Such plants could easily be shipped to specific locations (e.g., developing countries) for a wide range of applications (e.g., local epidemics or military use). Reductions in floor space are also beneficial to reduce investment costs, although higher costs can be expected for process analytical technology (PAT) tools. Nevertheless, if a CM plant is accurately designed with integrated PAT tools, labor work in offline quality control can be vastly reduced [2,42]. CM further enables the design of safer primary manufacturing routes of small molecules, stoichiometric-reactions or catalytic systems, which usually have moderate reaction rates to avoid explosions at large reaction volumes. CM processes can be designed in a way that reaction volumes are in the order of milliliters and flow chemistry can be used to enable safer and more efficient production routes. Much faster and more exothermic reactions can be applied with more selective catalytic routes, containing unstable intermediates or products in higher temperature and pressure environment.

Last but not least, CM will positively affect the societal needs for safer drugs with reduced costs. Using CM, high-tech jobs will be created and new chemical entities (NCE) can be developed in a wider extend, specifically for the patient's needs. The quality of medicines will be increased and the costs will be reduced.

1.2 Purification of pharmaceuticals

The purity of pharmaceutical compounds is of great importance to produce high quality drugs and meet regulatory requirements. Purity criteria must be fulfilled within the process chain for intermediates (e.g. purified API after synthesis) as well as for the final drug product (e.g. tablets, consisting of API and excipients). A key aspect in primary manufacturing is therefore the purification step to remove impurities, thereby ensuring a production of high quality pharmaceuticals. Impurities can diminish the pharmacological efficacy of the API, or sometimes have negative effects as they can be teratogenic, mutagenic or carcinogenic [43]. An impurity is defined according to guidelines from the International Conference on Harmonization (ICH) by "Any component of the drug product that is not the chemical entity defined as the drug substance or an excipient in the drug product." (ICH Q6A: Specifications) [44]. Impurities associated with APIs are divided in

different groups: organic impurities, inorganic impurities, residual solvents, polymorphic forms and enantiomeric impurities [45]. Organic impurities are the most common impurities found, originating from incomplete chemical reactions of the unreacted raw material during the synthesis, byproducts or degradation. Inorganic impurities are also formed during the manufacturing process and might be reagents, ligands, catalysts, heavy metals and other materials like filters, charcoal, etc.

Removal of impurities is frequently done by distillation, adsorption-desorption, solvent exchange, membrane-assisted liquid-liquid extraction, crystallization and chromatography [46,47]. Most organic synthesis reactions are carried out in a liquid state, where the API, impurities and different solvents are present. API and impurities are usually homogeneously mixed in the solvent mixture and cannot be separated without further process steps like a solvent exchange. The conventional solvent exchange is done via distillation, which is able to separate solvents with different boiling points. This purification procedure has some drawbacks because it is vastly energy consuming and may damage heat-sensitive APIs [48].

An alternative way to remove impurities can be done by a solvent exchange through cascades of washing and filtration. This purification cascade follows directly after the crystallization phase (mother liquor with API and impurities), where particles with tailored properties are produced. After the crystallization, a washing liquid (anti-solvent) is added to the mother liquor to provoke a change of the liquid regime. The API should not be soluble in the washing liquid, whereas the impurities should be soluble. Therefore, the API remains in crystal state (particles) and the impurities are dissolved in the liquid mixture. Separation of the API and the impurities can be easily achieved after the solvent exchange washing by a filtration process. Depending on the number of impurities, washing and filtration must be done in multiple steps to achieve sufficient purity of the API crystals.

After the crystallization the API is mainly in solid state with only a few amounts dissolved in the mother liquor. Addition of the washing liquid to the mother liquor is used to remove impurities on the one hand, but could also shift the solubility of residual dissolved API on the other hand. Usually, the solubility of the API in the washing liquid is lower than in the mother liquor. After addition of the washing liquid, dissolved API might precipitate on API crystals, influencing the API morphology (shape and size) and the process stability. Precipitation occurs preferentially on seeds (API crystals) and therefore the particle size increases. Furthermore, precipitation can also influence the process

stability, because precipitation might take place on surfaces of the equipment resulting in solid material buildup.

The purification process can be done in batch mode (e.g. agitated filter dryer [18,49]) or in continuous operation via a cascade arrangement of washing and filtration equipment. The continuous purification line can be realized through a solvent exchange washing in static mixers, following a membrane filter to separate API crystals from the liquid mixture. In the washing sequence, the API/impurity mother liquor enters together with the washing liquid the static mixer, where mixing of the two components is intensified through the static mixing elements. The static mixer elements ensure a good miscibility between the API/impurity mother liquor with the washing liquid, to create the regime change with API crystals and dissolved impurities. Afterwards, the solid API material is separated from the liquid mixture through a filtration process [50,51]. The continuous purification cascade of washing and filtration is repeated until a crystalline API material with low impurities is obtained.

1.3 Drying of pharmaceuticals

The definition of the drying process is the thermal removal of volatile substances (moisture) to obtain a solid, dry product [52]. During drying of a wet solid material, two processes occur simultaneously: At first, energy transfer from the environment to evaporate the surface moisture and secondly, moisture transport from the inside to the surface of the solid, following evaporation due to the first process. The heat energy from the surrounding environment is either provided through convection, conduction, radiation, or a combination of them. Usually, heat is transferred to the surface of the wet solid material and then further to the interior. Nevertheless, heat can also be generated within the solid through radio frequency or microwaves, resulting in a flow to the outer surface. Drying operations are applied to convert a solid, semi-solid or liquid feedstock into a solid product by application of heat to evaporate the liquid into the vapor phase. Most drying technologies evaporate the moisture by changing the physical state of the moisture from liquid to gaseous. An exception from this drying procedure is freeze drying, where drying occurs by sublimation of the solid phase into the vapor phase. In this case, drying takes place below the triple point of the liquid that is removed.

Drying is a complex process and involves physical or chemical transformations, which influences the product quality and the mechanisms of heat and mass transfer. Physical transformations can be shrinkage, puffing, crystallization or glass transitions, and chemical

transformations can be changes in color, odor, or other properties of the solid product [52]. Therefore, the dried product particle properties are influenced by a large number of external process variables as temperature, humidity, rate and direction of air flow, the physical form of the solid, the desirability of agitation, and the method of supporting the solid during the drying operation [53]. These variables are very important during the initial phase of drying, where unbound surface moisture is removed. In addition to the external factors of air temperature and humidity, the solid characteristics are important parameters. As drying progresses, a temperature gradient is formed within the solid during moisture evaporation from the surface. As a consequence of the temperature gradient, the moisture is transported from within the solid to the surface through the mechanisms of diffusion, capillary flow, internal pressure differences through shrinkage during drying and progressive occurring vaporization and condensation of moisture on the surface [52].

Drying of a wet solid in a gaseous medium loses moisture, until the vapor pressure of the moisture in the solid is equal to the partial pressure of the vapor in the gas. At this point, solid and gas are in equilibrium and the moisture content of the solid is called equilibrium moisture content. Continuing drying beyond this point will not reduce the moisture content in the solid any further.

The moisture content of solids depends on the physical properties of the particles, which can be classified in three different properties [54]:

Nonhygroscopic capillary-porous media, such as polymer particles, some ceramics, sand, crushed minerals, and nonhygroscopic crystals. These solids are defined by a (1) clearly recognizable pore space, which is either filled with liquid if the capillary-porous medium is completely saturated or is filled with air when the medium is completely dry, (2) physically bound moisture can be neglected, and (3) the solid does not shrink during drying.

Hyroscopic-porous media, such as textiles, wood, molecular sieves, and clay. These solids are defined by a (1) clearly recognizable pore space, (2) large amount of physically bound liquid, and (3) shrinkage often occurs in the initial stages of drying.

Colloidal (nonporous) media, such as various food products, soap, polymers (e.g., nylons). These solids are defined by a (1) non existing pore space (evaporation can take place only at the surface), and (2) all liquid is physically bond.

Moisture within these different types of solids might be bound (e.g., solution with the solid, retention in capillaries, or chemical or physical adsorption on the solid surface) or unbound (e.g., all the moisture content in a non-hygroscopic material, or in a hygroscopic material, the moisture in excess of the equilibrium moisture content corresponding to the saturation humidity) [52]. Removal of unbound moisture is either done through evaporation, when the vapor pressure of the moisture on the solid surface is equal to the atmospheric pressure, or vaporization, where moisture is removed through convection by transporting warm air over the product. Characterization of the drying behavior of solids is done by measuring the moisture content decrease as a function of time. Methods as continuous weighing, intermittent weighing or humidity difference are used to measure the drying behavior [55].

Figure 4 depicts a drying rate curve of a hygroscopic material. Drying starts with the first drying stage, where a constant removal of moisture occurs due to vaporization. During this stage, the moisture on the surface is drawn back toward the solid surface, which might result in shrinkage. Drying is mainly controlled by the diffusion of the liquid vapor across the interface between air and moisture, and the rate at which the diffusion surface is removed. At the end of the first drying stage, moisture is transported from the solids inside to the surface by capillary forces and this drying process may still be constant. When the critical moisture content is reached, the moisture film on the surface has been reduced by evaporation so that dry spots occur by further drying on the surface. At this drying behavior, the period of unsaturated surface drying starts, which is known as the second drying stage or the first part of the falling rate period. This drying period ends until the liquid film on the surface is completely evaporated. Afterwards, drying continues with the third drying stage or the second falling rate period. During this phase, the driving force for moisture removal is the concentration gradient within the solid and the removal rate is controlled by the surface. Drying at this stage is either controlled by conduction or diffusion.
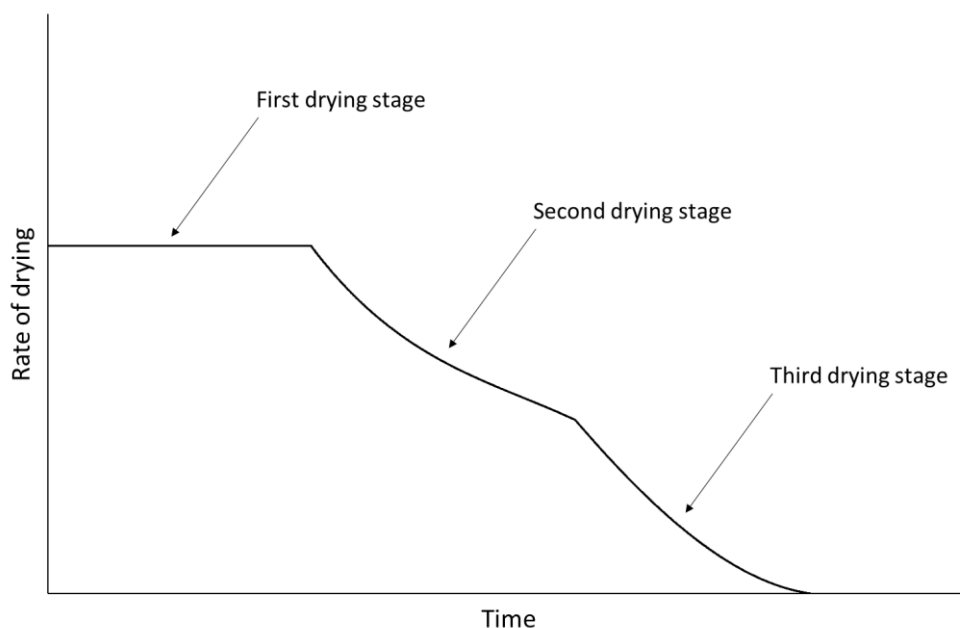
Figure 4. Drying rate curve for constant drying conditions [52].

Drying of pharmaceuticals is one of the most challenging unit operations in primary manufacturing, which follows directly after the purification. Usually, the particle properties such as size, shape and morphology are tailored during crystallization and should be unaltered in downstream processes [17]. After crystallization, API crystals are purified, for example, through the procedure described in chapter 1.2. The purified API crystals are then transferred to the drying unit operation, where the API crystals are dried and finally resulting in a dried powder as end product in primary manufacturing. Drying is a very complex process and several phenomena like agglomerate formation, attrition, (re-)crystallization and re-dissolution, can occur simultaneously. Agglomeration or attrition change the size to larger or smaller particles. Both effects are not desired while preserving particle size during drying. Furthermore, larger particles may result in lower dissolution rates, which might influence the drug's bioavailability profile, and smaller particles can have poor flowability, which might affect blending or tableting performance [18]. During a drying process, particle size reduction occurs via induced shear stresses on the particles by colliding with each other or with the equipment surface [22–25,56], or by pressure or temperature induced stresses inside the machine [26–28]. In addition to particle size reduction by environmental aspects, the attrition rate is strongly affected by the particle shape [57,58]. It has been reported that needle shaped particles have less resistance to attrition than cubic particles [22].

Most processes for drying of pharmaceuticals are still conducted via batch processing [18,27,49,59–61]. A semi-continuous drying method was developed with six small batch fluidized bed compartments linked together [38,62]. Such operations might work for free-flowing materials, but are limited in their applicability for non-free-flowing, cohesive materials, since such materials do not fluidize [63–65]. For this reason, new processes have to be developed to enable continuous drying of hard to dry substances with cohesive flow behavior.

References

(1)   Higgins, B. Pharmaceutical Manufacture by Continuous Processing. Process Eng. 1984, 35.

(2)   Cole, K. P.; Groh, J. M.; Johnson, M. D.; Burcham, C. L.; Campbell, B. M.; Diseroad, W. D.; Heller, M. R.; Howell, J. R.; Kallman, N. J.; Koenig, T. M.; et al. Kilogram-Scale Prexasertib Monolactate Monohydrate Synthesis under Continuous-Flow CGMP Conditions. Science (80-.). 2017, 356, 1144–1150.

(3)   FDA. Pharmaceutical CGMPs for the 21s Century - A Risk-Based Approach. Food Drug Adm. 2004, No. September, 32.

(4)   Lionberger, R. A.; Lee, S. L.; Lee, L.; Raw, A.; Yu, L. X. Quality by Design: Concepts for ANDAs. AAPS J. 2008, 10, 268–276.

(5)   Fisher, A. C.; Lee, S. L.; Harris, D. P.; Buhse, L.; Kozlowski, S.; Yu, L.; Kopcha, M.; Woodcock, J. Advancing Pharmaceutical Quality: An Overview of Science and Research in the U.S. FDA's Office of Pharmaceutical Quality. Int. J. Pharm. 2016, 515, 390–402.

(6)   Yu, L. X.; Woodcock, J. FDA Pharmaceutical Quality Oversight. Int. J. Pharm. 2015, 491, 2–7.

(7)   Nasr, M. M.; Krumme, M.; Matsuda, Y.; Trout, B. L.; Badman, C.; Mascia, S.; Cooney, C. L.; Jensen, K. D.; Florence, A.; Johnston, C.; et al. Regulatory Perspectives on Continuous Pharmaceutical Manufacturing: Moving From Theory to Practice: September 26-27, 2016, International Symposium on the Continuous Manufacturing of Pharmaceuticals. J. Pharm. Sci. 2017, 106, 3199–3206.

(8)   Allison, G.; Cain, Y. T.; Cooney, C.; Garcia, T.; Bizjak, T. G.; Holte, O.; Jagota, N.; Komas, B.; Korakianiti, E.; Kourti, D.; et al. Regulatory and Quality Considerations for Continuous Manufacturing May 20-21, 2014 Continuous Manufacturing Symposium. J. Pharm. Sci. 2015, 104, 803–812.

(9)   Welch, C. J.; Hawkins, J. M.; Tom, J. Precompetitive Collaboration on Enabling Technologies for the Pharmaceutical Industry. Org. Process Res. Dev. 2014, 18, 481–487.

(10)   Mascia, S.; Heider, P. L.; Zhang, H.; Lakerveld, R.; Benyahia, B.; Barton, P. I.; Braatz, R. D.; Cooney, C. L.; Evans, J. M. B.; Jamison, T. F.; et al. End-to-End Continuous Manufacturing of Pharmaceuticals: Integrated Synthesis, Purification, and Final Dosage Formation. Angew. Chemie - Int. Ed. 2013, 52, 12359–12363.

(11)   Khinast, J.; Bresciani, M. Continuous Manufacturing: Definitions and Engineering Principles. In *Continuous Manufacturing of Pharmaceuticals*; John Wiley & Sons, Ltd: Chichester, UK, 2017; pp 1–31.

(12)   Srai, J. S.; Badman, C.; Krumme, M.; Futran, M.; Johnston, C. Future Supply Chains Enabled by Continuous Processing-Opportunities and Challenges May 20-21, 2014 Continuous Manufacturing Symposium. J. Pharm. Sci. 2015, 104, 840–849.

(13)   Leuenberger, H. New Trends in the Production of Pharmaceutical Granules: Batch versus Continuous Processing. Eur. J. Pharm. Biopharm. 2001, 52, 289–296.

(14)   Teżyk, M.; Milanowski, B.; Ernst, A.; Lulek, J. Recent Progress in Continuous and Semi-Continuous Processing of Solid Oral Dosage Forms: A Review. Drug Dev. Ind. Pharm. 2016, 42, 1195–1214.

(15) Remon, J. P.; Vervaet, C. Continuous Processing of Pharmaceuticals. In *Encyclopedia of Pharmaceutical Technology*; Swarbrick, J., Ed.; Taylor & Francis: New York, 2013; pp 743–749.

(16) Byrn, S.; Futran, M.; Thomas, H.; Jayjock, E.; Maron, N.; Meyer, R. F.; Myerson, A. S.; Thien, M. P.; Trout, B. L. Achieving Continuous Manufacturing for Final Dosage Formation: Challenges and How to Meet Them May 20-21, 2014 Continuous Manufacturing Symposium. J. Pharm. Sci. 2015, 104, 792–802.

(17) Burgbacher, J.; Wiss, J. Industrial Applications of Online Monitoring of Drying Processes of Drug Substances Using NIR. Org. Process Res. Dev. 2008, 12, 235–242.

(18) Lekhal, A.; Girard, K. P.; Brown, M. A.; Kiang, S.; Glasser, B. J.; Khinast, J. G. Impact of Agitated Drying on Crystal Morphology: KCl-Water System. Powder Technol. 2003, 132, 119–130.

(19) Seville, J. P. K.; Willett, C. D.; Knight, P. C. Interparticle Forces in Fluidisation: A Review. Powder Technol. 2000, 113, 261–268.

(20) Kreimer, M.; Aigner, I.; Sacher, S.; Krumme, M.; Mannschott, T.; van der Wel, P.; Kaptein, A.; Schroettner, H.; Brenn, G.; Khinast, J. G. Mechanical Strength of Microspheres Produced by Drying of Acoustically Levitated Suspension Droplets. Powder Technol. 2018, 325, 247–260.

(21) Birch, M.; Marziano, I. Understanding and Avoidance of Agglomeration during Drying Processes: A Case Study. Org. Process Res. Dev. 2013, 17, 1359–1366.

(22) Bemrose, C. R.; Bridgwater, J. A Review of Attrition and Attrition Test Methods. Powder Technol. 1987, 49, 97–126.

(23) Neil, A. U.; Bridgwater, J. Attrition of Particulate Solids under Shear. Powder Technol. 1994, 80, 207–219.

(24) Bravi, M.; Di Cave, S.; Mazzarotta, B.; Verdone, N. Relating the Attrition Behaviour of Crystals in a Stirred Vessel to Their Mechanical Properties. Chem. Eng. J. 2003, 94, 223–229.

(25) Hare, C.; Ghadiri, M.; Dennehy, R. Prediction of Attrition in Agitated Particle Beds. Chem. Eng. Sci. 2011, 66, 4757–4770.

(26) Bika, D. G.; Gentzler, M.; Michaels, J. N. Mechanical Properties of Agglomerates. Powder Technol. 2001, 117, 98–112.

(27) MacLeod, C. S.; Muller, F. L. On the Fracture of Pharmaceutical Needle-Shaped Crystals during Pressure Filtration: Case Studies and Mechanistic Understanding. Org. Process Res. Dev. 2012, 16, 425–434.

(28) Kowalski, S. J.; Rajewska, K.; Rybicki, A. Destruction of Wet Materials by Drying. Chem. Eng. Sci. 2000, 55, 5755–5762.

(29) Warikoo, V.; Godawat, R.; Brower, K.; Jain, S.; Cummings, D.; Simons, E.; Johnson, T.; Walther, J.; Yu, M.; Wright, B.; et al. Integrated Continuous Production of Recombinant Therapeutic Proteins. Biotechnol. Bioeng. 2012, 109, 3018–3029.

(30) Poechlauer, P.; Manley, J.; Broxterman, R.; Ridemark, M. Continuous Processing in the Manufacture of Active Pharmaceutical Ingredients and Finished Dosage Forms: An Industry Perspective. Org. Process Res. Dev. 2012, 16, 1586–1590.

(31) Yu, L. X.; Kopcha, M. The Future of Pharmaceutical Quality and the Path to Get There. Int. J. Pharm. 2017, 528, 354–359.

(32)   Collins, P. C. Chemical Engineering and the Culmination of Quality by Design in Pharmaceuticals. AIChE J. 2018, 64, 1502–1510.

(33)   Lee, S. L.; O'Connor, T. F.; Yang, X.; Cruz, C. N.; Chatterjee, S.; Madurawe, R. D.; Moore, C. M. V.; Yu, L. X.; Woodcock, J. Modernizing Pharmaceutical Manufacturing: From Batch to Continuous Production. J. Pharm. Innov. 2015, 10, 191–199.

(34)   Hashimoto, K.; Adachi, S.; Shirai, Y.; Horie, M. Continuous Separation of α-Cyclodextrin and Glucose Using a Simulated Moving-Bed Adsorber. J. Food Eng. 1988, 8, 187–200.

(35)   Schaber, S. D.; Gerogiorgis, D. I.; Ramachandran, R.; Evans, J. M. B.; Barton, P. I.; Trout, B. L. Economic Analysis of Integrated Continuous and Batch Pharmaceutical Manufacturing: A Case Study. Ind. Eng. Chem. Res. 2011, 50, 10083–10092.

(36)   Vervaet, C.; Remon, J. P. Continuous Granulation in the Pharmaceutical Industry. Chem. Eng. Sci. 2005, 60, 3949–3957.

(37)   Myerson, A. S.; Krumme, M.; Nasr, M.; Thomas, H.; Braatz, R. D. Control Systems Engineering in Continuous Pharmaceutical Manufacturing May 20-21, 2014 Continuous Manufacturing Symposium. J. Pharm. Sci. 2015, 104, 832–839.

(38)   Vercruysse, J.; Delaet, U.; Van Assche, I.; Cappuyns, P.; Arata, F.; Caporicci, G.; De Beer, T.; Remon, J. P.; Vervaet, C. Stability and Repeatability of a Continuous Twin Screw Granulation and Drying System. Eur. J. Pharm. Biopharm. 2013, 85, 1031–1038.

(39)   Markarian, J. Rutgers University Research Center and Janssen Develop Continuous Manufacturing Process http://www.pharmtech.com/rutgers-university-research-center-and-janssen-develop-continuous-manufacturing-process-0 (accessed Apr 20, 2018).

(40)   Plumb, K. Continuous Processing in the Pharmaceutical Industry. Chem. Eng. Res. Des. 2005, 83, 730–738.

(41)   O'Connor, T. F.; Yu, L. X.; Lee, S. L. Emerging Technology: A Key Enabler for Modernizing Pharmaceutical Manufacturing and Advancing Product Quality. Int. J. Pharm. 2016, 509, 492–498.

(42)   Laske, S.; Paudel, A.; Scheibelhofer, O.; Sacher, S.; Hoermann, T.; Khinast, J.; Kelly, A.; Rantannen, J.; Korhonen, O.; Stauffer, F.; et al. A Review of PAT Strategies in Secondary Solid Oral Dosage Manufacturing of Small Molecules. J. Pharm. Sci. 2017, 106, 667–712.

(43)   Rama Rao, N.; Mani Kiran, S. S.; Prasanthi, N. L. Pharmaceutical Impurities: An Overview. Indian J. Pharm. Educ. Res. 2010, 44, 301–310.

(44)   Keitel, S. Impurity Profiles in Active Pharmaceutical Ingredients; EU/Swissmedic GMP Workshop: Beijing University, 2006.

(45)   Chandrawanshi, H.; Pilaniya, U.; Manchandani, P.; Jain, P.; Singh, N.; Pilaniya, K. Recent Trends in the Impurity Profile of Pharmaceuticals. J. Adv. Pharm. Technol. Res. 2010, 1, 302.

(46)   Székely, G.; Gil, M.; Sellergren, B.; Heggie, W.; Ferreira, F. C. Environmental and Economic Analysis for Selection and Engineering Sustainable API Degenotoxification Processes. Green Chem. 2013, 15, 210–225.

(47)   Siew, W. E.; Livingston, A. G.; Ates, C.; Merschaert, A. Continuous Solute Fractionation with Membrane Cascades - A High Productivity Alternative to Diafiltration. Sep. Purif. Technol. 2013, 102, 1–14.

(48)   Lin, J. C. Te; Livingston, A. G. Nanofiltration Membrane Cascade for Continuous Solvent Exchange. Chem. Eng. Sci. 2007, 62, 2728–2736.

(49)   Lekhal, A.; Girard, K. P.; Brown, M. A.; Kiang, S.; Khinast, J. G.; Glasser, B. J. The Effect of Agitated Drying on the Morphology of L-Threonine (Needle-like) Crystals. Int. J. Pharm. 2004, 270, 263–277.

(50)   Gursch, J.; Hohl, R.; Toschkoff, G.; Dujmovic, D.; Brozio, J.; Krumme, M.; Rasenack, N.; Khinast, J. Continuous Processing of Active Pharmaceutical Ingredients Suspensions via Dynamic Cross-Flow Filtration. J. Pharm. Sci. 2015, 104, 3481–3489.

(51)   Gursch, J.; Hohl, R.; Dujmovic, D.; Brozio, J.; Krumme, M.; Rasenack, N.; Khinast, J. Dynamic Cross-Flow Filtration: Enhanced Continuous Small-Scale Solid-Liquid Separation. Drug Dev. Ind. Pharm. 2016, 42, 977–984.

(52)   Mujumdar, A. Handbook of Industrial Drying, Fourth Edition; Mujumdar, A. S., Ed.; CRC Press, 2015; Vol. 4.

(53)   Williams-Gardner, A. Industrial Drying; Godwin: London, 1976.

(54)   van Brackel, J. Mass Transfer in Convective Drying. In *Advances in Drying*; Hemisphere Publishing: New York, 1980; pp 217–168.

(55)   Keey, R. B. Introduction to Industrial Drying Operations, 1st ed.; Pergamon Press: New York, 1978.

(56)   Keey, R. B. Drying of Loose and Particulate Materials; Hemisphere Publishing, 1992.

(57)   Gahn, C.; Krey, J.; Mersmann, a. The Effect of Impact Energy and the Shape of Crystals on Their Attrition Rate. J. Cryst. Growth 1996, 166, 1058–1063.

(58)   Schæfer, T.; Mathiesen, C. Melt Pelletization in a High Shear Mixer. VII. Effects of Product Temperature. Int. J. Pharm. 1996, 134, 105–117.

(59)   Leuenberger, H.; Betz, G.; Junker-Bürgin, P. Batch and Continuous Processing in the Production of Pharmaceutical Granules #. Pharm. Dev. Technol. 2003, 8, 289–297.

(60)   Cypes, S. H.; Wenslow, R. M.; Thomas, S. M.; Chen, A. M.; Dorwart, J. G.; Corte, J. R.; Kaba, M. Drying an Organic Monohydrate: Crystal Form Instabilities and a Factory-Scale Drying Scheme to Ensure Monohydrate Preservation. Org. Process Res. Dev. 2004, 8, 576–582.

(61)   Kougoulos, E.; Chadwick, C. E.; Ticehurst, M. D. Impact of Agitated Drying on the Powder Properties of an Active Pharmaceutical Ingredient. Powder Technol. 2011, 210, 308–314.

(62)   Kemp, I. C. Drying of Pharmaceuticals in Theory and Practice. Dry. Technol. 2017, 35, 918–924.

(63)   Geldart, D. The Effect of Particle Size and Size Distribution on the Behaviour of Gas-Fluidised Beds. Powder Technol. 1972, 6, 201–215.

(64)   Geldart, D. Types of Gas Fluidization. Powder Technol. 1973, 7, 285–292.

(65)   Visser, J. Van Der Waals and Other Cohesive Forces Affecting Powder Fluidization. Powder Technol. 1989, 58, 1–10.

„The task is not to see what has never been seen before,
but to think what has never been thought before
about what you see everyday."

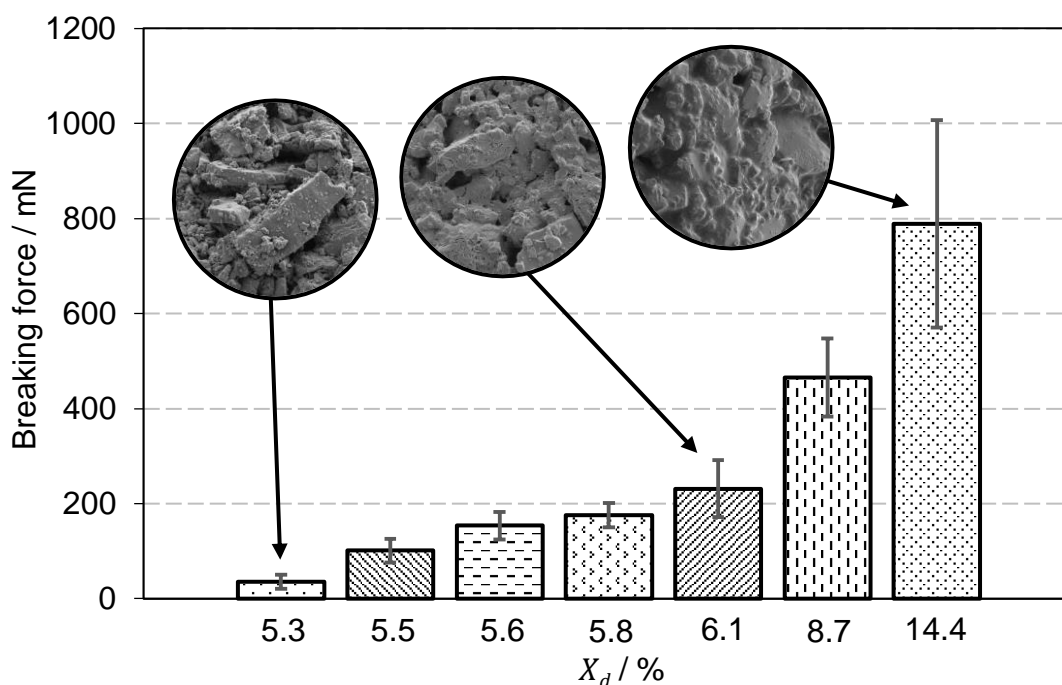*Erwin Schrödinger (1887-1961)*

2. Mechanical Strength of Microspheres Produced by Drying of Acoustically Levitated Suspension Droplets

M. Kreimer, I. Aigner, S. Sacher, M. Krumme, T. Mannschott, P. van der Wel,

A. Kaptein, H. Schroettner, G. Brenn, J.G. Khinast

Graphical abstract:

Key words acoustic levitation, spray drying, suspensions, microspheres, morphology, mechanical properties

Mechanical Strength of Microspheres Produced by Drying of Acoustically Levitated Suspension Droplets

M. Kreimer[1], I. Aigner[1], S. Sacher[1], M. Krumme[2], T. Mannschott[2], P. van der Wel[3], A. Kaptein[3], H. Schroettner[4,5], G. Brenn[6], J.G. Khinast[1,7]

[1] Research Center Pharmaceutical Engineering (RCPE) GmbH, 8010 Graz, Austria

[2] Novartis Pharma AG, Novartis Campus, 4056 Basel, Switzerland

[3] Hosokawa Micron B.V., Gildenstraat 26, 7005 BL Doetinchem, Netherlands

[4] Graz University of Technology, Institute for Electron Microscopy and Nanoanalysis, 8010 Graz, Austria

[5] Austrian Centre for Electron Microscopy and Nanoanalysis (FELMI-ZFE), 8010 Graz, Austria

[6] Graz University of Technology, Institute of Fluid Mechanics and Heat Transfer, 8010 Graz, Austria

[7] Graz University of Technology, Institute for Process and Particle Engineering, 8010 Graz, Austria

Corresponding author: J.G. Khinast

      Tel. number: 0043 316 873 30400

      E-mail address: khinast@tugraz.at

Highlights

- Solubility measurements of lactose in isopropanol-water mixtures.

- Drying experiments of suspension droplets by means of acoustic levitation.

- Microsphere formation at different mass of suspended and dissolved solids.

- Hardness tests of individual microspheres.

- Relevance of single microsphere drying experiments for industrial spray drying.

Abstract

Spray drying is widely used in pharmaceutical manufacturing to produce microspheres from solutions or suspensions. The mechanical properties of the microspheres are reflected by the morphology formed in the drying process. In suspension drying, solids dissolved in the carrier liquid may form bridges between the suspended primary particles, producing a microsphere structure which is resistant against mechanical loads. Experiments with individual, acoustically levitated droplets were performed to investigate the drying of suspension droplets. The suspensions studied consisted of a binary liquid mixture as the carrier liquid, and primary particles of a suspended solid material partially soluble in the liquid. The solubility of the solid was varied by the composition of the liquid mixture. The experiments revealed longer first and second drying stages for higher solids solubility. Electron micrographs revealed the morphology of individual microspheres produced by drying in the levitator. Microspheres with only primary particles and no visible crust were obtained for low solids solubility, whereas higher contents of dissolved solids resulted in a more densely packed microsphere with crust formation. To quantify the hardness of individual microspheres, the maximum breaking force upon mechanical loading was measured for a range of varying suspension compositions. These measurements confirmed that densely packed structures with a thick crust reveal high mechanical strength. It was shown that, for primary particles to be conserved in spray drying, the dissolved solid loading X_d must be below $5.2 \cdot 10^{-2}$.

Key words acoustic levitation, spray drying, suspensions, microspheres, morphology, mechanical properties

Nomenclature

A	Decreasing droplet surface area of an oblate spheroid / m^2
A_0	Initial droplet surface area of an oblate spheroid / m^2
$A_{s,o}$	Droplet surface area of an oblate spheroid / m^2
m	Mass of droplet / g
m_d	Mass of dissolved solids / g
m_{H_2O}	Mass of water / g

m_I	Mass of isopropanol / g
m_{liq}	Mass of liquids / g
m_s	Mass of suspended solids / g
m_{sol}	Mass of dissolved and suspended solids / g
q_3	Particle size density distribution
Re	Reynolds number
t_d	Drying time in levitator / min
w_d	Dissolved solid mass fraction
w_{H_2O}	Water mass fraction
w_s	Suspended solid mass fraction
w_{sol}	Dissolved and suspended solid mass fraction
X_d	Dissolved solid mass loading
X_L	Solubility of lactose in isopropanol-water mixtures
ρ_s	Density of suspension / $g \cdot cm^{-3}$
ρ_{sol}	Density of solution / $g \cdot cm^{-3}$

2.1 Introduction

Spray drying is a widely used technique transforming an atomized liquid feed into dry particles by evaporation of the liquid phase in a gaseous drying medium [1]. The technique is used for heat-sensitive products, such as food and pharmaceuticals, since the temperature of the drying liquid remains below the wet-bulb temperature [2]. A big advantage of spray drying is that drying of emulsions, slurries or pastes may be carried out in one unit operation [3]. Independent of the feed composition, production of spray dried powders with a narrow particle size distribution requires consistent droplet size formation. In general, production of fine droplets yields individual particle drying with reduced tendency for agglomeration during drying.

Single droplet drying and particle formation during spray drying are difficult to investigate, because of the complex two-phase flow in spray dryers and other difficulties as described by Vehring et al. [4]. Therefore, the drying behavior of individual droplets was studied in the literature with various experimental methods of droplet positioning, such as droplets free flying [5], free falling [6], or pending from a capillary or a filament [7, 8]. Other techniques trap droplets on a concave hot plate [9] or freely levitate them using optical, acoustic or electrodynamic forces [10, 11]. An acoustic levitator generates a standing acoustic wave with equally spaced pressure nodes and a corresponding quasi-steady pressure distribution allowing individual droplets to be levitated. Investigations of the progression of drying with this technique was successful for droplets of liquid mixtures [12], aqueous solutions [13] and aqueous suspensions [14]. The drying of droplets in an acoustic levitator is similar to the process in a spray dryer, as described by Schiffter [15]. One limitation in an acoustic levitator is the droplet size, which is determined by wavelengths between 2.2 and 0.34 cm for ultrasound frequencies between 15 and 100 kHz [16]. Furthermore, the maximum droplet volume and mass for acoustic levitation are limited by the liquid surface tension against the ambient air and the liquid density [17], [18]. Typical densities of suspensions for acoustic levitation experiments range between 0.5 and 8 g/ml [19].

Drying may be enhanced by convection through a gas flow, but independent of that the droplet undergoes two drying stages until a final dry particle is formed. The first drying stage is known as the constant-rate period, since the surface of the droplet decreases at a constant rate due to evaporation of the liquid from the surface. This drying stage therefore follows the so-called d^2 law [20]. Suspension droplets exhibit this behavior as long as the surface is wetted [21]. The mass loss of the liquid leads to an increase of the solid mass

fraction in the droplet. At high ratios of droplet-shrinkage-rate-to-diffusivity in the liquid phase, a non-uniform radial distribution of the solid may arise, leading to crust formation [14]. These phenomena may further influence the evaporation rate and, consequently, the duration of the first and the second drying stages. Different mechanisms of heat and mass transport may occur inside the microsphere (transport of liquid and liquid vapor, heat transfer, migration of the liquid surface into the microsphere). The local porosity of the solid, surface roughness and solids distribution inside the microsphere may result in a highly complex evolution of the second drying stage [14].

In the course of the first drying stage, the solid fraction of the droplet increases due to evaporation of the liquid. The end of the first drying stage is defined by the rise of the droplet temperature above wet-bulb level. In the second drying stage, evaporation is reduced by the resistance against liquid transport from the inside of the droplet (which slowly becomes a solid microsphere) to the surface. In this period, volume change due to the shrinkage is negligible. The liquid evaporation results in a loss of mass, which can be detected by a change of the microsphere position in the acoustic levitator. As the microsphere loses weight, it moves upward towards the nearest pressure node. The remaining liquid may evaporate inside the porous structure rather than on the most outer surface. Solids dissolved in the liquid may precipitate on the way to the surface or on the surface, resulting in a dense packing of the primary particles of the suspension or the formation of a completely closed solid layer on the surface.

The drying of pure liquid [12, 22], solution [23, 24] and suspension droplets [21, 25] was investigated in the literature. Drying of suspension droplets with dissolved solids, however, has been studied to a much lesser extent. A better understanding of the drying of suspension droplets is needed to evaluate the influence of the suspension composition on the dried particle properties. Knowing the influencing factors during spray drying of suspensions will make it possible to choose process parameters during drying which avoid change of particle properties. This is an advantage in manufacturing of API.

In a pharmaceutical continuous manufacturing process, drying is one of the last unit operations of primary manufacturing, before entering processes further downstream (secondary manufacturing), such as blending, granulation, tableting or capsule filling [26]. Looking at this process from the beginning, production starts with the synthesis of the API and continues with crystallization. Afterwards, several washing [27] and filtration [28, 29] steps are needed to obtain a purified solid drug product. The purification steps are vital to remove impurities. Finally, the drug crystals are dried [30, 31] where care has to be taken

to avoid major changes of final powder properties, such as the particle size distribution. If the carrier liquid of the suspension to be dried contains significant amounts of dissolved solids, agglomeration of primary particles by precipitated solids is likely to occur. The amount of dissolved solids (and thus, of the solid bridges) will then determine the mechanical strength of a dried agglomerate. If the connections (solid bridges) between primary particles are weak enough, the primary particles can be obtained by break-up of the agglomerates due to low-grade mechanical forces.

For this reason, there is interest in characterizing material's mechanical properties of spray-dried pharmaceutical microspheres. Methods characterizing the bulk properties of powders, such as the bulk density, the cohesive strength, the angle of repose and other parameters do not reveal information about individual particles [32]. In contrast to this, recently developed methods assess the individual particles by micro- and nano-indentation techniques [33-36]. Mechanical properties of individual particles, such as the hardness, the elastic modulus, the stiffness, or the load displacement curves, are determined by atomic force microscopy nano-indentation experiments [37-41]. Transferring the results from microscopic single particle measurements to a macroscopic level, however, is difficult. Some attempts were recently made to assess the mechanical strength of individual or agglomerated particles of ceramics [42], catalyst carriers [43] and calcium carbonate granules [44-47].

In the present work we studied the evaporation kinetics of suspension droplets, with solids dissolved in various carrier liquids, and the resulting microsphere morphology of pharmaceutical excipients. Furthermore, the mechanical properties of individual microspheres were evaluated by hardness measurements and related to the solid's solubility in the liquid. Our hypothesis is that the more solid material is dissolved in the liquid, the stronger solid bridges (obtained upon drying) will be, increasing the mechanical strength of the microspheres.

2.2 Materials and methods

2.2.1 Materials

Lactose GranuLac® 230 was obtained from Molkerei Meggle Wasserburg (Wasserburg, Germany) with a particle size distribution (PSD) as shown in Figure 1 and particle shapes as shown in Figure 2. Water of analytical grade was produced with an Ultrapure Water

System from TKA (Niederelbert, Germany). Isopropanol in high purity (≥99.8%) was obtained from Carl Roth (Karlsruhe, Germany).
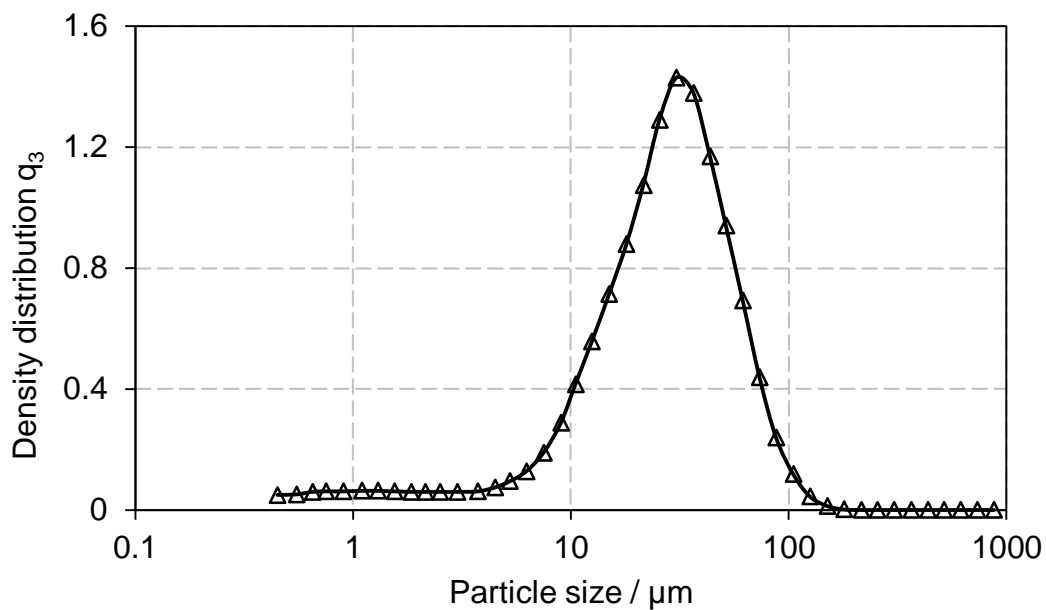
Figure 1. Particle size distribution of raw material GranuLac® 230.
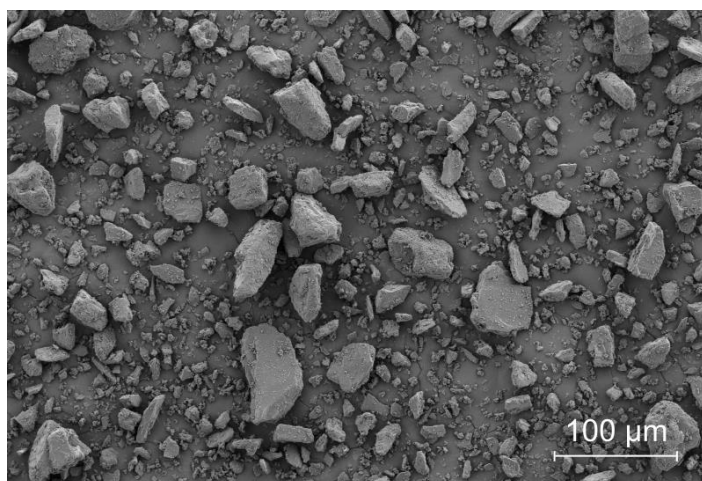
Figure 2. Scanning electron micrograph of raw material GranuLac® 230.

2.2.2   Solubility measurements of lactose in isopropanol-water mixtures

The following definitions were chosen, i.e., the mass of the liquid mixture m_{liq} consisting of H₂O and solvent I (isopropanol) in Eq. 1, the water mass fraction w_{H_2O} in Eq. 2 and the solubility of lactose X_L in Eq. 3.

$$m_{liq} = m_{H_2O} + m_I \qquad (1)$$

$$w_{H_2O} = \frac{m_{H_2O}}{m_{liq}} \qquad (2)$$

$$X_L = \frac{m_d}{m_{liq}} \qquad (3)$$

Here m_d is the mass of the dissolved excipient (alpha-lactose monohydrate). Solubility measurements of alpha-lactose monohydrate in different water-isopropanol mixtures were carried out by measuring the solution densities with DSA 5000 M from Anton Paar (Graz, Austria). The measurements were carried out at the constant temperature of 25°C and covered solvents with five different water mass fraction w_{H_2O} between 40 % and 90 %.

For determination of the solubility, the densities of the mixtures m_{liq} were measured in the following manner. The density of each isopropanol-water mixture was measured. Afterwards, for each of the mixtures, four solutions with known amounts of dissolved lactose m_d were prepared, as depicted by the square symbols in Figure 3. All the lactose concentrations were below the saturation concentration. Solid concentrations were increased with increasing water mass fraction w_{H_2O}. For the solution preparation, a known amount of lactose was suspended in the solvent mixture and the suspensions were placed in an incubating orbital shaker 3500l from VWR (Pennsylvania, United States) at 25°C for 24h. After this time, the lactose was completely dissolved. The density of each solution was measured five times. The RSD of all the measurements was below 0.02%. With these data, a linear relation was obtained for the unsaturated regime between solution densities ρ_{sol} and the dissolved lactose mass loading in isopropanol-water mixtures X_L. The linear relation is depicted in Figure 3**Error! Reference source not found.** for a water mass fraction w_{H_2O} of 50 %. This procedure was carried out for all water mass fractions w_{H_2O} and enabled the calculation of linear fit curves ρ_{sol} as depicted in Table 1.
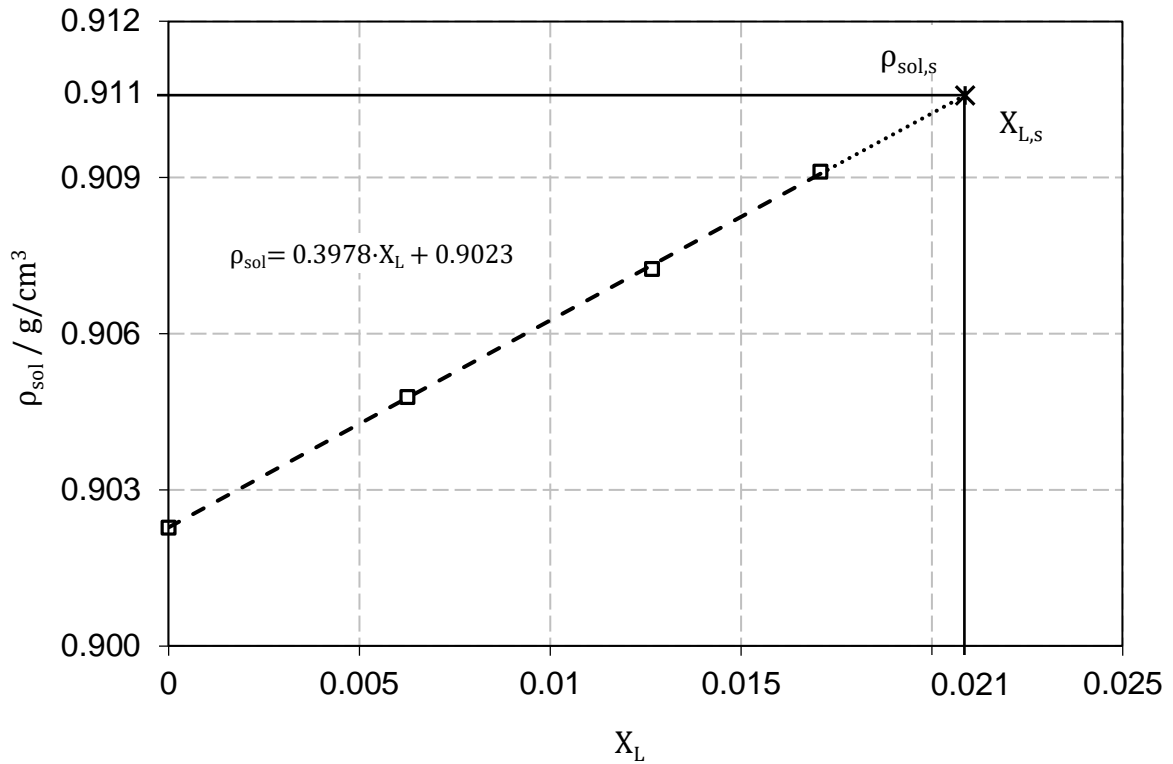
Figure 3. Determination of the solubility $X_{L,s}$ from different solution densities ρ_{sol} for a water mass fraction w_{H_2O} of 50 % at 25°C. The square symbols represent solution densities ρ_{sol} with known mass of dissolved solids m_d and the dashed line shows the linear fit curve ρ_{sol}. The dotted line depicts the extrapolation to calculate the solubility $X_{L,s}$ (star symbol) from the measured saturated solution density $\rho_{sol,s}$.

Table 1. Measured saturation densities $\rho_{sol,s}$ and calculated solubilities $X_{L,s}$ from the linear fit curve ρ_{sol} at different water mass fractions w_{H_2O}.

w_{H_2O} / %	Linear fit curve ρ_{sol}	R^2	$\rho_{sol,s}$ / g/cm³	$X_{L,s}$ / %
40	$0.4637 \cdot X_L + 0.8786$	0.9477	0.883	0.92
50	$0.3978 \cdot X_L + 0.9023$	0.9998	0.911	2.06
60	$0.3906 \cdot X_L + 0.9256$	0.9992	0.941	3.80
80	$0.3769 \cdot X_L + 0.9667$	0.99997	1.005	9.95
90	$0.4007 \cdot X_L + 0.9807$	0.9987	1.041	14.72

To determine the concentration at saturation, saturated lactose solutions were prepared for all the five solvent mixtures. A surplus of lactose was suspended in the liquids, and the

mixtures were placed in an orbital shaker at 25°C for 48h. The saturated solutions $\rho_{sol,s}$ were decanted and, before measurement, filtered with a syringe filter from Merz Brothers GmbH (Vienna, Austria) with a pore size of 0.22 μm. The concentration of the saturated solutions $\rho_{sol,s}$ was measured five times. The RSD for all the measurements was below 0.02%. The solubility $X_{L,s}$ of the saturated solutions $\rho_{sol,s}$ was calculated from the density using the previously determined linear fit curves ρ_{sol}. The densities $\rho_{sol,s}$ of the saturated pure water and pure isopropanol solutions were not measured to calculate the lactose solubility, because these values were available from the literature [48,49]. Figure 4 represents the solubility of lactose $X_{L,s}$ in the isopropanol-water mixtures in the form of water mass fractions w_{H_2O}.
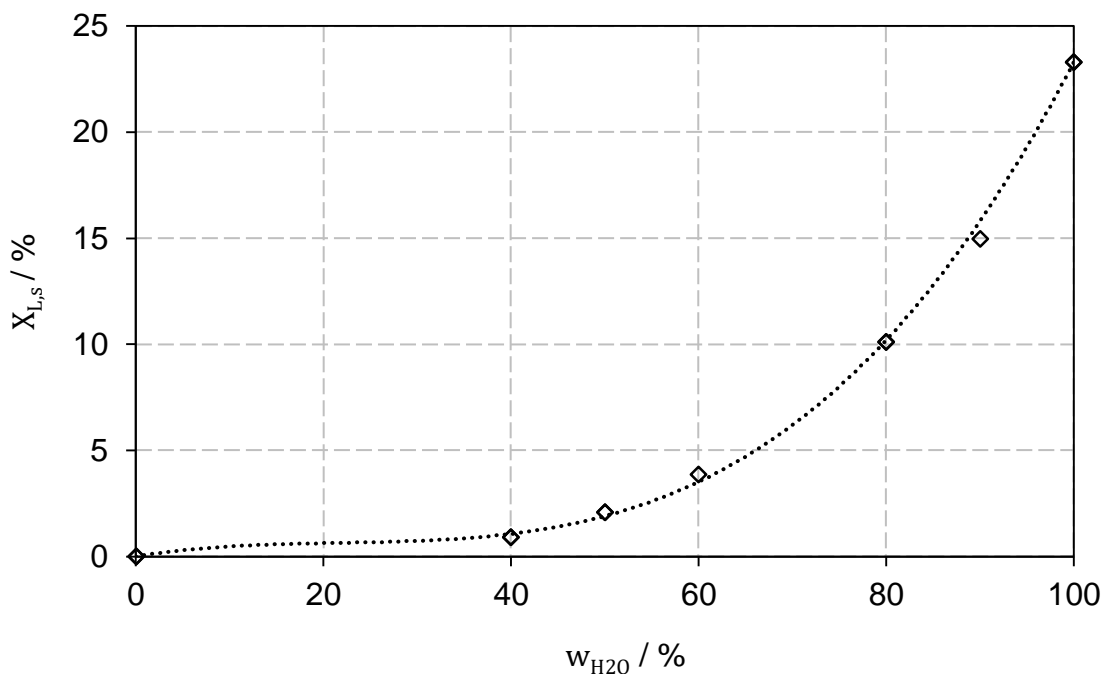
Figure 5. Solubility $X_{L,s}$ of alpha-lactose monohydrate in isopropanol-water mixtures at 25°C.

2.2.3 Levitation drying setup

Experiments for assessing the drying kinetics of lactose suspensions with different lactose mass fractions and solvent compositions were carried out using an acoustic levitator. Acoustic levitation is commonly used for studying transport processes with individual objects suitable for being positioned in the quasi-steady pressure field of the resonator. This levitation technique works without mechanical contact between the levitated object and a solid body. Heat and mass transfer from the object are therefore influenced by the

acoustic streaming field of the resonator only, and they may be controlled by additional air streams around the object.

The ultrasound transducer of the levitator used in the drying experiments was supplied by tec5 AG (Oberursel, Germany). The experimental setup can be seen in Figure 5. The standing ultrasound wave is generated by an acoustic resonator consisting of the transducer and a reflector. The vibrating horn of the transducer is made of stainless steel and driven by a piezo-crystal at the frequency of 58 kHz. The interaction of the ultrasound with the reflector produces standing soundwaves with a quasi-steady pressure distribution in the resonator. Proper coaxial relative alignment of the transducer and the reflector allows for a sound-pressure level in the resonator strong enough for levitating the object, and low enough to keep the deformation of the object to a minimum. The presence of the object in the resonator produces a steady acoustic-streaming flow which influences the transport processes from the object. The acoustic streaming vortices, however, rather form a closed flow system in the air around the object and are saturated by the vapor produced by the drying process. To prevent a retarding effect from this vapor content of the vortices, an additional upward flow of drying air is provided through a hole in the reflector plate. This air flow is provided from the in-house pressurized air system and controlled by a mass flow controller from Bronkhorst (AK Ruurlo, Netherlands).

The temperature in the acoustic levitator during the drying experiments was in the range of 25 ± 2°C. The drying air flow was set at a velocity of 0.66 m/s, corresponding to a Reynolds number of 170 at the exit hole of the air supply. Additional experiments were carried out without air flow around the droplet for comparison.

The process of droplet drying was recorded using a CCD camera Sony XCD-X710 (Tokyo, Japan) with a CCD chip of 1024 x 768 pixels. The image resolution was 166 pixels/mm. The CCD camera was used with a macro lens Pentax, 50 mm, 1:2.8 (Tokyo, Japan). The data evaluation of the images was carried out with the public domain software ImageJ, version 1.49, to obtain the surface area of the droplet, the aspect ratio of its shape, and the coordinates of the center of gravity relative to a reference point in space. The droplet surface area of an oblate spheroid $A_{s,o}$ was calculated via Eq. 4 through the half-major (a) and the half-minor (b) axes lengths [50]:

$$A_{s,o} = 2\pi a^2 \left(1 + \frac{b/a}{\sqrt{a^2/b^2 - 1}} arcsin\sqrt{a^2/b^2 - 1}\right) \tag{4}$$

The raw data were analyzed as functions of time to calculate the droplet surface decay, assuming axial symmetry. The vertical displacement of the droplet due to the mass loss was measured as well. Thus, drying kinetics can be studied also in the second drying stage, where the drop has a constant size and shape. The images were recorded with a frequency between 0.5 and 0.067 Hz, depending on the state of evaporation. Every experiment was repeated five times for each droplet liquid composition.
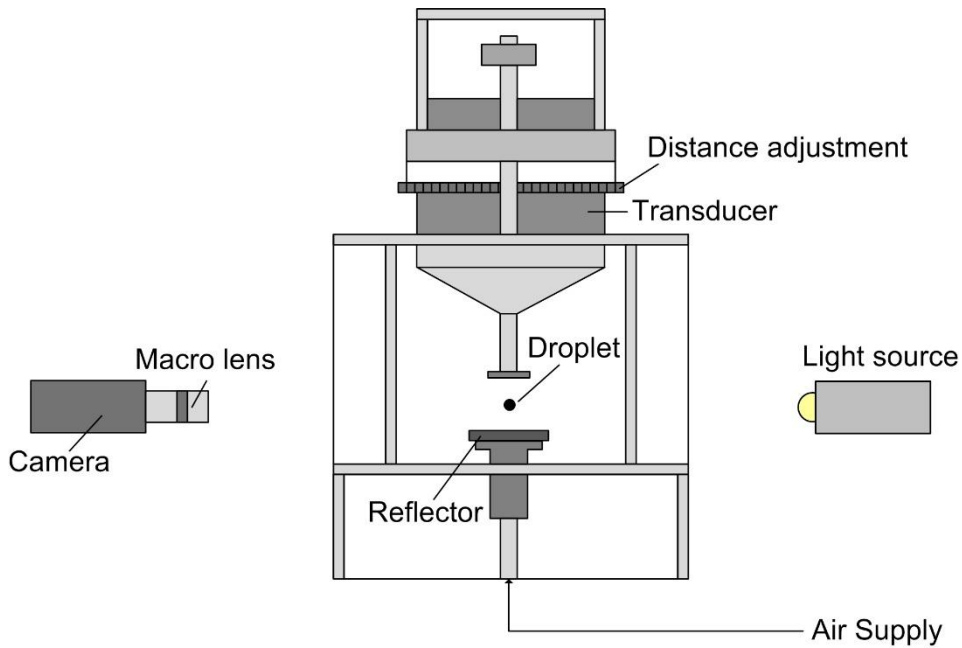
Figure 5. Ultrasonic levitator and imaging equipment for measuring individual droplet drying kinetics.

2.2.4 Preparation of suspensions and droplet formation

The suspensions investigated consisted of one solid material (lactose) in mixtures of water and isopropanol (or in the pure species) as the carrier liquids. A part of the solid material was dissolved in the liquid, according to its solubility. A droplet with the mass m therefore consists of the dissolved mass m_d and the suspended mass m_s of the solid material in a mixture of the liquid masses m_{H_2O} and m_I of water and isopropanol. We can therefore write

$$m = m_d + m_s + m_{H_2O} + m_I \tag{5}$$

Depending on the water mass fraction w_{H_2O} (Eq. 2), different mass of solids m_{sol} (Eq. 6) were present in one suspension droplet. The solids mass m_{sol} consists of dissolved m_d and suspended solids m_s.

$$m_{sol} = m_d + m_s \tag{6}$$

In terms of definition, the mass m was used as reference to define the dissolved solid mass fraction w_d (Eq. 7), the suspended solid mass fraction w_s (Eq. 8) and the total solid mass fraction w_{sol} (Eq. 9).

$$w_d = \frac{m_d}{m} \tag{7}$$

$$w_s = \frac{m_s}{m} \tag{8}$$

$$w_{sol} = \frac{m_{sol}}{m} = w_d + w_s \tag{9}$$

For the preparation of a suspension, a saturated solution of lactose was prepared beforehand as the carrier liquid to avoid changes of the particle size or shape due to dissolution of the lactose. Water and isopropanol were mixed in different ratios in sealable flasks and stirred for one hour to ensure homogeneous solvent mixtures. Lactose was then added in surplus to the liquids and shaken with an incubating orbital shaker 3500l from VWR (Pennsylvania, United States) for 48 hours at 25 °C. The saturated solutions were decanted and filtered with MN 618 from Macherey-Nagel (Düren, Germany). Solid lactose particles were then added to obtain the suspensions. The suspensions were ranked by the dissolved lactose mass loading X_d (Eq. 10), which is further used as naming convention in the results and discussion part.

$$X_d = \frac{m_d}{m_{sol}} \tag{1}$$

The first three investigated compositions in Table 2 were done in pure isopropanol with variations in the suspended lactose mass fraction w_s from 10 % to 50 %. Afterwards, the measurement series was continued with the same suspended lactose mass fraction w_s of 10 % and varying dissolved lactose mass fractions w_d, ranging from 0.0072 % to 17 %. These variations are due to different water mass fractions w_{H_2O}, ranging from 0 % to 100%. In addition, the water mass fraction w_{H_2O} determined the drying time t_d in the levitator. This time was varied between 10 and 35 minutes to guarantee complete drying of the microspheres.

Table 2. Compositions of suspensions for drying experiments.

X_d / %	w_d / %	w_s / %	w_{solid} / %	w_{H_2O} / %	$X_{L,s}$ / %	ρ_s / g/cm³	t_d / min
0.072	0.0072	10	10.01	0	0.008	0.819	10

0.019	0.0056	30	30.01	0	0.008	0.913	10
0.008	0.004	50	50.00	0	0.008	1.031	10
4.00	0.42	10	10.42	10	0.47	0.865	10
5.3	0.56	10	10.56	20	0.62	0.898	10
5.5	0.58	10	10.58	22.5	0.64	0.904	10
5.6	0.60	10	10.60	25	0.67	0.910	15
5.8	0.62	10	10.62	27.5	0.69	0.915	15
6.1	0.65	10	10.65	30	0.73	0.920	15
8.7	0.95	10	10.95	40	1.06	0.935	20
14.4	1.68	10	11.68	50	1.90	0.948	25
34.4	5.25	10	15.25	70	6.19	0.980	30
55.1	12.28	10	22.28	90	15.80	1.048	30
63.0	17.00	10	27.00	100	23.29	1.104	35

At the beginning of the drying experiments, droplets with volumes in the order of 2-3 µl were inserted into the acoustic field with a microliter syringe from Terumo (Tokyo, Japan). The inserted droplet volumes were slightly different for different suspensions, since releasing a droplet from the syringe with higher suspension solid loadings was only possible with bigger droplets. Thus, larger droplets were obtained for higher solids loadings. This experimental difficulty was described as well by Yarin et al. [21]. However, a uniform initial droplet volume was achieved for a given constant solids loading.

Achieving a consistent solid loading in the levitator droplets is another experimental concern. Thus, the lactose content in the droplets was verified by weighing to ensure that drying starts always at the same initial conditions. For this purpose, droplets were formed with a microliter syringe, inserted in a sealable plastic pipe from Eppendorf (Hamburg, Germany), and weighed before and after drying with an analytical balance XP205 DR from Mettler Toledo (Giessen, Germany). Suspended lactose mass fraction w_s of 10 %, 30 % and 50 % were examined in pure isopropanol as solvent. After droplet insertion, the sealable plastic pipe was closed immediately before weighing, to avoid evaporation of volatile components. Afterwards, the sealable plastic pipe was opened to enable evaporation of volatile components under controlled conditions in a compartment drier from Binder (Tuttlingen, Germany) at 40°C for 30 minutes. The mass of dried lactose in a single droplet was calculated and compared with the set solid content in the prepared suspension.

Table 3 depicts the results for the measured solid mass fraction in one droplet for lactose isopropanol suspensions.

Table 3. Set suspended lactose mass fraction w_s in comparison with the measured suspended lactose mass fraction w_s in one droplet for pure isopropanol as solvent.

Set w_s / %	Measured w_s / %	RSD / %
10	10.07	2.8
30	31.19	3.2
50	50.67	4.2

Scanning electron micrographs of the microspheres were recorded with the Zeiss Ultra 55 from Carl Zeiss AG (Oberkochen, Germany) with an Everhart-Thornley detector and an acceleration voltage of 5 keV. The microspheres were sputtered with the sputter coater EM ACE600 from Leica (Wetzlar, Germany) with a 15 nm gold-platinum (80 % - 20 %) layer to enable good electrical conductivity.

2.2.5   Hardness measurement setup

The hardness of individual microspheres was measured with the side-crushing-strength (SCS) test in a slightly modified version. This test method is applied to determine the compressive strength of individual particles. In this test, the sample is placed between two platens and compressed by linear movement of one plate [43,51]. An exact procedure for this test method is described in ASTM Standard D4179-01 for crushing of single catalyst pellets[52]. In our work, the agglomeration strength of individual dried microspheres was measured using a rheometer MCR 300 from Anton Paar (Graz, Austria) in the plate-plate configuration with a normal force range from 10 to 5000 mN and a normal force resolution of 5 mN. For this measurement, individual microspheres dried in the acoustic levitator were placed in the center of the bottom plate, and the upper plate was moved downward at the constant velocity of $5 \cdot 10^{-6}$ m·s^{-1} (see Figure 6). The normal forces were recorded while the upper plate was moving.

Investigations of the mechanical strength of granules produced in continuous granulators were also reported in the literature [44-47]. In these experiments, a minimum of 100 granules were analyzed to obtain statistically reliable results. In our experiments, measurements with such a large numbers of microspheres were not possible.

Nevertheless, at least five individual microspheres were crushed for each suspension composition to have statistical information on the results.

(a)   (b)

Figure 6. Microsphere on the rheometer plate (a) before and (b) after hardness test

2.3   Results and discussion

2.3.1   Drying kinetics and morphology of lactose-isopropanol suspensions

The pressure forces from the acoustic field levitating the droplet result in oblate spheroidal droplet shapes [53]. Therefore, the diameter of a sphere cannot be used to track the temporal drying progress in the acoustic field. Thus, drying kinetics were obtained through the surface decrease as described in chapter 2.3.

Individual droplet drying experiments with mixtures of lactose and pure isopropanol with a suspended lactose mass fraction w_s of 10 %, 30 % and 50 % were performed at 25°C without drying air flow. Lactose has a very low solubility in isopropanol. The data from the experiments in Figure 7 reveal that the first drying stage depends on the solids content. Higher solids content in the droplet resulted in smaller changes of the droplet diameter and, consequently, shorter first drying stages. As long as the droplet surface is wetted with isopropanol, the drying occurs at the same rate for each solids content. This constant-rate period is known as the first drying stage. After its end, the drying continues at constant microsphere volume in the second drying stage. The kinetics of the transition from the first to the second drying stage is similar for each solid content, resulting in similar shapes of the curves in Figure 7.
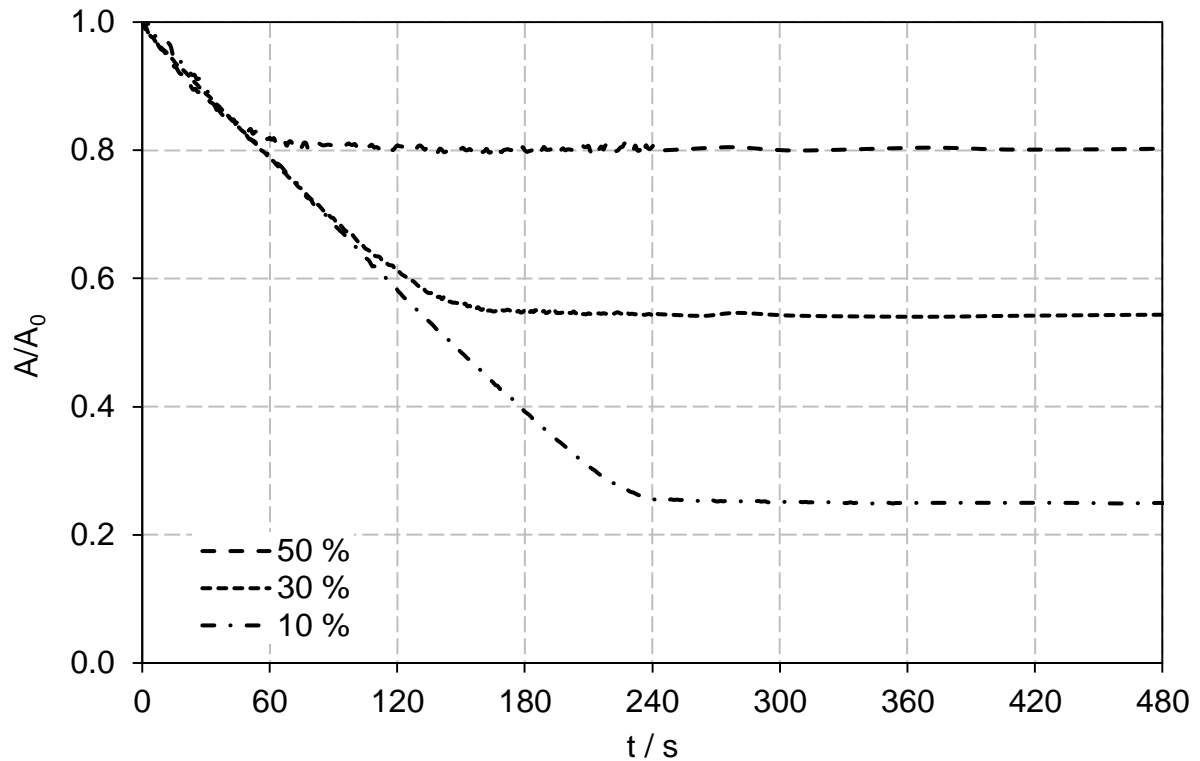
Figure 7. Drying of lactose-isopropanol suspensions with different suspended lactose mass fractions w_s of 10 %, 30 % and 50 % at ambient air temperature of 25°C without drying air flow.

Dried particles from these experiments are shown in Figure 8. As mentioned above, initial droplet size varied with the solids content of the suspension. The larger droplets exhibit more strongly deformed shapes, which can be attributed to a balance of the levitating force from the acoustic field and the droplet weight [54]. An almost spherical droplet (and as result, a spherical microsphere) with an aspect ratio of 1.05 was obtained for a w_s of 10 % lactose (Figure 8a). The aspect ratio increased to 1.2 for a w_s of 30 % lactose (Figure 8b), and the spheroidal droplet with the highest aspect ratio of 1.5 was observed for the highest w_s value of 50 % lactose (Figure 8c), which had the highest suspension density ρ_s.
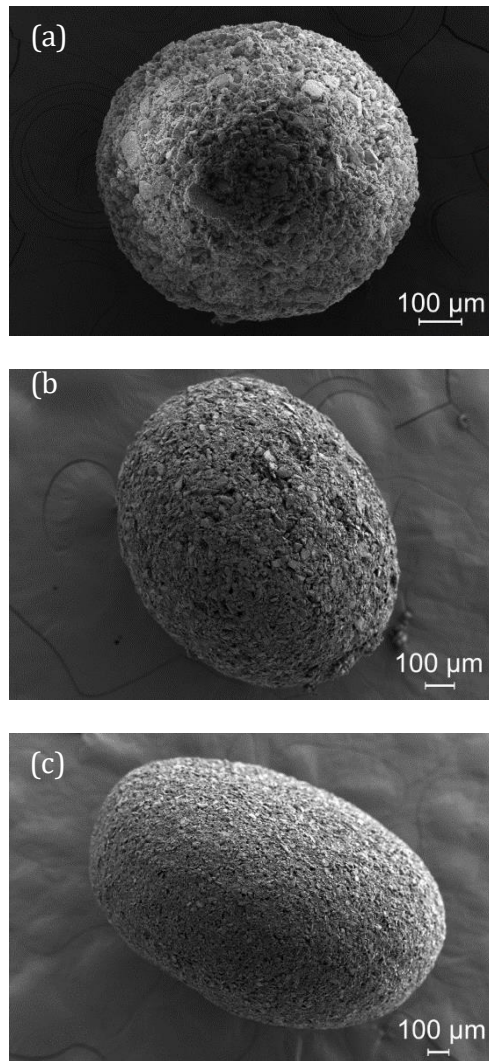
Figure 6. Scanning electron micrographs of microspheres collected from the levitator after drying at 25°C. Drying of lactose-isopropanol mixtures with a suspended solid mass fraction w_s of (a) 10 %, (b) 30 %, (c) 50 %.

The solubility of lactose in isopropanol of 0.008 g/l is very low [49] compared to the solubility in water. The resulting small amount of dissolved solids enables drying of primary particles. Moreover, no significant solid bridges are formed between primary particles upon drying. For all three cases, the morphologies of the dried microspheres (Figure 8) were the same. No bonding of primary particles due to precipitated solid bridges was observed for these compositions. Different microsphere sizes were observed for the different solids contents, as seen in Figure 8**Figure 6**. Clearly, initially more dilute suspensions resulted in smaller microspheres than the more concentrated ones due to lower solid contents.

A drying air flow with the volume flow rate-equivalent velocity of 0.66 m/s in the reflector hole reduced the duration of the first drying period for a suspended lactose mass fraction w_s of 10 % by a factor of 3, as depicted in Figure 9. Additionally, drying with air flow resulted in a shorter transition between the first and second drying stages. In contrast to this, drying without air flow revealed a longer transition with a more rounded curve. The differences in the drying kinetics observed are due to the ventilation of the acoustic streaming vortices near the drying droplet. Thus, the reduced vapor content of the vortices allows for the observed higher drying rate. An additional convective influence from the drying air flow on the droplet is not the reason for this effect [15].
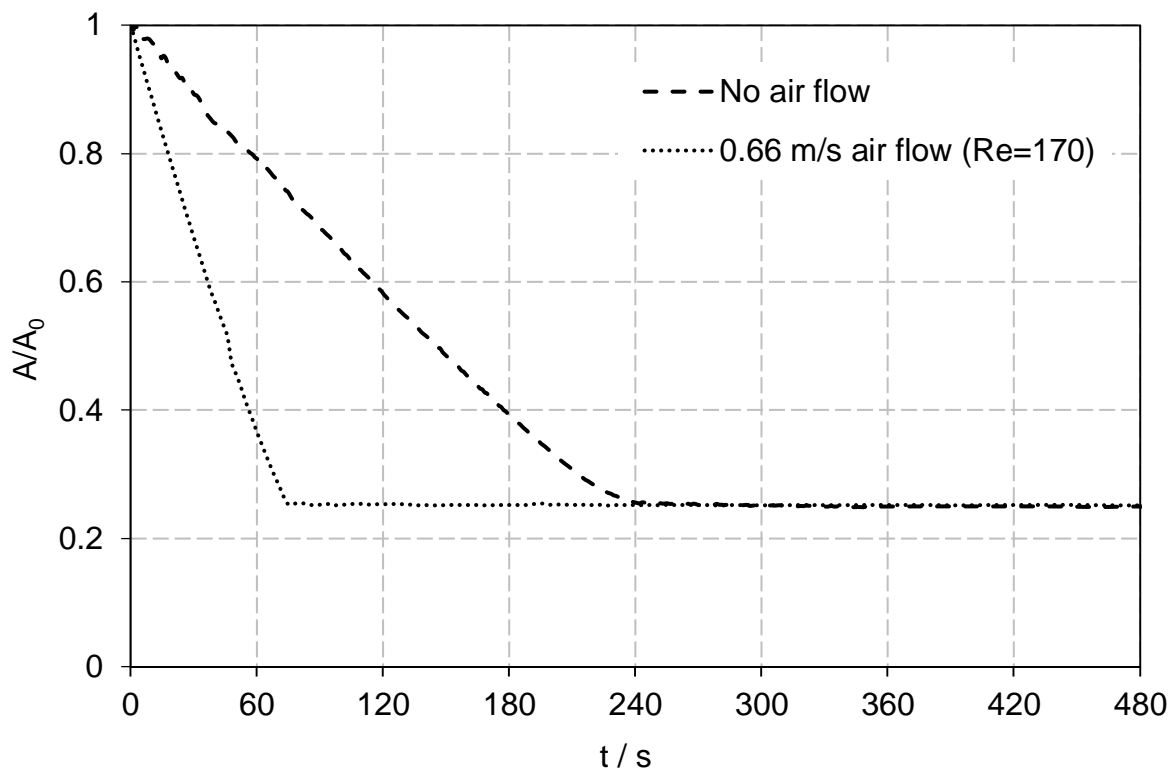
Figure 9. Drying of lactose-isopropanol suspensions with a suspended solid mass fraction w_s of 10 % at ambient air temperature of 25°C without and with 0.66 m/s drying air flow.

### 2.3.2 Drying kinetics and morphology of lactose-isopropanol-water suspensions

In this section, individual droplet drying experiments were performed for the fixed suspended lactose mass fraction w_s of 10 % and different compositions of the carrier liquid of the suspension. The varying liquid compositions (water mass fractions w_{H_2O} from 0 % to 70 %) exhibit different solubility of lactose, and therefore, resulted in different dissolved

lactose mass loadings X_d from 0.072 % to 34.4 %. The saturation concentrations of lactose in pure water and in pure isopropanol are 233 g/l and 0.008 g/l, respectively [48,49]. Liquids with higher water content allow for higher dissolved lactose concentrations, as shown in Figure 4. Furthermore, water reduced the evaporation rate of the suspension carrier liquid, because water is less volatile (pure water vapor pressure at 25°C is 3.169 kPa) [55] than isopropanol (pure isopropanol vapor pressure at 25°C is 5.846 kPa) [56].

Figure 10 depicts the drying of individual droplets with the same suspended lactose mass fraction w_s of 10 % and different compositions of the carrier liquid. The drying air flow with 0.66 m/s (Re = 170) was again applied to control the vapor content of the acoustic streaming vortices.

The drying of an individual droplet consisting of lactose and isopropanol without water revealed the fastest evaporation rate in the first drying stage. Adding water to the droplet liquid reduced the evaporation rate, resulting in a longer first drying stage. Water mass fractions w_{H_2O} up to 20 % showed pure liquid drying kinetics and negligible influences of the slower evaporating water. Water mass fractions w_{H_2O} above 20 % resulted in a change of the drying kinetics due to higher water mass fractions w_{H_2O} in the liquid mixture. These compositions showed different slopes of the drying kinetics, the first one with a steeper slope and the second one with a lower slope. This indicates that the more volatile component (isopropanol) evaporates preferentially first and afterwards the less volatile component (water) [57,58]. These drying kinetics of binary liquid mixtures are due to the different activities of the two liquid components, which furthermore depend on the composition of the liquid phase.

Another effect that reduces the drying rate at higher amounts of dissolved solid is the formation of bridges and shells. As pointed out above, the amount of dissolved solids increased with the water content of the liquid, resulting in a higher total solid loading in the droplet. The dissolved solids precipitated during the drying process and formed bridges between primary particles or a skin on the surface, which reduced the rate of evaporation of the volatile components [3]. At low concentration, the dissolved solids formed a porous structure allowing for fast solvent evaporation. In contrast to this, high amounts of dissolved solids precipitated at the surface and sealed the pores, hindering the evaporation of the liquids.
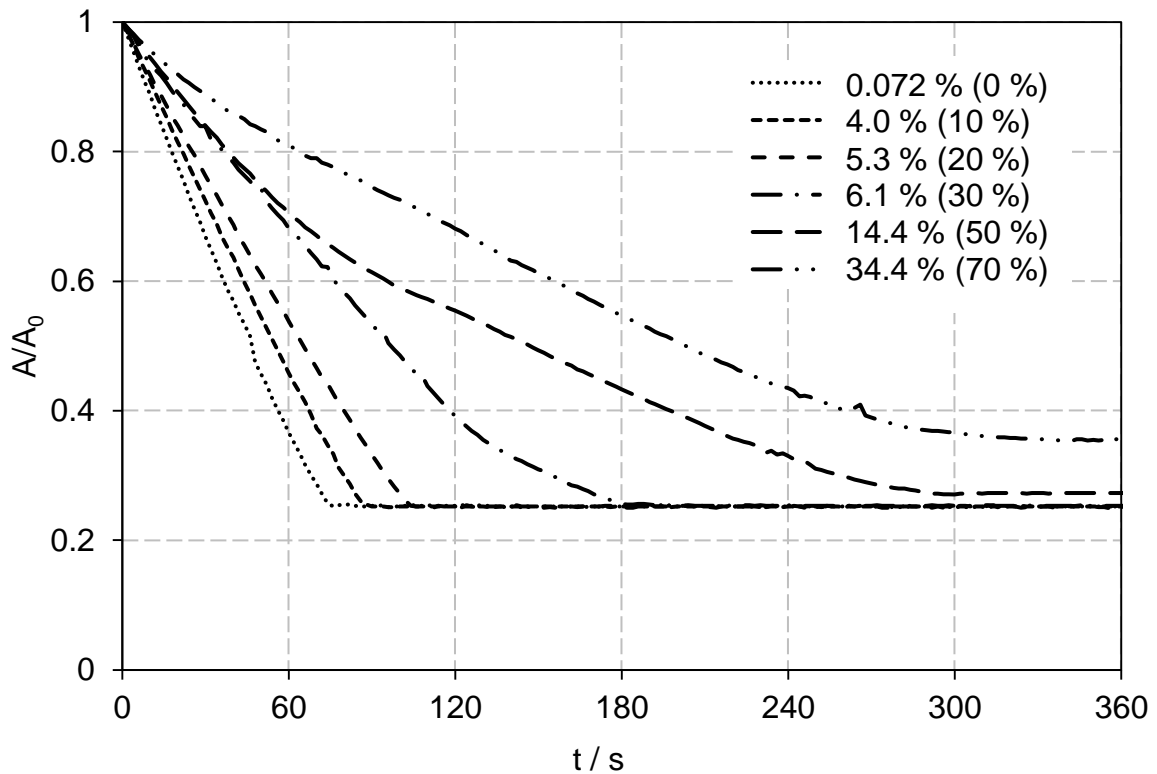
Figure 10. Drying of lactose suspensions with the same suspended lactose mass fraction w_s of 10 % and different dissolved lactose mass loadings X_d between 0.072 % and 34.4 % (water mass fractions w_{H_2O} between 0 % and 70 %).

The electron micrographs in Figure 11 depict the surface and bulk morphologies of microspheres dried in the levitator with the constant suspended lactose mass fraction w_s of 10 % and different dissolved lactose mass loadings X_d between 5.3 % and 34.4 %.

For low levels of X_d no significant effects of the dissolved solid could be observed, and primary particles had no visible connections by precipitated material. For example, the structure for a dissolved lactose mass loading X_d of 5.3 % (Figure 11a) was very similar to the one in Figure 8a for a much lower X_d of 0.072 %. However, raising the water mass fraction w_{H_2O} to 30 % and, therefore, the dissolved lactose mass loading X_d to 6.1 %, resulted in visible connections of the primary particles with precipitated solids on the surface (Figure 11b(i)). The precipitated mass acts as a binder and "glues" the primary particles together, resulting in a more densely packed network structure. The particle packing at the droplet surface becomes more intense as the dissolved lactose mass loading X_d increases to 14.4 % (Figure 11c(i)). An additional increase of X_d can even lead to full covering of the microsphere surface with precipitated solids (Figure 11d(i)). At the dissolved lactose mass loading X_d of 34.4 %, no primary particles were visible any more.

(i)   (ii)

(a)

(b)

(c)

(d)
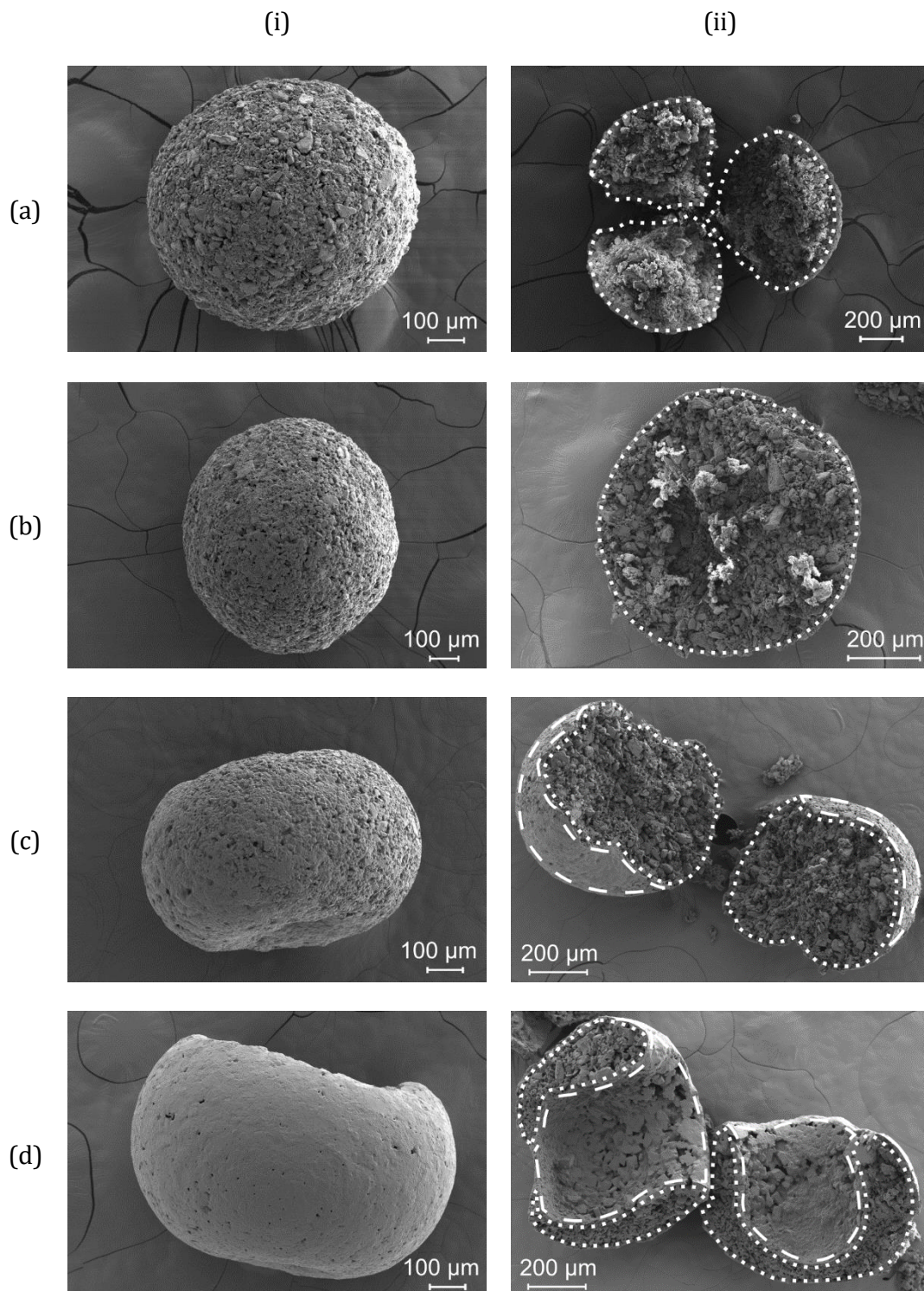
Figure 11. Scanning electron micrographs of microspheres collected from the levitator after drying at 25°C with 0.66 m/s air flow. Drying of lactose isopropanol-water mixtures with the suspended lactose mass fraction w_s of 0.1. Left column (i) shows the surface, and right column (ii) the inside structure (area enclosed by dotted line) and the surface (indicated by dashed line) of the microspheres. The

dissolved lactose mass loadings X_d and the water mass fractions w_{H_2O} in brackets are (a) 5.3 % (20 %), (b) 6.1 % (30 %), (c) 14.4 % (50 %) and (d) 34.4 % (70 %).

In addition to the skin on the microsphere, another effect on the microsphere shape occurred at high dissolved lactose mass loadings X_d: the spherical shape was lost from the dissolved lactose mass loading X_d of 14.4 % on, resulting in an ellipsoidal microsphere shape (Figure 11c(i)). The reasons for this change of shape are maybe twofold: First, high dissolved lactose mass loadings X_d resulted in high droplet densities and higher mass of the drying droplet. The weight of the droplet was too high to maintain a spherical shape by the levitation force. Second, higher dissolved lactose mass loadings X_d resulted in more precipitated mass, resulting in an unevenly distributed precipitated mass around the droplet. This can even lead to the collapse of the microsphere due to high concentration gradients, resulting in the formation of hollow microspheres (Figure 11d(i)). This highly concentrated surface leads to an increased viscosity with subsequent crust formation. Remaining solvents can evaporate through pores in the formed crust. Afterwards, the hollow microsphere may collapse, depending on the mechanical properties of the crust [59].

It is known for spray drying of suspensions that during the drying process diffusion of the liquid phase from the core to the surface can lead to voids in the particle. Similar effects have been attributed to the liquid drawn to the surface by capillary forces. Thus a pressure difference across the droplet surface is formed, resulting in a collapse of the formed microsphere [60,61].

Further information on the inside structure of the microsphere was obtained by electron micrographs of crushed microspheres. At low dissolved lactose mass loading X_d of 5.3 %, as in Figure 11a(ii), no crust was formed on the surface and no solids precipitated inside the particle, resulting in a loosely packed microsphere. Variations in the composition of the suspension to a higher dissolved lactose mass loading X_d of 6.1 % altered the microsphere surface towards a more densely packed structure, since more primary particles were connected by precipitated material (Figure 11b(ii)). Most of the dissolved solids precipitated on the surface. Therefore, a minor proportion precipitated inside the microsphere. Further increase of the dissolved lactose mass loading X_d resulted in the formation of a thicker crust and additional precipitation of material inside the microsphere. This can be clearly seen in Figure 11c(ii) (X_d = 14.4 %) and Figure 11d(ii) (X_d = 34.4 %), where larger agglomerates are visible throughout the cross section.

Figure 12 shows the particulate structure of the dried microspheres at higher magnification of the surface and the inside, showing clearly the relation between increased dissolved solids and a more coherent and less porous crust.

Comparing the results from microscopy and drying kinetics revealed deviations of drying curves for different compositions of the suspension. Similar progression of the drying curves (almost linear) were obtained up to a dissolved lactose mass loading X_d of 5.3 %, as depicted in Figure 10. A more curved progression was observed for a dissolved lactose mass loading X_d of 6.1 % and above, as previously described. Increasing the dissolved lactose mass loading X_d to 14.4 % or beyond causes a stronger deviation of the drying curve, as the microsphere shape changed from a solid sphere to a hollow ellipsoid.
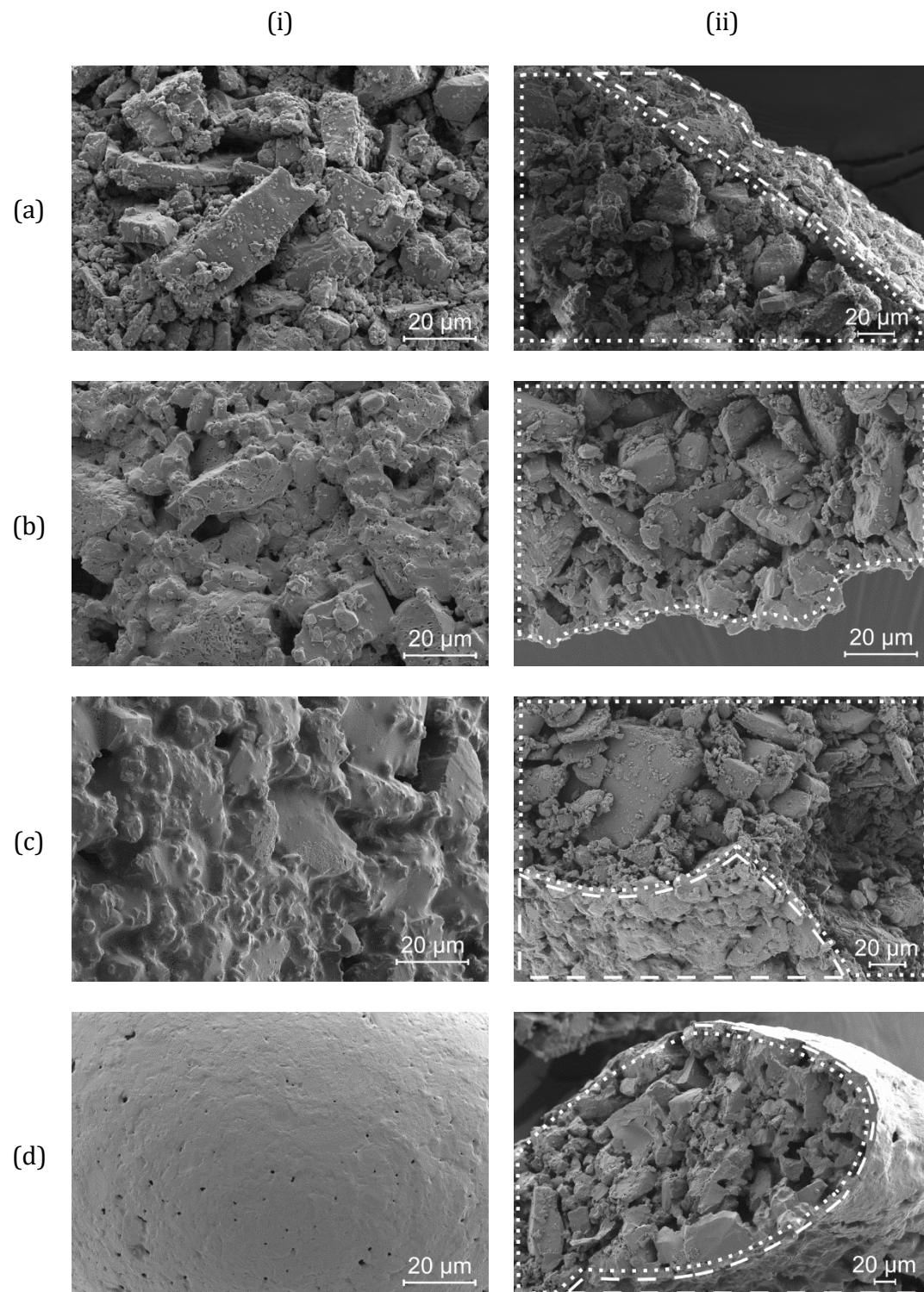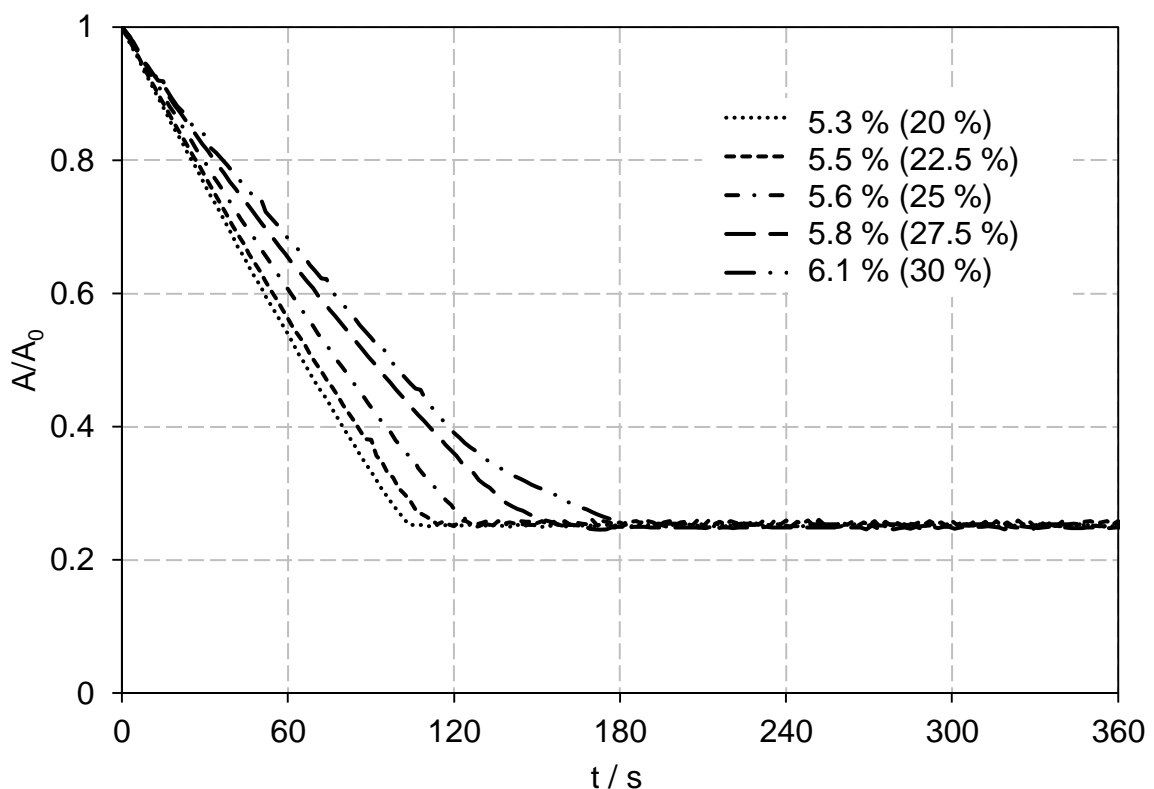
Figure 12. Scanning electron micrographs of microspheres collected from the levitator after drying at 25°C with 0.66 m/s air flow. Drying of lactose isopropanol-water mixtures with the suspended lactose mass fraction w_s of 10 %. Left column (i) shows the surface, and right column (ii) the inside structure (area enclosed by dotted line) and the surface (indicated by dashed line) of the microspheres at higher magnification. The dissolved lactose mass loadings X_d and the water mass

fractions w_{H_2O} in brackets are (a) 5.3 % (20 %), (b) 6.1 % (30 %), (c) 14.4 % (50 %) and (d) 34.4 % (70 %).

The formation of the first connecting solid bridges between primary particles was studied in more detail. This analysis was carried out by raising the water mass fraction w_{H_2O} in steps of 2.5 % from 20 % to 30 %. Figure 13 reveals clearly that increased water mass fractions w_{H_2O}, and therefore higher dissolved lactose mass loadings X_d, lead to longer drying times. Although longer drying times were observed for higher dissolved lactose mass loadings X_d, no visual differences were observed as depicted in the electron micrographs of Figure 14. The microsphere surface, as well as the crushed microsphere, showed no clear connections between primary particles. Nevertheless, the hardness measurements in chapter 3.4 show measurable differences in the dissolved lactose mass loadings X_d of the microspheres.

Figure 13. Drying of lactose suspensions with the suspended lactose mass fraction w_s of 10 %, but different dissolved lactose mass loadings X_d between 5.3 %and 6.1 %. Water mass fractions w_{H_2O} between 20 % and 30 % shown in brackets.
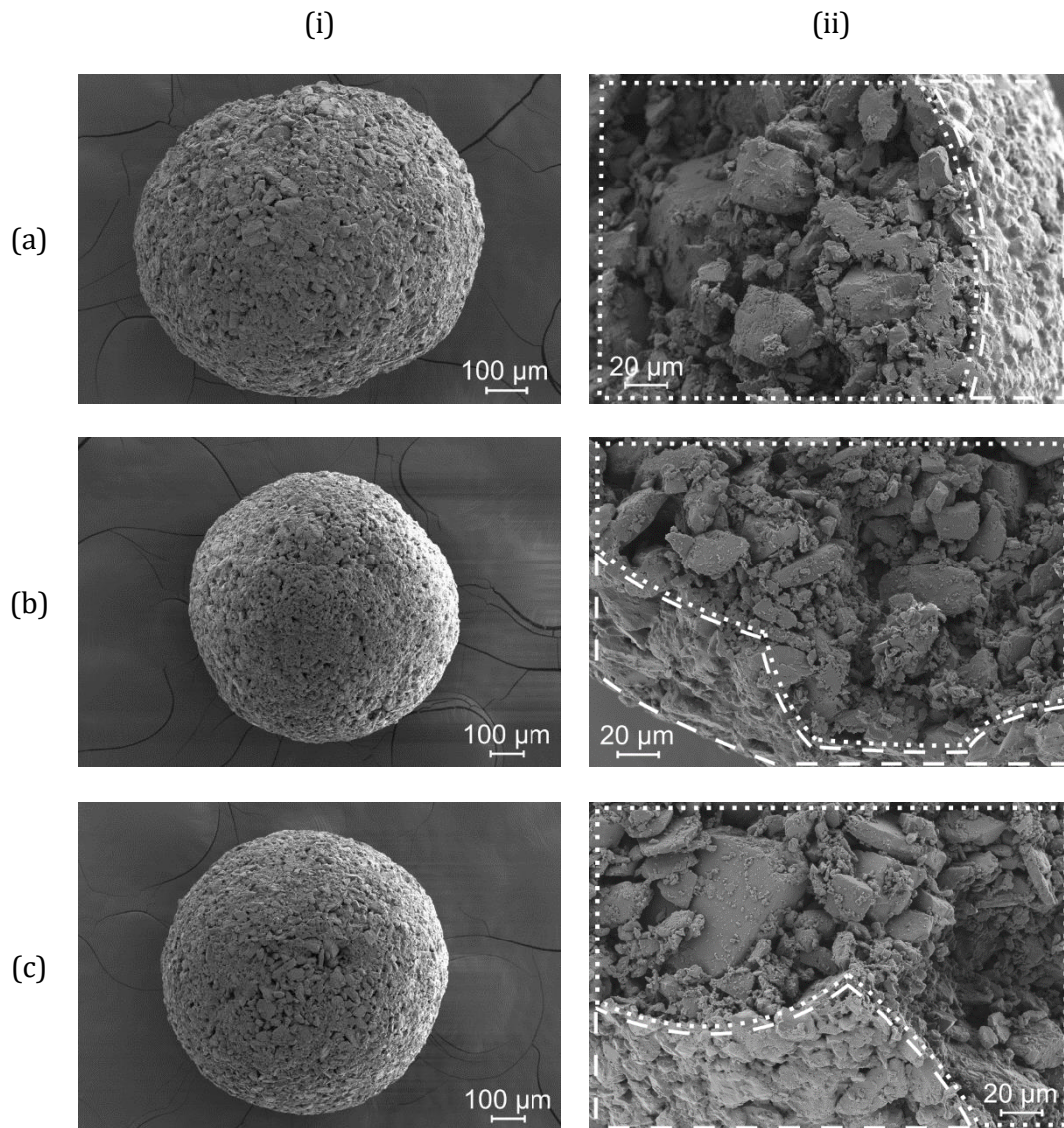
Figure 14. Scanning electron micrographs of microspheres collected from the levitator after drying at 25°C with 0.66 m/s air flow. Drying of lactose isopropanol-water mixtures with the suspended lactose mass fraction w_s of 10 %. Left column (i) shows the surface, and right column (ii) shows the inside structure (area enclosed by dotted line) and the surface (indicated by dashed line) of the microspheres. The dissolved lactose mass loadings X_d and the water mass fractions w_{H_2O} in brackets are (a) 5.5 % (22.5 %), (b) 5.6 % (25 %) and (c) 5.8 % (27.5 %).

2.3.3 Relevance of suspension drying kinetics for industrial spray drying process design

In addition to the analysis of the first drying stage, the second drying stage was investigated by evaluation of the vertical position of a droplet in the acoustic field. The drying droplet

moves upward in the acoustic field as it loses mass due to the drying. This additional data z - z$_0$, with the initial droplet position z_0, enabled a complete analysis of both the first and the second stages of the drying process. Figure 15 depicts the droplet drying kinetics for a suspended lactose mass fraction w_s of 10 % and the dissolved lactose mass loading X_d varying from 0.072 % to 34.4 % due to different liquid compositions.
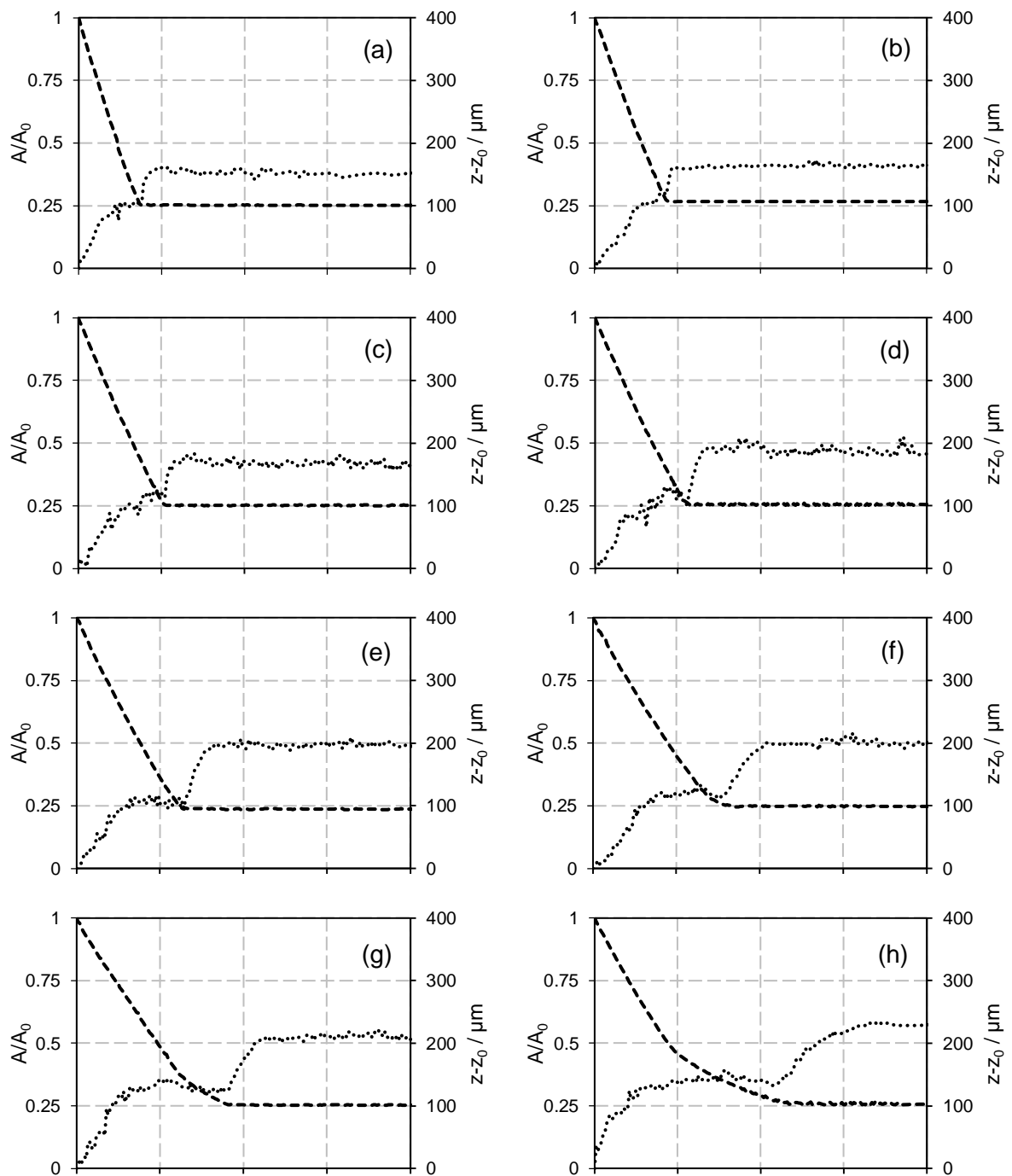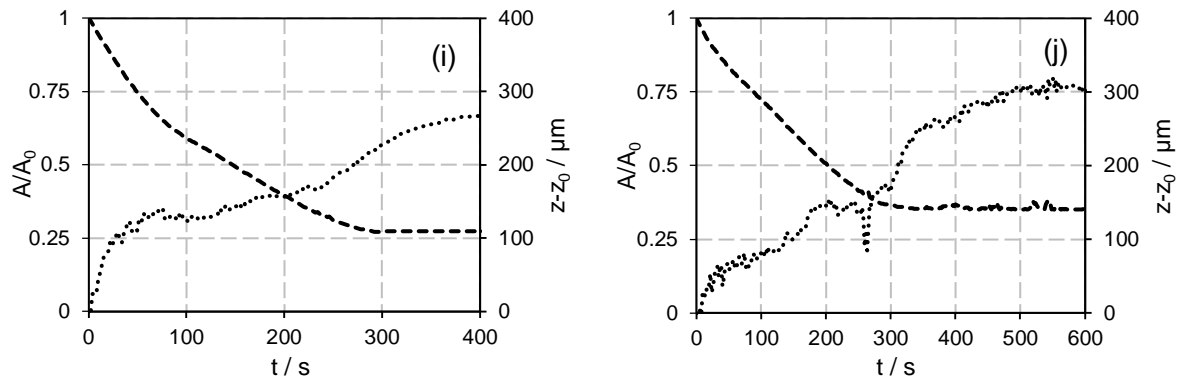
Figure 15. Drying of individual lactose suspension droplets with the suspended lactose mass fraction w_s of 10 % and ten different dissolved lactose mass loadings X_d between 0.072 %and 34.4 % (water mass fractions w_{H_2O} between 0 % and 70 %). The dashed lines depict the evolution of the normalized droplet surface, the dotted lines the vertical droplet position in the acoustic field. The dissolved lactose mass loadings X_d and the water mass fractions w_{H_2O} in brackets are (a) 0.072 % (0 %), (b) 4.0 % (10 %), (c) 5.3 % (20 %), (d) 5.5 % (22.5 %), (e) 5.6 % (25 %), (f) 5.8 % (27.5 %), (g) 6.1 % (30 %), (h) 8.7 % (40 %), (i) 14.4 % (50 %) and (j) 34.4 % (70 %).

Drying lactose suspension droplets with pure isopropanol as the solvent (Figure 15a) show a sharp transition between the first and second drying periods since the solvent is a pure substance with a high volatility. The droplet moves upward during the whole drying process, and it continues to do so after the end of the first drying period, where the droplet shape and surface remain constant with time, but the droplet still loses mass due to solvent transport through the solid microsphere surface. The second drying stage ends seven seconds after the end of the first drying stage. The vertical position of the droplet remains constant after that. An increase of the solvent composition to the water mass fraction w_{H_2O} of 10 % reveals a similar drying profile, as shown in Figure 15b. The influence of the water content on the drying kinetics becomes more apparent at higher amounts, leading to a longer duration of the first and second drying periods and a stronger change of the vertical position. The latter was a result of the larger mass loss of the droplets due to the water evaporation with higher water mass fractions w_{H_2O}.

The shapes of the normalized droplet surface profiles show a significant change in shape as the water content (and thus, the dissolved solid mass) is increased. For water mass fractions w_{H_2O} of 30 % and above, a significant change of slope of the droplet surface profiles occurs, the drying kinetics start to become impacted by significant crust formation,

leading even to the formation of hollow spheres for even higher water mass fractions w_{H_2O}. Interestingly, the onset of the secondary drying stage, signified by another increase of the droplet position after a steady phase, is delayed for higher water mass fractions w_{H_2O}, likely due to the formation of a significant crust. Apparently, after crust formation, solvent is captured inside the droplet and has to form channels for transport to the outer surface.

Table 4 depicts the durations of the first (normalized droplet area reaches steady state) and second drying periods (height curve reaches steady state) and the changes of vertical droplet position relative to the initial state during drying. These relations between suspension composition and drying time are important for the spray drying process. Suspensions with higher dissolved solids contents or lower rate of solvent evaporation require longer drying times and the primary drying stage (after which shape does not change anymore) is longer as well [62]. Thus, the time to obtain mechanically stable microspheres (which still are wet) is increased: Change of the suspension composition from a dissolved lactose mass loading X_d of 0.072 % (water mass fraction w_{H_2O} of 0 %) to 8.7 % (0.4 40 %) resulted in a three times longer first and a 16 times longer second drying stage. Thus, also the relative duration of the second drying stage increased compared to the primary one.

Further increase of the dissolved lactose mass loading X_d to 14.4 % and 34.4 % resulted in the formation of solid or hollow ellipsoidal microspheres (Figure 11c and 11d), possibly due to stronger concentrations gradients of precipitated solids in the crust. Thus, a collapse of the microsphere was observed (hollow ellipsoidal shape) and the temporal tracking of the surface via backlight images took these indentations (Figure 11c) or hollow voids (Figure 11d) not into account (backlight images may show larger surfaces as in reality). Therefore, the drying kinetics for dissolved lactose mass loadings X_d of 14.4 % (Figure 15i) and 34.4 % (Figure 15j) differed: First, the onset of the secondary drying stage was delayed for an X_d of 14.4 %, whereas the delay was diminished for an X_d of 34.4 %. Secondly, the surface ratio of A/A_0 was increased from 0.27 for an X_d of 14.4 % to 0.35 for an X_d of 34.4 %. The reason for this could be the increased crust of the microspheres and the change from a full microsphere structure to a hollow microsphere with voids. Nevertheless, the results emphasize the trend of prolonged drying times for higher dissolved lactose mass loadings X_d as well as higher water mass fractions w_{H_2O}.

Clearly, drying of such suspensions in a spray dryer will be faster under elevated temperatures and higher drying gas flow rates. Nevertheless, similar effects as the ones

observed in our study will be prevalent, and the suspension composition is apparently an important parameter in the design of a spray drying process.

Table 4. Duration of first and second drying stages and rise $z\text{-}z_0$ of the droplet in the acoustic field in the first and second drying stages for the initial suspended lactose mass fraction w_s of 10 % and dissolved lactose mass loadings X_d varying between 0.072 % and 34.4 %.

X_d / %	w_{H_2O} / %	Duration of first drying period / s	Duration of second drying period / s	$z\text{-}z_0$ first drying period / μm	$z\text{-}z_0$ second drying period / μm
0.072	0	76	7	108	41
4.0	10	86	8	113	46
5.3	20	102	24	116	59
5.5	22.5	115	26	117	66
5.6	25	129	36	118	74
5.8	27.5	152	44	120	80
6.1	30	178	50	123	86
8.7	40	220	112	135	95
14.4	50	292	104	167	99
34.4	70	322	218	163	140

2.3.4 Mechanical strength of the microspheres

We present a new approach for quantifying the mechanical strength of individual microspheres produced by drying in the acoustic levitator. The method of measuring the mechanical strength was introduced in chapter2.5. Figure 16 depicts characteristic profiles of the normal force on individual particles, produced and measured by the rheometric device. The independent variable is the displacement of the upper plate of the rheometer. The starting position of the upper plate is at the distance of 750 μm from the bottom plate, and the measurement is stopped at the distance of 500 μm to avoid damages to the equipment. The first change in the normal force is observed as the upper plate takes up contact with the microsphere. This contact point indicates a typical dimension of the microsphere of 685 μm. Thereafter, the normal force increases rapidly until a maximum force is reached, which indicates the force needed for breaking the microsphere and, therefore, the mechanical strength of the object against normal stress. As the microsphere

breaks, the recorded force decreases immediately. Further linear motion of the upper plate leads to normal forces due to the compression of the fragmented microsphere.

Figure 16 depicts this force for different initial compositions of the suspension. The small dissolved lactose mass loading X_d of 5.5 % results in a low breaking force of 101 mN. Increased water content, and therefore, higher dissolved lactose mass loading X_d of 5.8 %, results in a higher breaking force of 176 mN. This behavior continues with a further increase of the dissolved lactose mass loading X_d to 8.7 %, resulting in an even higher breaking force of 466 mN. Different normal forces are observed for the fragments as well, after breaking of the microsphere, indicating the strength of connections between primary particles. These fragments are weakly connected for a low dissolved lactose mass loading X_d of 5.5 %, resulting in low normal crushing forces close to zero. In contrast, higher normal forces are obtained for the fragments for higher dissolved lactose mass loadings X_d.
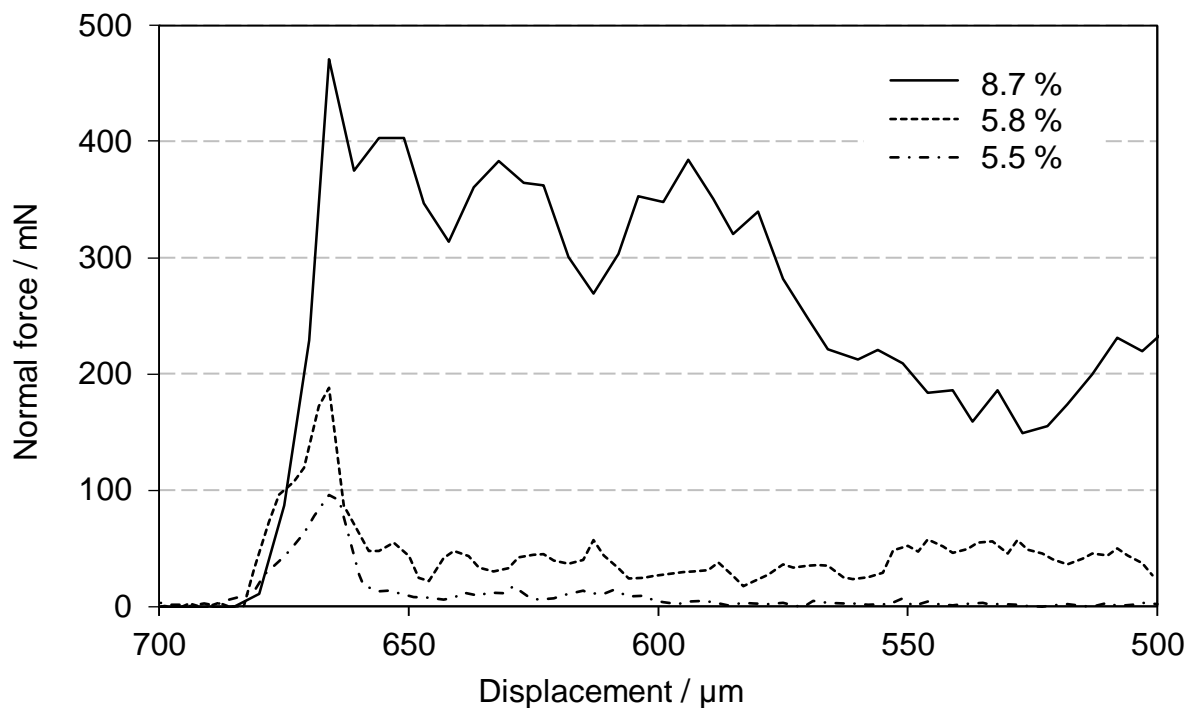
Figure 16. Normal force on individual microspheres dried in the acoustic levitator as a function of plate distance. The normal force is applied and recorded by a rheometer. The suspended lactose mass fraction w_s was 10 %. The dissolved lactose mass loading X_d varied between 5.5 % and 8.7 %.

Tests of the microsphere mechanical strength for the measurement series in Table 2 reveal a strong dependence of the breaking force on the amount of dissolved solids. Due to limitations of the force measurement accuracy, the breaking force could not be recorded for dissolved lactose mass loadings X_d below 4 %.

The first measurable breaking force was obtained for the dissolved lactose mass loading X_d of 5.3 %, as depicted in Figure 17a. Small changes in the dissolved lactose mass loadings X_d from 5.5 % to 6.1 % resulted in an increase of the breaking force. This increase can be explained by inspection of the micrographs in Figure 11b and Figure 14. More dissolved solids connected the primary particles, resulting in stronger bonds and a significant increase of the breaking force within this transition zone. Increasing dissolved lactose mass loading X_d up to 6.1 % resulted in the formation of stronger agglomerates between primary particles, revealing a stronger increase of the breaking force.
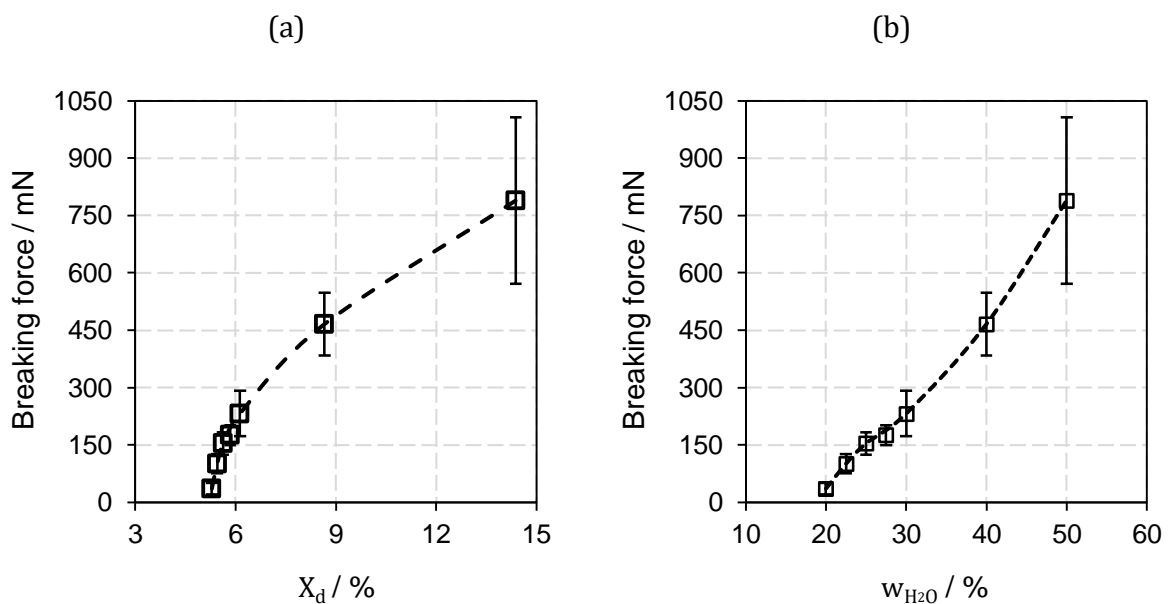
At the dissolved lactose mass loading X_d of 14.4 %, the measurement method reaches its limitations due to changes of the particle morphology. As depicted in Figure 11c, the spherical shape is lost and ellipsoidal microspheres are formed. The stress distribution in an ellipsoidal microsphere under normal force is different from a spherical body. This deviation of the shape may be responsible for the higher standard deviation. However, it is clear that stronger microspheres with higher breaking forces are formed at higher dissolved lactose mass loadings X_d. Above a dissolved lactose mass loading X_d of 14.4 %, hollow ellipsoidal microspheres are formed, resulting in largely different breaking forces.

The change of the breaking force with variation of the suspension composition is illustrated in Figure 17a. The transition zone of the dissolved lactose mass loading X_d between 5.5 % and 6.1 % revealed a non-linear dependency of the breaking force on the dissolved lactose mass content. This effect may be explained by the gradual filling of the voids between primary particles with precipitated solids, resulting in a more densely packed structure, and therefore, higher mechanical strength against normal force. A further increase of dissolved solids content formed a denser packed crust around the microsphere with the effect of a linear relation between higher dissolved lactose mass loadings X_d and maximum breaking forces. The same relation is observed by depicting the breaking force as a function of the water mass fraction w_{H_2O} in the suspension, as in Figure 17b

Based on these data, by extrapolation the point was calculated where no force is needed to break the microsphere. This point reflects a suspension composition with a dissolved lactose mass loading X_d of 5.2 % or, equivalently, a water mass fraction w_{H_2O} of

19 %. This corresponds to our observation that quite loose microspheres are formed below these values. Microspheres from drying of suspensions with dissolved lactose mass loadings X_d between 0.072 % and 4.0 % broke during collection from the acoustic levitator.

These results demonstrate the strong influence of the suspension composition on the mechanical strength of spray-dried particles. There exists a threshold value of the dissolved lactose loading X_d below which loose microspheres are formed. Primary particles are then loosely bonded by precipitated solids, so that the microspheres easily break up, even by weak forces.

(a) (b)

Figure 17. The breaking force as a function of (a) the dissolved lactose mass loading X_d and (b) the water mass fraction w_{H_2O}.

2.4   Conclusions

The present work investigates the influence of initial suspension droplet composition on the drying kinetics via acoustic levitation and the resulting microsphere properties in relation to spray drying. Single droplet drying experiments of a model substance consisting of lactose particles suspended in saturated isopropanol-water lactose solutions were studied at different lactose solubilities. It is found that the dissolved lactose mass loading X_d, which depends on the initial solvent composition, determines the drying kinetics and has a strong influence on the dried microsphere morphology and mechanical strength. The individual microsphere structure changes from loosely packed primary particles with

isopropanol as the solvent to denser packing with increasing water mass fraction w_{H_2O}. The dissolved solids precipitate during drying and bond the primary particles. Most of the precipitation occurs at the droplet surface and forms a crust.

The hardness of individual microspheres was measured by a compression strength test. These measurements enabled the mechanical strength of individual microspheres against normal forces to be quantified. Loosely agglomerated microspheres were formed below the threshold X_d = 5.2 % for the investigated model substance. Based on these findings, drying should be carried out below this threshold to enable drying either of primary particles (i.e. tailored particle properties after crystallization remain unaltered during drying), or above this threshold to produce larger, agglomerated particles (i.e. improved powder flowability as favored in direct compression). In conclusion, transferring the results from small scale droplet studies to spray drying emphasizes the importance of fine atomization (small droplets with small amounts of suspended and dissolved solids) of the suspension to produce powders of primary particles mainly. Based on the experimental data presented here, modelling of the dry microsphere formation is underway.

Acknowledgements

References

[1] K. Masters, Spray drying in practice. Charlottenlund, 2002.

[2] J. Dlouhy and W. H. Gauvin, "Heat and mass transfer in spray drying," McGill University, 1957.

[3] A. Mujumdar, Handbook of Industrial Drying, Fourth Edition, vol. 4. CRC Press, 2015.

[4] R. Vehring, "Pharmaceutical particle engineering via spray drying," Pharm. Res., vol. 25, no. 5, pp. 999–1022, 2008.

[5] P. C. Nordine and R. M. Atkins, "Aerodynamic levitation of laser-heated solids in gas jets," Rev. Sci. Instrum., vol. 53, no. 9, pp. 1456–1464, 1982.

[6] G. D. Kinzer and R. Gunn, "The Evaporation, Temperature and Thermal Relaxation-Time of Freely Falling Waterdrops," J. Meteorol., vol. 8, no. 2, pp. 71–83, 1951.

[7] W. E. Ranz and W. R. Marshall, "Evaporation from drops - Part I," Chem Eng Pro, vol. 48, no. 3, pp. 141–146, 1952.

[8] D. H. Charlesworth and W. R. Marshall, "Evaporation from drops containing dissolved solids," AIChE J., vol. 6, no. 1, pp. 9–23, 1960.

[9] N. Tsapis et al., "Onset of Buckling in Drying Droplets of Colloidal Suspensions," Phys. Rev. Lett., vol. 94, no. 1, p. 18302, 2005.

[10] E. James Davis, P. Ravindran, and A. K. Ray, "Single aerosol particle studies," Adv. Colloid Interface Sci., vol. 15, no. 1, pp. 1–24, 1981.

[11] E. J. Davis and G. Schweiger, The Airborne Microparticle. Berlin, Heidelberg: Springer Berlin Heidelberg, 2002.

[12] G. Brenn, L. J. Deviprasath, F. Durst, and C. Fink, "Evaporation of acoustically levitated multicomponent liquid droplets," Int. J. Heat Mass Transf., vol. 50, no. 25–26, pp. 5073–5086, 2007.

[13] H. Schiffter and G. Lee, "Single-Droplet Evaporation Kinetics and Particle Formation in an Acoustic Levitator. Part 2: Drying Kinetics and Particle Formation From Microdroplets of Aqueous Mannitol, Trehalose, or Catalase," J. Pharm. Sci., vol. 96, no. 9, pp. 2284–2295, 2007.

[14] O. Kastner, G. Brenn, D. Rensink, and C. Tropea, "The acoustic tube levitator - A novel device for determining the drying kinetics of single droplets," Chem. Eng. Technol., vol. 24, no. 4, pp. 335–339, 2001.

[15] H. A. Schiffter, "Single droplet drying of proteins and protein formulations via acoustic levitation," Friedrich-Alexander University Erlangen-Nürnberg, 2006.

[16] F. Priego-Capote and L. de Castro, "Ultrasound-assisted levitation: Lab-on-a-drop," TrAC Trends Anal. Chem., vol. 25, no. 9, pp. 856–867, 2006.

[17] E. G. Lierke, "Akustische Positionierung - Ein umfassender Überblick über Grundlagen und Anwendungen," Acustica, vol. 82, pp. 220–237, 1996.

[18] A. Anilkumar, C. Lee, and T. Wang, "Stability of an acoustically levitated and flattened drop: An experimental study," Phys. Fluids A Fluid Dyn., vol. 5, no. 11, pp. 2763–2775, 1993.

[19] S. Santesson and S. Nilsson, "Airborne chemistry: Acoustic levitation in chemical analysis," Anal. Bioanal. Chem., vol. 378, no. 7, pp. 1704–1709, 2004.

[20] A. L. Yarin, G. Brenn, O. Kastner, D. Rensink, and C. Tropea, "Evaporation of acoustically levitated droplets," J. Fluid Mech., vol. 399, pp. 151–204, 1999.

[21] A. L. Yarin, G. Brenn, O. Kastner, and C. Tropea, "Drying of acoustically levitated droplets of liquid-solid suspensions: Evaporation and crust formation," Phys. Fluids, vol. 14, no. 7, pp. 2289–2298, 2002.

[22] A. L. Yarin, G. Brenn, and D. Rensink, "Evaporation of acoustically levitated droplets of binary liquid mixtures," Int. J. Heat Fluid Flow, vol. 23, no. 4, pp. 471–486, 2002.

[23] D. H. Charlesworth and W. R. Marshall, "Evaporation from drops containing dissolved solids," AIChE J., vol. 6, no. 1, pp. 9–23, 1960.

[24] G. Brenn, "Concentration fields in evaporating droplets," Int. J. Heat Mass Transf., vol. 48, no. 2, pp. 395–402, 2005.

[25] N. Kawahara, A. L. Yarin, G. Brenn, O. Kastner, and F. Durst, "Effect of acoustic streaming on the mass transfer from a sublimating sphere," Phys. Fluids, vol. 12, no. 4, p. 912, 2000.

[26] S. Mascia et al., "End-to-end continuous manufacturing of pharmaceuticals: Integrated synthesis, purification, and final dosage formation," Angew. Chemie - Int. Ed., vol. 52, no. 47, pp. 12359–12363, 2013.

[27] S. Lawton, G. Steele, P. Shering, L. Zhao, I. Laird, and X. W. Ni, "Continuous crystallization of pharmaceuticals using a continuous oscillatory baffled crystallizer," Org. Process Res. Dev., vol. 13, no. 6, pp. 1357–1363, 2009.

[28] J. Gursch et al., "Continuous Processing of Active Pharmaceutical Ingredients Suspensions via Dynamic Cross-Flow Filtration," J. Pharm. Sci., vol. 104, no. 10, pp. 3481–3489, 2015.

[29] J. Gursch et al., "Dynamic cross-flow filtration: enhanced continuous small-scale solid-liquid separation," Drug Dev. Ind. Pharm., vol. 42, no. 6, pp. 977–984, 2016.

[30] J. Gursch et al., "Continuous Drying of Small Particles for Pharmaceutical Applications – An Evaluation of Selected Lab-Scale Systems," Org. Process Res. Dev., vol. 19, no. 12, pp. 2055–2066, 2015.

[31] M. Kreimer, I. Aigner, G. Koscher, D. Lepek, and J. G. Khinast, "Continuous Drying of Powders and Slurries in an Extruder without Changing Product Particle Size Distribution," in AIChE Annual Meeting, 2016.

[32] J. W. Carson and B. H. Pittenger, "Bulk Properties of Powders," ASM Handb. Vol. 7, Powder Met. Technol. Appl., vol. 7, pp. 148–159, 1998.

[33] R. C. Rowe and R. J. Roberts, "The Mechanical Properties of Powders," Adv. Pharm. Sci., vol. 7, pp. 1–62, 1995.

[34] C. Oliver and M. Pharr, "An improved technique for determining hardness and elastic modulus using load and displacement sensing indentation experiments," Journal of Materials Research, vol. 7, no. 11. pp. 1564–1583, 1992.

[35] L. J. Taylor et al., "Predictive milling of pharmaceutical materials using nanoindentation of single crystals," Org. Process Res. Dev., vol. 8, no. 4, pp. 674–679, 2004.

[36] L. Taylor, D. Papadopoulos, P. Dunn, A. Bentham, J. Mitchell, and M. Snowden, "Mechanical characterisation of powders using nanoindentation," Powder Technol., vol. 143–144, pp. 179–185, 2004.

[37] M. Perkins et al., "Elastic modulus measurements from individual lactose particles using atomic force microscopy," Int. J. Pharm., vol. 332, no. 1–2, pp. 168–175, 2007.

[38] X. Liao and T. S. Wiedmann, "Measurement of process-dependent material properties of pharmaceutical solids by nanoindentation," J. Pharm. Sci., vol. 94, no. 1, pp. 79–92, 2005.

[39] K. J. Ramos and D. F. Bahr, "Mechanical behavior assessment of sucrose using nanoindentation," J. Mater. Res., vol. 22, no. 7, pp. 2037–2045, 2007.

[40] X. Liao and T. S. Wiedmann, "Characterization of pharmaceutical solids by scanning probe microscopy," J. Pharm. Sci., vol. 93, no. 9, pp. 2250–2258, 2004.

[41] V. M. Masterson and X. Cao, "Evaluating particle hardness of pharmaceutical solids using AFM nanoindentation," Int. J. Pharm., vol. 362, no. 1–2, pp. 163–171, 2008.

[42] I. C. van den Born, A. Santen, H. D. Hoekstra, and J. T. M. De Hosson, "Mechanical strength of highly porous ceramics.," Phys. Rev. B. Condens. Matter, vol. 43, no. 4, pp. 3794–3796, 1991.

[43] C. Couroyer, "Methodology for Investigating the Mechanical Strength of Reforming Catalyst Beads," Oil Gas Sci. Technol. Rev. Linstitut Fr. Dupetrole, vol. 55, no. 1, p. 67, 2000.

[44] N. Rahmanian, M. Ghadiri, and Y. Ding, "Effect of scale of operation on granule strength in high shear granulators," Chem. Eng. Sci., vol. 63, no. 4, pp. 915–923, 2008.

[45] N. Rahmanian, M. Ghadiri, X. Jia, and F. Stepanek, "Characterisation of granule structure and strength made in a high shear granulator," Powder Technol., vol. 192, no. 2, pp. 184–194, 2009.

[46] N. Rahmanian, A. Naji, and M. Ghadiri, "Effects of process parameters on granules properties produced in a high shear granulator," Chem. Eng. Res. Des., vol. 89, no. 5, pp. 512–518, 2011.

[47] N. Rahmanian and M. Ghadiri, "Strength and structure of granules produced in continuous granulators," Powder Technol., vol. 233, pp. 227–233, 2013.

[48] J. J. . Machado, J. A. Coutinho, and E. A. Macedo, "Solid–liquid equilibrium of α-lactose in ethanol/water," Fluid Phase Equilib., vol. 173, no. 1, pp. 121–134, 2000.

[49] F. Montañés, A. Olano, E. Ibáñez, and T. Fornari, "Modeling solubilities of sugars in alcohols based on original experimental data," AIChE J., vol. 53, no. 9, pp. 2411–2418, 2007.

[50] G. Brenn, Analytical Solutions for Transport Processes. Berlin, Heidelberg: Springer Berlin Heidelberg, 2017.

[51] H. J. Ryu and F. Saito, "Single particle crushing of nonmetallic inorganic brittle materials," Solid State Ionics, vol. 47, no. 1–2, pp. 35–50, 1991.

[52] C. Gauge and T. S. Anvils, "Standard Test Method for Single Pellet Crush Strength of Formed Catalysts and Catalyst Carriers," ASTM D4179-11, 2011.

[53] Y. Tian, R. G. Holt, and R. E. Apfel, "Deformation and location of an acoustically levitated liquid drop," J. Acoust. Soc. Am., vol. 93, no. 6, pp. 3096–3104, 1993.

[54] S. Zhao and J. Wallaschek, "A standing wave acoustic levitation system for large planar objects," Arch. Appl. Mech., vol. 81, no. 2, pp. 123–139, 2011.

[55] W. M. Haynes, CRC Handbook of Chemistry and Physics, 97th Edition. CRC Press, 2016.

[56] S. J. Ashcroft, A. D. Clayton, and R. B. Shearn, "Isothermal Vapor-Liquid Equilibria for the Systems Toluene-n-Heptane, Toluene-Propan-2-ol, Toluene-Sulfolane, and Propan-2-ol-Sulfolane," J. Chem. Eng. Data, vol. 24, no. 3, pp. 195–199, 1979.

[57] K. Sefiane, L. Tadrist, and M. Douglas, "Experimental study of evaporating water-ethanol mixture sessile drop: Influence of concentration," Int. J. Heat Mass Transf., vol. 46, no. 23, pp. 4527–4534, 2003.

[58]   K. Hasegawa, Y. Abe, and A. Goda, "Microlayered flow structure around an acoustically levitated droplet under a phase-change process," npj Microgravity, vol. 2, no. 1, p. 16004, 2016.

[59]   R. Vehring, W. R. Foss, and D. Lechuga-Ballesteros, "Particle formation in spray drying," J. Aerosol Sci., vol. 38, pp. 728–746, 2007.

[60]   S. J. Lukasiewicz, "Spray-drying ceramic powders," J. Am. Ceram. Soc., vol. 72, no. 4, pp. 617–624, 1989.

[61]   G. Bertrand, P. Roy, C. Filiatre, and C. Coddet, "Spray-dried ceramic powders: A quantitative correlation between slurry characteristics and shapes of the granules," Chem. Eng. Sci., vol. 60, no. 1, pp. 95–102, 2005.

[62]   E. Wulsten, F. Kiekens, F. van Dycke, J. Voorspoels, and G. Lee, "Levitated single-droplet drying: Case study with itraconazole dried in binary organic solvent mixtures," Int. J. Pharm., vol. 378, no. 1–2, pp. 116–121, 2009.
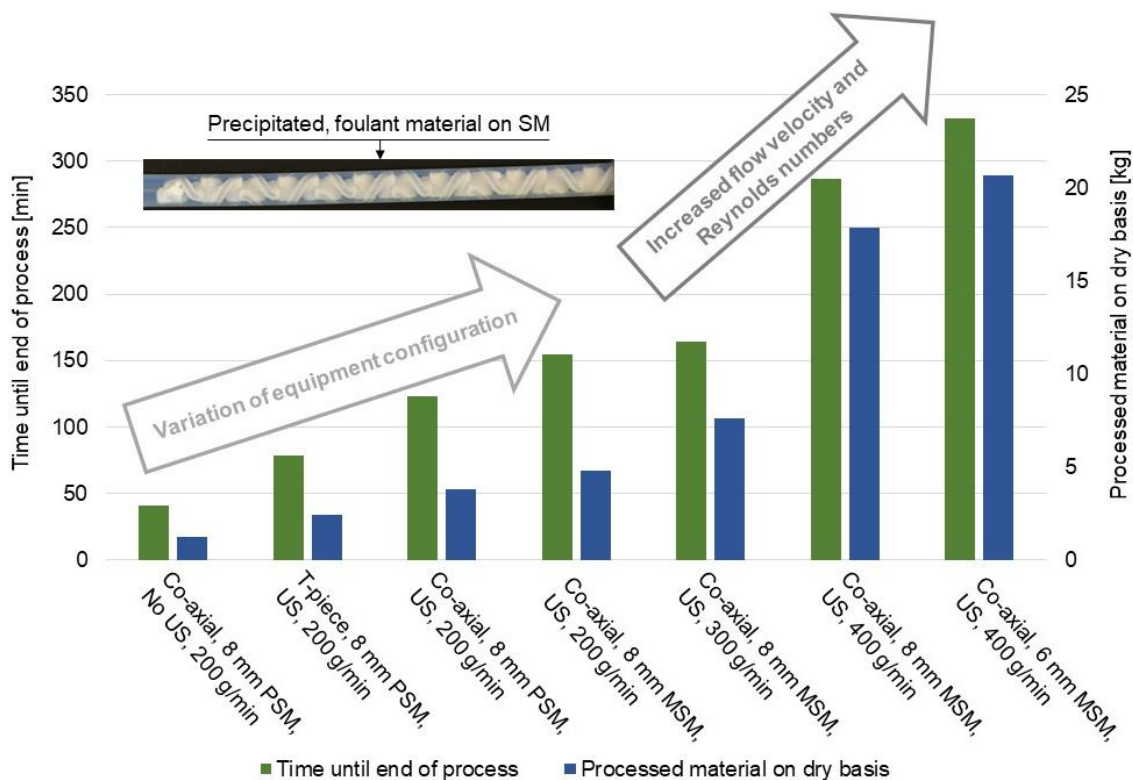
3. Performance Characterization of Static Mixers in Precipitating Environments

M. Kreimer[1], M. Zettl[1], I. Aigner[1], T. Mannschott[2], P. van der Wel[3], J.G. Khinast[1,4*],

M. Krumme[2]

TOC Graphic:

Performance characterization of static mixers in precipitating environments

M. Kreimer[1], M. Zettl[1], I. Aigner[1], T. Mannschott[2], P. van der Wel[3], J.G. Khinast[1,4]*, M. Krumme[2]

[1] Research Center Pharmaceutical Engineering (RCPE) GmbH, 8010 Graz, Austria

[2] Novartis Pharma AG, 4056 Basel, Switzerland

[3] Hosokawa Micron B.V., Gildenstraat 26, 7005 BL Doetinchem, Netherlands

[4] Graz University of Technology, Institute for Process and Particle Engineering, 8010 Graz, Austria

*Corresponding author: J.G. Khinast

Tel. number: 0043 316 873 30400

E-mail address: khinast@tugraz.at

Abstract

Static mixers are extensively used in various industries (pharmaceutical, food processing, chemical, pulp and paper, polymer synthesis, water treatment and petrochemical). They offer several advantages with regard to continuous operation (e.g., intensified mixing, byproduct reduction and sharp residence time distribution, no moving parts) and are frequently used in harsh chemical environments, in which fouling could cause serious problems like clogging or reduction of heat transfer or lead to a shut-down of the entire production line. Fouling has diverse mechanisms: precipitation fouling, particulate fouling, corrosion fouling, chemical reaction fouling, solidification, biofouling and composite fouling. This work investigates the application of static mixers in precipitating environments as present in pharmaceutical processes, in which the undesired side effect of precipitation of the residual dissolved fraction leads to equipment fouling and process stability challenges. The tests were conducted using saturated suspensions mixed with an anti-solvent to challenge the system with a step change of solubility in the presence of seeds and static mixers. Various equipment configurations were investigated and fouling probability and stability was analyzed for different precipitation rates. Process stability was highly influenced from the setup configuration, in which the most stable and

satisfactory process was achieved by co-axial mixing of the fluids before the static mixer and ultrasound irradiation in a unique configuration. Furthermore, the particle size in various feed and outlet suspensions was analyzed and correlations between the amount of suspended particles and the particle growth were determined.

Nomenclature

d_{SM}	Diameter of static mixer / mm
d_{50}	Median mean diameter / µm
l_{SM}	Length of static mixer / mm
l/d	Length to diameter ratio of static mixing elements
m_d	Processed material on dry basis / kg
$\dot{m}_{c,p}$	Crystallized solid mass flow rate in outlet / g/min
$\dot{m}_{d,p}$	Dissolved solid mass flow rate in outlet / g/min
$\dot{m}_{s,f}$	Suspended solid mass flow rate in feed / g/min
$\dot{m}_{s,p}$	Suspended solid mass flow rate in outlet / g/min
$\dot{m}_p$	Total mass flow rate of outlet / g/min
$N_{elements}$	Number of static mixer elements
R	Radius of pipe / m
Re	Reynolds number in empty pipe
SMD	Sauter mean diameter / µm
t	Time until end of process / min
VMD	Volume mean diameter / µm
$\dot{V}$	Volume flow rate / m^3/s
$w_{d,f}$	Dissolved solid mass fraction in feed / wt.%
$w_{d,p}$	Dissolved solid mass fraction in outlet / wt.%
$w_{H_2O,f}$	Water mass fraction in feed / wt.%
$w_{H_2O,p}$	Water mass fraction in outlet / wt.%
$w_{I,p}$	Isopropanol mass fraction in outlet / wt.%
$w_{s,f}$	Suspended solid mass fraction in feed / wt.%
$w_{s,p}$	Suspended solid mass fraction in outlet / wt.%

$X_{c/s}$ kg/kg	Ratio of crystallized mass in outlet to suspended mass in feed /
ϕ_f	Suspended solid volume fraction in feed / V.%
ϕ_p	Suspended solid volume fraction in outlet / V.%
ρ_f	Density of feed suspension / g·cm^{-3}
ρ_p	Density of outlet suspension / g·cm^{-3}

3.1 Introduction

Static mixers (SM) are extensively used in industrial applications to improve mixing and heat transfer. SM, in the context of continuous manufacturing, can help to improve productivity and safety, as well as reduce waste production and energy consumption [1], in contrast to mechanically stirred vessels used in batch processing. Due to their small space requirement, narrow residence time distribution, intensified mixing and isothermal operation, byproduct reduction and enhanced safety, SMs are commonly used in a broad range of applications in pharmaceutical, food processing, chemical, pulp and paper, polymer synthesis, water treatment and petrochemical industries [2-5].

The mixing mechanisms in SMs include macromixing (mixing on the scale of the entire vessel), mesomixing (coarse-scale turbulent exchange between the fresh feed and its surroundings) and micromixing (molecular mixing because of diffusion and turbulent dispersion) [6, 7]. Deviations from ideal plug flow behavior of SMs can be characterized via the residence time distribution for temporal variations [8, 9] and the striation thickness distribution for spatial variations [9, 10]. In contrast, SMs operated in the turbulent flow regimes create intensive radial mixing, even close to the wall. The effect of intensified mixing is more important for the laminar flow and the intensification effect is reduced in turbulent regimes [11]. However, the level of turbulence can be increased in SMs without changing the pipe diameter and the flow rate, although higher pressure drops can be expected. Such an increase in turbulence levels enhances the wall turbulence and may prevent plugging or fouling [4]. Besides the flow regime, understanding and describing the degree of mixing is important. To that end, qualitative techniques (e.g., estimating the mixing time by observing a color change [12, 13]) or quantitative techniques (e.g., monitoring species concentration [14, 15]) can be applied.

A major engineering challenge in chemical industrial processes is fouling. Fouling mechanisms include precipitation fouling, particulate fouling, corrosion fouling, chemical reaction fouling, solidification, biofouling or a combination of them (composite fouling) [16,17]. Considering this variety of mechanisms, fouling is a complex process influenced by a large number of variables. In general, fouling on a surface consists of the following consecutive stages: initiation, transport, attachment, removal and aging [18]. The initiation period starts with a new or cleaned equipment and may last from a few seconds to several weeks. This period is shorter for increased chemical reaction rates and rougher surface texture [19]. In the transport period, fouling substances are transported towards the deposit-fluid interface (e.g., SM or tube). Diffusion, sedimentation and thermophoresis are the

driving forces [20]. At the attachment stage, the deposits adhere to the surface and to each other. Deposition of particles is a function of several variables: the particle size and concentration, bulk fluid density and bulk fluid velocity, stickiness and attractive or repulsive forces between particles [21]. Fouling material accumulates on the surface, prompting a competition between the removal and deposition of foulants [19]. This continues until steady growth of the deposition on the surface occurs. The removal depends on the velocity gradients at the surface, the viscosity of the fluid and surface roughness. The last stage in a fouling process, aging, commences as soon as the first depositions are formed. In its course, deposits might be strengthened or weakened [22].

SMs used in harsh industrial environments, such as the considered mixing experiments, undergo a composite fouling effect, mainly determined by particulate fouling (i.e., sedimentation) [23, 24] and precipitation fouling (i.e., precipitation of solids out of solutions or suspensions) [25]. The precipitation takes place either directly on a surface (i.e., SM) resulting in difficult-to-remove deposits or via the formation of solids in the bulk liquid which are rather loose and easily removed [25]. Yet during the process more depositions may be created, reducing the cross-sectional area and increasing the flow velocity. Therefore, the deposits should be periodically removed and extend the resistance against fouling from linear to asymptotic behavior [19]. However, as soon as precipitation occurs in a chemical reaction, the fouling probability is drastically accelerated [26]. This fouling acceleration by precipitation is a well-known issue amongst several industries from the oil industry [27, 28], to chemical synthesis [29], pharma [30], and food industry [31].

Dong et al. [32] and Hu et al. [33] investigated anti-solvent precipitation during static mixing processes with regard to production of nanoparticles, but not in the sense of process stability. In our work, the application of SMs in harsh, precipitating environments was examined. Technical opportunities and limitations of SM designs were evaluated for different equipment sizes and under various environmental conditions. The process stability and fouling probability were analyzed for various design approaches, i.e., mixing the feed suspensions and the anti-solvent co-axially and perpendicularly. During this process, dissolved components in the feed suspension precipitate by anti-solvent addition (change of the solubility from higher to lower values), where precipitates might adhere to surfaces forming foulant material. Process optimization was performed by applying ultrasound irradiation, variation of the mixer material (i.e., plastic or metal) and by varying the mass flow rate and equipment size. Ultrasound prevents - to some degree - the material accumulation via precipitation of solids on a surface and slows down fouling. Similarly, process times could be extended by using a metal static mixer (MSM) instead of a plastic

static mixer (PSM). Moreover, higher mass flow rates and smaller equipment size further increased process stability. The most stable process was achieved via co-axial mixing of the feed suspension with the anti-solvent on the smallest equipment scale, using MSMs and ultrasound irradiation. In addition, the feed composition was varied to evaluate the influence of the precipitation rate during the experiments on the outlet particle size.

## 3.2 Materials and methods

3.2.1 Process equipment

Precipitation fouling experiments were carried out using the mixing equipment, as depicted in Figure 1. Two eccentric screw pumps MX10S-10/20® from Knoll Maschinenbau GmbH (Bad Salgau, Germany) were used to transport the feed suspension and the anti-solvent from the storage tanks to the SM. The pressure in the system was measured using a Krohne Optibar P 3050 C (Duisburg, Germany) on the feed and anti-solvent side to detect possible blockages of the system by precipitated material. Experiments were carried out by mixing the feed and the anti-solvent in the SM with or without ultrasound (US) irradiation (in an US bath). This is illustrated in Figure 1. The water temperature in the US bath was maintained at 25 °C by a cooler LAUDA Alpha RA 12 (Lauda-Königshofen, Germany) to avoid a temperature increase due to the US-input. After mixing of the two liquids, the outlet was collected in a tank, which was placed on a scale to monitor the outlet mass flow. The feed suspension was stirred with a Heidolph mixer RZR 200 (Schwabach, Germany) to avoid sedimentation of particles enabling a consistent feed composition throughout the experiments.
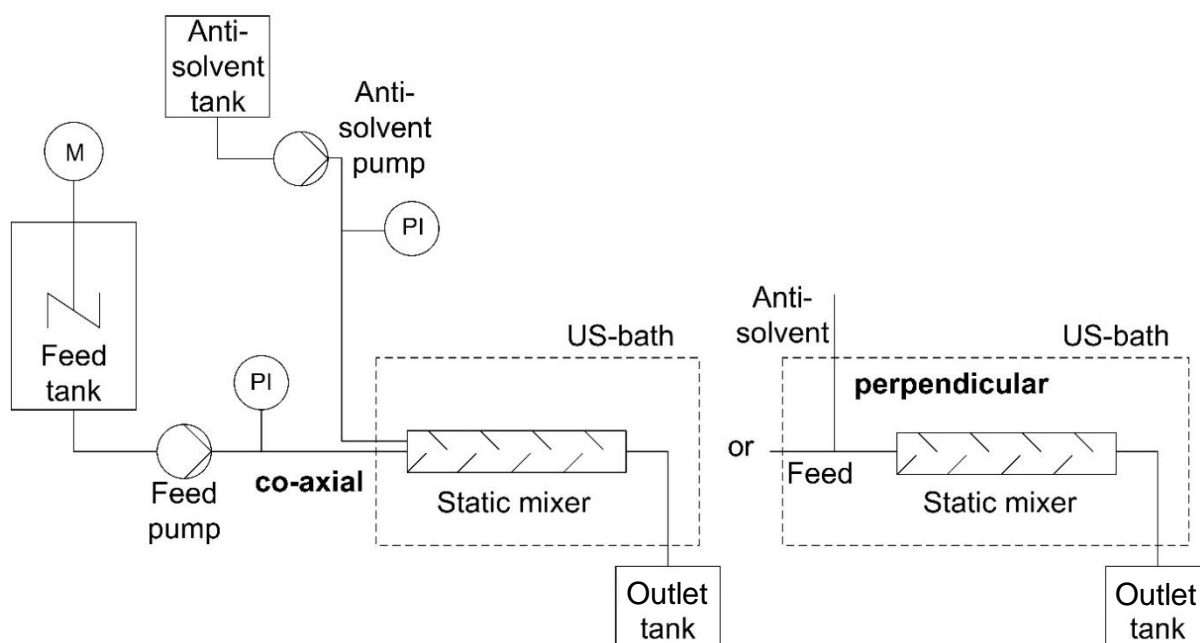
Figure 1. Flow sheet of experimental setup for precipitation experiments with SMs.

Mixing of the feed and anti-solvent was either done co-axially or perpendicular, as shown in Figure 2. Thus, the mixing point (denoted by a "*") of the feed suspension and anti-solvent, and therefore the first point of precipitation was located either directly after the co-axial outlet or in the T-piece. In the case of co-axial mixing, the SM was 7 cm away from the mixing point and the inner feed pipe had an inside diameter of 2.4 mm and an outside diameter of 3 mm (Figure 3). In the case of perpendicular mixing, the SM was also 7 cm away from the mixing point in the T-piece. In between the distance mixing point – SM, precipitation occurs before mixing is intensified in the SM. The SM was placed in pipes with diameters of 8 mm and 6 mm. Three SMs of Kenics type were used for the experiments, as depicted in Table 1. The elements of Kenics mixers are twisted by 180° to each other, providing a helical structure with alternating left- and right-turning elements. For this type of mixers, mixing is achieved by distribution of the flow at the leading edge of each element. In ideal mixing conditions, 2^n distributions (striations) are created, where 'n' represents the number of mixing elements. In practice 1.45^n striations are formed [34], which means 86 striations for the used SMs with 12 elements. The PTFE SM was supplied by Esska GmbH (Hamburg, Germany) and the metal SMs were supplied by Schumacher Verfahrenstechnik GmbH (Wiehl Bomig, Germany). The surface of the MSM was electro-polished with a roughness Ra < 0.8 µm, and the surface of the PTFE static mixer (PSM) was not known. The inner surface of T-piece had the same surface quality as the MSM. Translucent PFA pipes

were used for the feed and anti-solvent supply pipes, as well as for the outlet suspension pipes, to make the flow regime before and in the SM visible during the experiments.
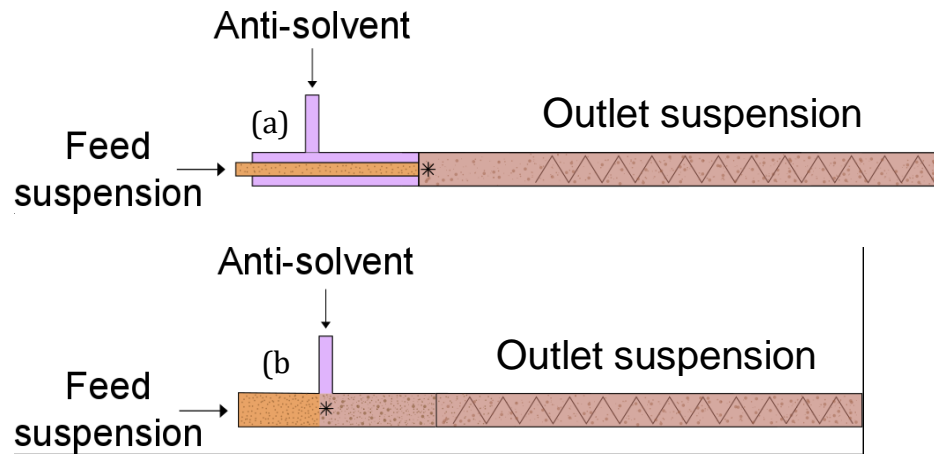
Figure 2. Co-axial (a) or perpendicular mixing (b) of feed suspension and anti-solvent. The star symbol shows the mixing point of feed suspension and anti-solvent in the equipment.
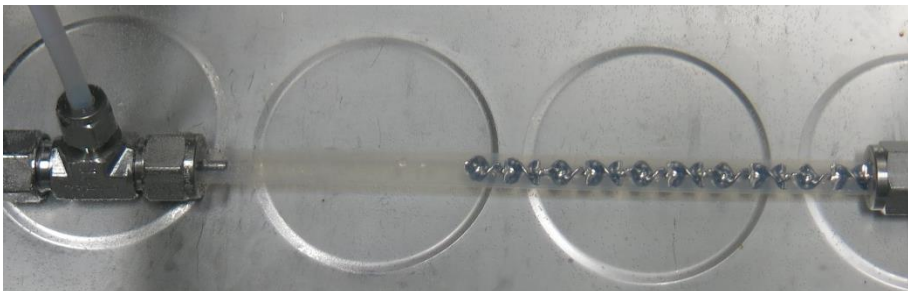
Figure 3. Experimental setup (8 mm) in the lab for co-axial mixing with the MSM in the US-bath.

**Table 1.** SMs used for the experiments.

| No.	d_{SM} [mm]	l_{SM} [mm]	$N_{elements}$	l/d	Material
1	7.9	95	12	1.00	PTFE
2	7.9	137	12	1.44	Stainless steel
3	5.9	110	12	1.55	Stainless steel

3.2.2 Materials

GranuLac® 230 (alpha-lactose monohydrate) was obtained from Molkerei Meggle Wasserburg (Wasserburg, Germany) with a particle shape and a particle size distribution (PSD) shown in Figure 4 and Figure 5, respectively. The volume mean particle size (VMD) was 30 μm.

Aqueous feed suspensions with different suspended solid mass fractions were prepared according to Table 2. Before adding the suspended solids, a saturated aqueous lactose solution was prepared at 25 °C ±1 °C either by adding exactly 233 g of lactose to 1 liter of water (lactose equilibrium solubility) [35] or by surplus addition of lactose. In the latter case, the solution was filtered after the dissolution phase. The solution mixtures were stirred for 18 h to ensure homogenous solutions. For long-term runs, the exact amount of lactose was added to the liquid, as for these test runs, large quantities of saturated solutions are needed and filtration of undissolved solids would be too time-consuming. After preparation of the saturated solution, suspended solids were added in the amount of 5 wt.%, 15 wt.% or 30 wt.%. Thus, added suspended solids might be dissolved because of the large metastable zone of lactose solutions. Such metastable zones in lactose solutions are well known from literature [36, 37]. Therefore, for the test runs with particle size measurements, saturated solutions were prepared by surplus addition of lactose to avoid later dissolution of suspended lactose particles. The saturated lactose solutions were decanted and afterwards filtered with MN 618 from Macherey-Nagel (Düren, Germany). Thus, the saturation of the solution was guaranteed and added suspended solids cannot be dissolved. The degree of saturation was proven by density measurements of the saturated solutions with DSA 5000 M from Anton Paar (Graz, Austria). The density of the saturated solutions was measured at 25 °C with 1.0560 ± 0.002 g·cm⁻³, which agrees with the value of 1.05599 g·cm⁻³ reported by [38]. Isopropanol (IPA) with a purity ≥ 98 % from VWR chemicals (Pennsylvania, United States) was used as anti-solvent.
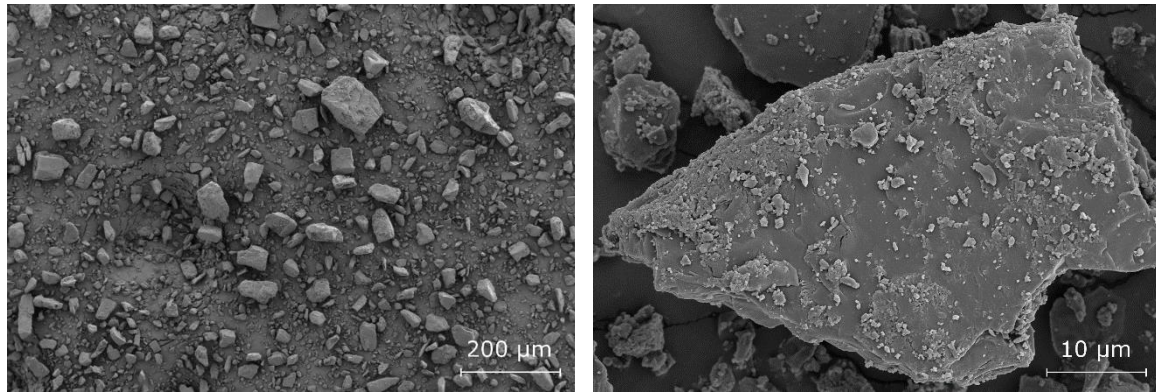
Figure 4. Particle shape of GranuLac® 230.
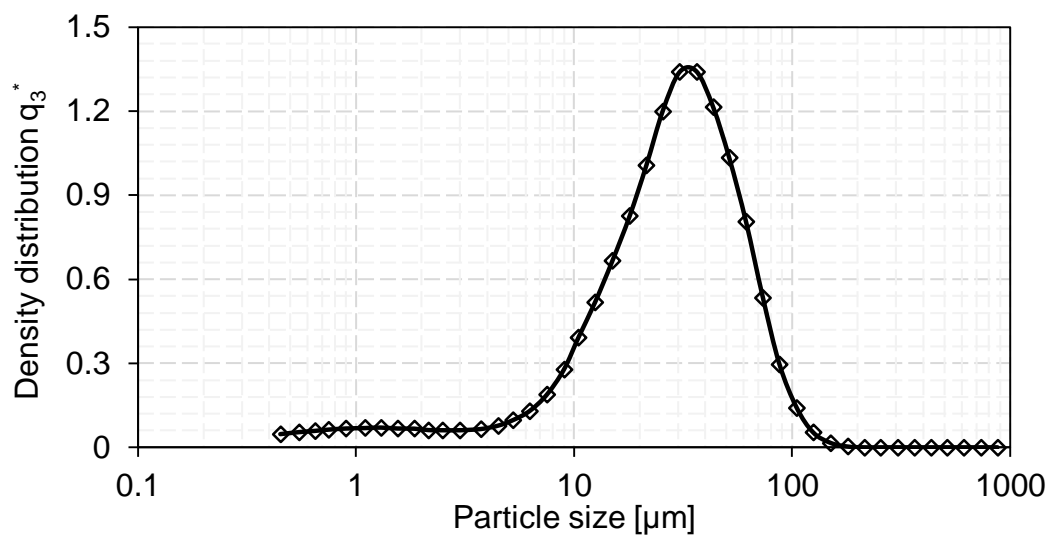
**Figure 5.** PSD of GranuLac® 230.

Table 2. Composition of feed suspensions with suspended solid mass fraction in feed ($w_{s,f}$), dissolved solid mass fraction in feed ($w_{d,f}$), water mass fraction in feed ($w_{H_2O,f}$), suspended solid volume fraction in feed (ϕ_f) and density of feed suspension (ρ_f).

$w_{s,f}$	$w_{d,f}$	$w_{H_2O,f}$	ϕ_f	ρ_f
[wt.%]	[wt.%]	[wt.%]	[V.%]	[g/cm³]
5	18.0	77	3.5	1.07
15	16.1	68.9	10.9	1.11
30	13.2	56.8	22.9	1.16

3.2.3   Material characterization

Feed and outlet suspensions were analyzed in detail. The particle size was measured in wet dispersion mode by laser diffraction with Helos KR from Sympatec GmbH (Clausthal-Zellerfeld, Germany). The particle size of feed and outlet suspensions were measured to assess the influence of the precipitation rate during the process on the outlet particle size. Measurements of the feed and outlet suspensions were done in the related saturated solutions to avoid particle size changes by dissolution or precipitation. For example, a larger quantity of outlet suspension was collected and filtered to obtain a saturated solution from the specific composition. Afterwards, this saturated solution was used as background medium to measure the particle size of the related outlet. The particle surface and shape of the feed material was examined with a scanning electron microscope (SEM) Zeiss Ultra 55 from Carl Zeiss AG (Oberkochen, Germany) with an Everhart-Thornley detector and an acceleration voltage of 5 keV. Sample preparation was done with a sputter coater EM ACE 600 from Leica (Wetzlar, Germany) by sputtering a 15 nm gold-platinum (80 % - 20 %) layer on the surface of the samples.

The viscosity of the feed and outlet suspensions was analyzed to calculate the empty pipe Reynolds numbers (Re) for different outlet mass flows. The measurements were done with a rotational rheometer MCR 300 from Anton Paar (Graz, Austria), equipped with a double-gap measuring system (DG26.7/Ti / TEZ 150P). The viscosity was measured in a shear rate range between $0.1 \ s^{-1}$ and $3000 \ s^{-1}$ in rotational mode with 46 measurement points and a measurement point duration of 5 s. The relevant shear rate range is shown in Figure 6 highlighting the (mostly) shear thinning behavior of the feed suspensions.
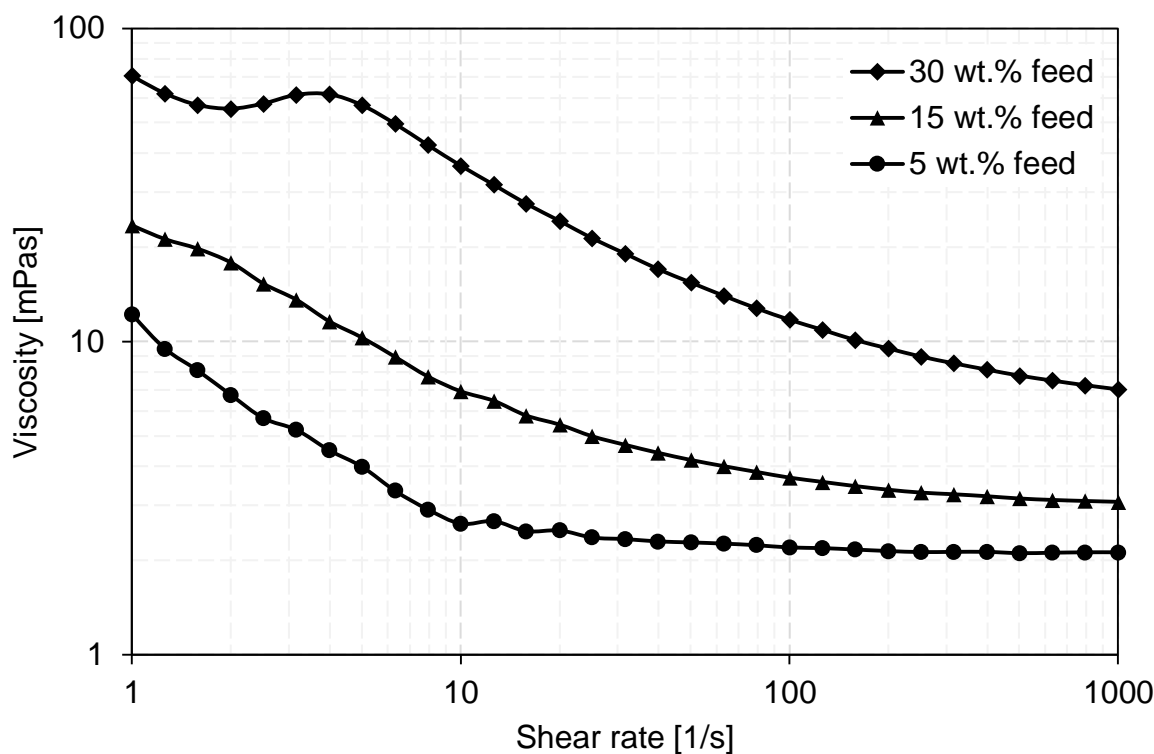
Figure 6. Viscosity as a function of shear rate of the feed suspensions with 5 wt.%, 15 wt.% and 30 wt.% suspended solids.

3.2.4 Methods

Before the precipitation experiments with SMs were performed, the necessity of SMs to improve miscibility (aqueous and organic phase as well as solids) was proven through mixing studies. For this reason, the co-axial setup was used without a SM to visualize the flow propagation in an empty pipe. The straight section of the pipe was 1 m long with an inner diameter of 8 mm. Instead of the used suspension for SM experiments, a saturated aqueous lactose solution was used as feed material to visualize the mixing point and the precipitation along the pipe. Using a suspension as feed material would already result in an opaque mixing point from the beginning on, because of the suspended solids and hence the precipitation point cannot be seen. Figure 7 depicts the mixing point and the precipitation along an empty pipe for mixing the solution and anti-solvent in a 1:1 ratio in total mass flow rates of 300 and 900 g/min. A pipe length of approx. 10 cm is shown, the outlet flow appearance was the same along the whole pipe. A total mass flow rate of 300 g/min resulted in an almost translucent outlet flow with little precipitated solids. The created turbulences at the mixing point were not strong enough to achieve visually homogenous mixing. Increasing the total mass flow rate up to 900 g/min increased the

opacity of the outlet flow, but still a translucent flow at the bottom was visible. The desired total mass flow rate of 200 g/min for the SM experiments was also tested. In this case, the outlet flow was almost translucent with little precipitated particles. In summary it can be said that mixing in an empty pipe will not be sufficient to achieve good mixing of feed suspension and anti-solvent.
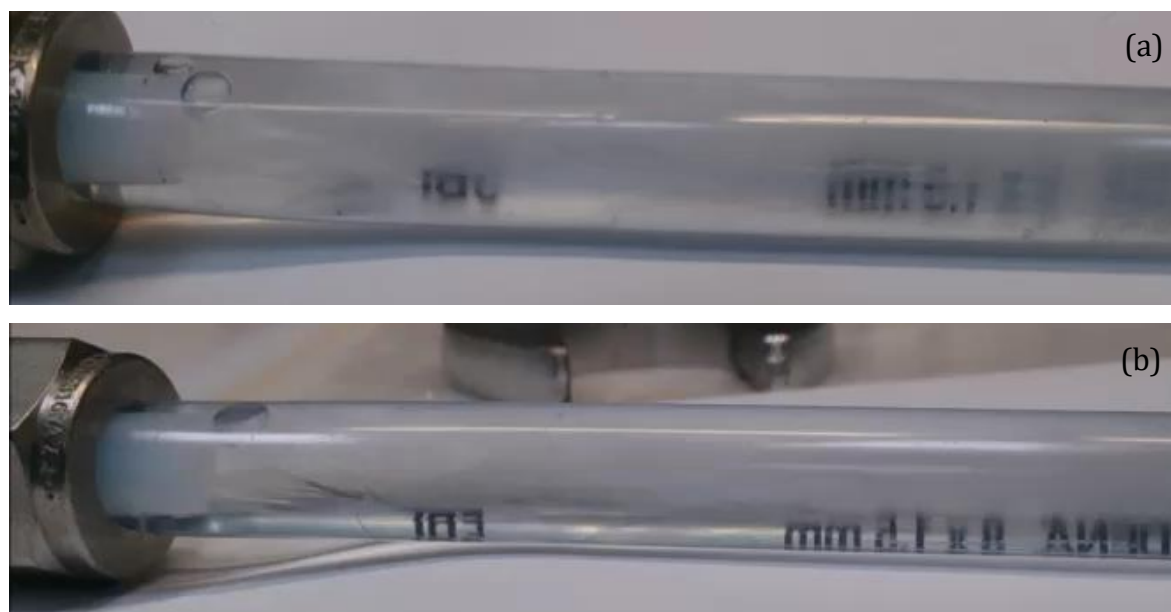
Figure 7. Visualization of the mixing point and the precipitation along an empty pipe for mixing of an aqueous saturated solution and anti-solvent in a 1:1 ratio with total mass flow rates of (a) 300 g/min and (b) 900 g/min.

For the performance characterization experiments of SMs in precipitating environments, the whole system was flushed with water before the start of the experiments for 5 min to avoid precipitation of lactose in the connection pipes. Afterwards, the feed was switched simultaneously from water to suspension and anti-solvent. Therefore, the first contact of the fluids and the first material precipitation occurred at the mixing point, which was in the T-piece or in front of the SM. The feed suspension was located in a continuously stirred tank and fed to the SM through an eccentric screw pump. Experiments were stopped if the pressure in the system exceeded 5 - 6 bar to avoid damage of the equipment.

A set of different experiments was carried out for the particle size evaluation and the performance characterization of SMs in precipitating environments. The setup for the evaluation of the particle size consisted of a PTFE SM in co-axial mixing arrangement, no ultrasound input and 200 g/min mass flow rate. The mixing ratio of feed suspension to

anti-solvent was in a 1:1 ratio, which means 100 g/min feed mass flow rate and 100 g/min anti-solvent mass flow rate. The start-up period was 15 min and samples were drawn after 5 min, 10 min and 15 min to measure the particle size of the outlet suspension. Samples from the feed suspensions were taken before and after the experiment for comparison with the outlet particle size. The suspended solid mass fraction was varied between 5 wt.%, 15 wt.% and 30 wt.% according to Table 2. Three experiments were performed for each composition, resulting in 9 experiments in total. Each of the drawn samples was analyzed in triplicate, resulting in 27 individual particle size measurements of the outlet suspension for one composition.

In our work, the mixing point was varied as well, as depicted in Table 3. Experiments were also conducted by variation of the feed suspension composition, but mainly with a suspended solid mass fraction of 15 wt.%. Feed suspension and anti-solvent were mixed in a 1:1 ratio. The process stability of a run was evaluated by calculation of the processed material on dry basis, which is basically the total amount of processed suspended and dissolved solids through the SM before blockage occurred.

Table 3. Experimental procedure and setup for performance characterization of SMs in precipitating environments (the changes to preceding experimental conditions are written in bold font).

No.	$\dot{m}_{tot}$ [g/min]	Mixing point	US input	SM material	d_{SM} [mm]
1	200	co-axial	No	PTFE	8
2	200	co-axial	**Yes**	PTFE	8
3	200	**perpendicular**	Yes	PTFE	8
4	200	**co-axial**	Yes	**Stainless steel**	8
5	**300**	co-axial	Yes	Stainless steel	8
6	**400**	co-axial	Yes	Stainless steel	8
7	400	co-axial	Yes	Stainless steel	**6**

The empty pipe Reynolds number (Re) was calculated via Eq. 1 with the fluid density ρ, the fluid velocity v, the pipe diameter d, and the dynamic viscosity η to compare different suspension compositions and setup dimensions. The dynamic viscosity η was determined from the viscosity – shear rate measurements for the occurring mean shear rate $\dot{\gamma}$, which was calculated via Eq. 2 by the volume flow rate $\dot{V}$ and the pipe radius R.

$$Re = \frac{\rho \cdot v \cdot d}{\eta} \tag{1}$$

$$\dot{\gamma} = \frac{4 \cdot \dot{V}}{\pi \cdot R^3} \tag{2}$$

3.3 Results and discussion

3.3.1 Material characterization

At first, the influence of the feed composition and the precipitation rate on the outlet particle size was evaluated (Figure 8). As can be seen, the PSD of the feed suspension was the same in the range for 5 wt.% and 30 wt.% suspended solids. Thus, no agglomeration or attrition occurred during preparation and pumping of the feed suspension. The PSD of the outlet suspensions changed significantly, depending on the amount of suspended solids. The 30 wt.% outlet in Figure 8refers to the feed suspension with 30 wt.% suspended solids; the same nomenclature was used for the other two compositions. It can be seen that the lowest amount of suspended solids in the feed resulted in the largest change of the outlet particle size and vice versa. The reason for this behavior is obvious: the feed suspension with 5 wt.% suspended solids contains 95 wt.% saturated lactose solution, consisting of 77 wt.% water and 18 wt.% dissolved solids. After addition of the anti-solvent, the solubility of lactose changed according to the solubility curve of lactose in isopropanol-water mixtures [39]. For example, the amount of dissolved solids in the feed suspension with 5 wt.% suspended solids changed from 18 wt.% to 1.2 wt.% (the solubility of lactose changed from 233 g/l to 13 g/l, based on the solvent mixture), as depicted in Table 4. Thus, during the solvent regime change by isopropanol, a high amount of dissolved solids precipitated on the 5 wt.% suspended solids from the feed suspension ($X_{c/s}$ = 3.14 kg/kg, ratio of crystallized mass in outlet to suspended mass in feed), resulting in a larger change of the particle size for the outlet suspension. On the contrary, for a higher amount of suspended solids in the feed suspension the precipitating material is distributed amongst more particles. In fact, less dissolved solids precipitate on a higher amount of suspended solids resulting in a smaller change of the outlet particle size. The smallest change of the particle size was observed for the feed suspension with the highest suspended mass flow of 30 wt.% and the lowest crystallized mass flow ($X_{c/s}$ = 0.39 kg/kg). Furthermore, particle size fractions smaller than 4 μm were drastically reduced in the PSD

of the 5 wt.% outlet. The disappearance of smaller size fractions is reduced for feed compositions with higher amounts of suspended solids.

Table 4. Composition of outlet suspensions

| $w_{s,f}$ [wt.%]	$w_{s,p}$ [wt.%]	$w_{d,p}$ [wt.%]	$w_{H_2O,p}$ [wt.%]	$w_{I,p}$ [wt.%]	ϕ_p [V.%]	ρ_p [g/cm^3]
5	10.3	1.2	38.5	50	6.8	0.933
15	14.6	0.9	34.5	50	9.6	0.948
30	20.9	0.7	28.4	50	13.8	0.970
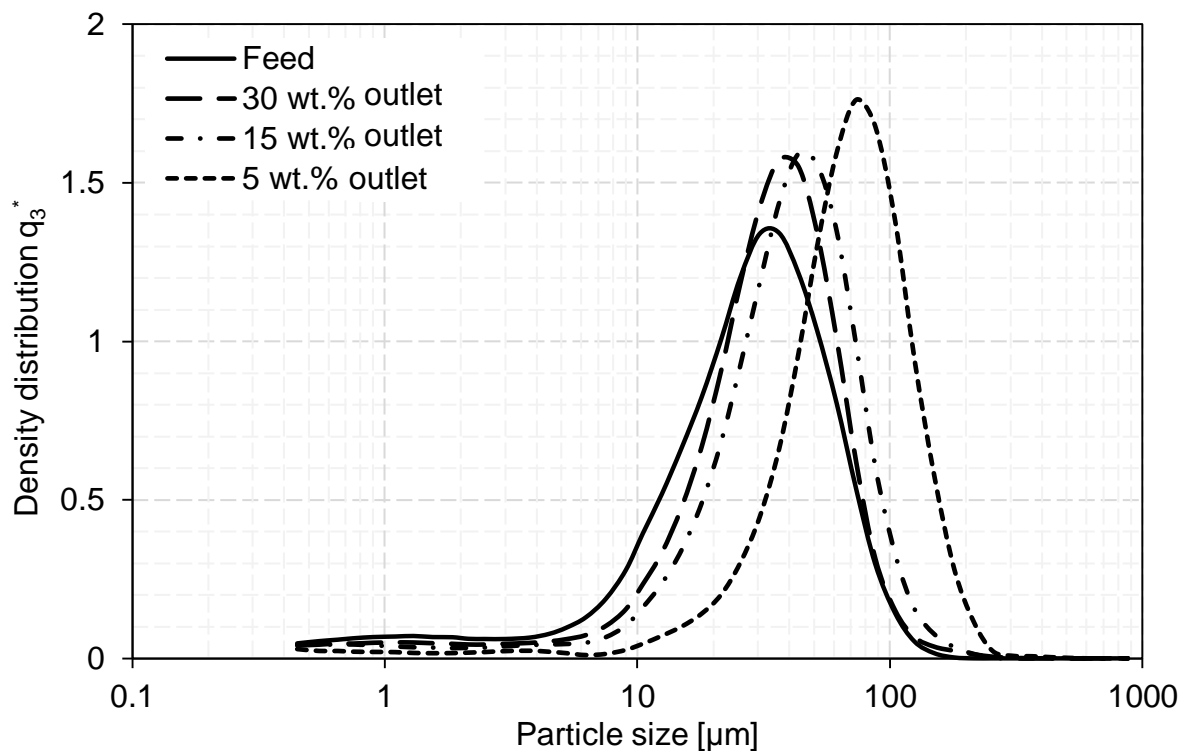
Figure 8. Density PSD q_3^* of feed and outlet suspensions after the precipitation experiments with 5 wt.%, 15 wt.% and 30 wt.% suspended solids in the initial feed suspension.

In general, the higher the number of seeds (suspended solids) and the lower the amount of dissolved solids, the smaller was the change of the particle size by precipitation. This can be also seen in the results of the Sauter mean diameter (SMD), the volume mean diameter (VMD) and the median diameter (d_{50}) in Figure 9(a-c). These diameters changed only slightly for the 30 wt.% outlet, whereas a large change was observed for the 5 wt.%

outlet. The d_{50} has more than doubled after the precipitation process for the 5 wt.% outlet from 26.5 μm to 63.8 μm. In contrast to this, the d_{50} of the 30 wt.% outlet increased only 17 % from 26.5 μm to 31.2 μm (Figure 9d). In that sense, process design in precipitating environments is a crucial part if particles with a desired size are demanded. Numerous other examples in the field of crystallization in SM (intentional) and reaction engineering (intentional or unintentional) can be relevant to the phenomena described here.
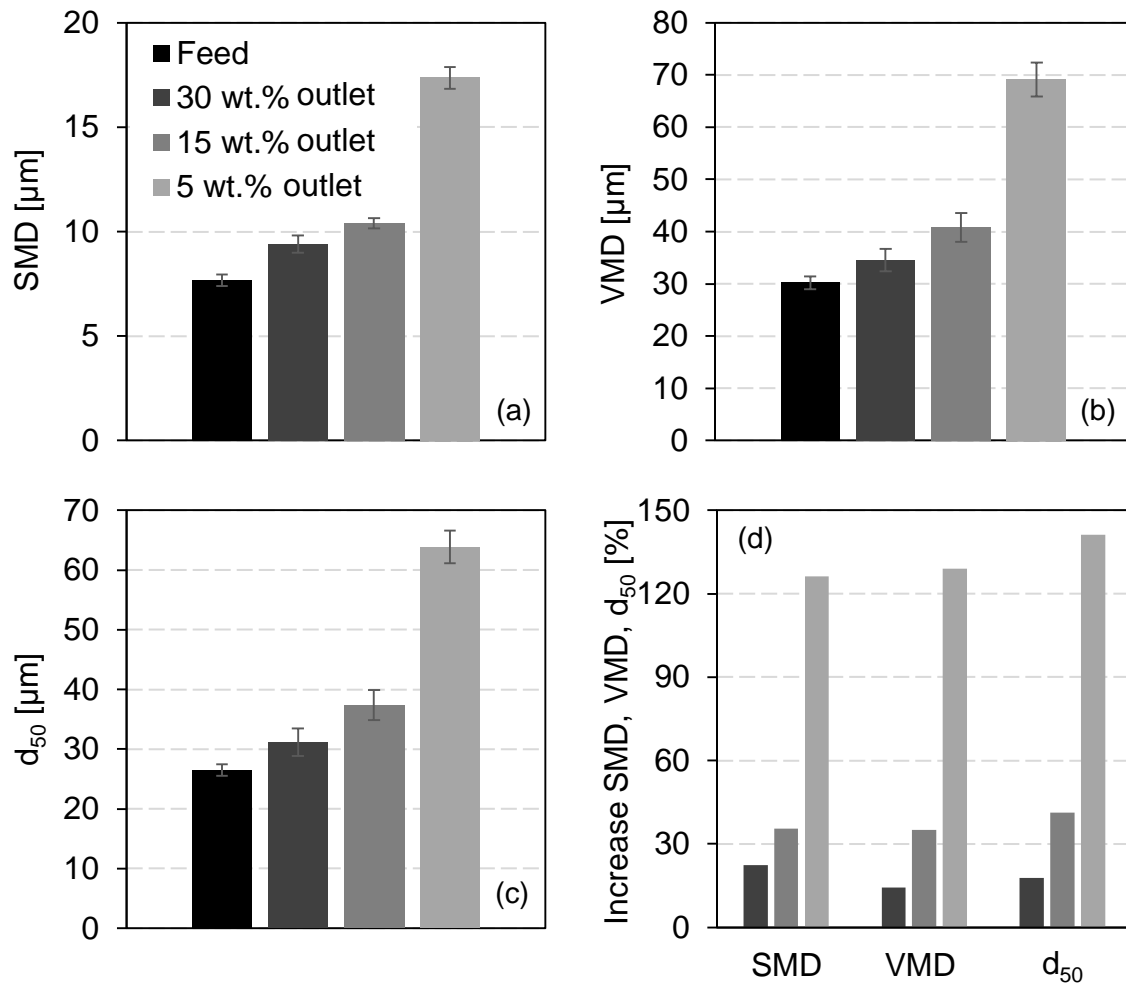

Figure 9. SMD (a), VMD (b) and d_{50} (c) of the feed material and the outlets after the precipitation experiments with 5 wt.%, 15 wt.% and 30 wt.% suspended solids in the initial feed suspension. Increase of SMD, VMD and d_{50} (d) of the outlet suspensions in relation to the feed suspension.

The viscosity of the feed and outlet suspensions is shown in Figure 10. Variations in the viscosities of feed and outlet suspensions are attributable to changes because of adding anti-solvent and therefore altered particle volume fraction, particle shape, interaction

between particles and the spatial arrangement of particles [40]. The 5 wt.% feed has a lower viscosity as the 5 wt.% outlet (Figure 10a). The higher viscosity was mainly caused by newly suspended mass through precipitation of dissolved solids (suspended solid volume fraction increased from 3.5 to 6.8 V.%), an altered PSD and the anti-solvent isopropanol. Isopropanol has a viscosity of 2.04 mPa·s at 25 °C and is higher than that of water (0.89 mPa·s) [41]. Solids suspended in liquids with lower viscosity show higher shear-thinning behavior at lower shear rates [42]. Thus, the shear-thinning behavior was higher for the 5 wt.% feed suspension in a shear rate range of 1-10 s-1. The viscosity of the 5 wt.% outlet decreased only slightly from 6.4 mPa·s for a shear rate of 1 s-1 to 5.7 mPa·s for 1000 s-1. Similar results of lower shear-thinning behavior were obtained for the 15 wt.% (Figure 10b) and 30 wt.% (Figure 10c) outlet suspensions. At shear rates between 100 s-1 to 1000 s-1 the viscosity decrease of the outlet suspension leveled off, especially for the 30 wt.% suspension. In general, the viscosity of the suspensions increased with higher suspended solid volume fraction (particle volume fraction) and with isopropanol content.
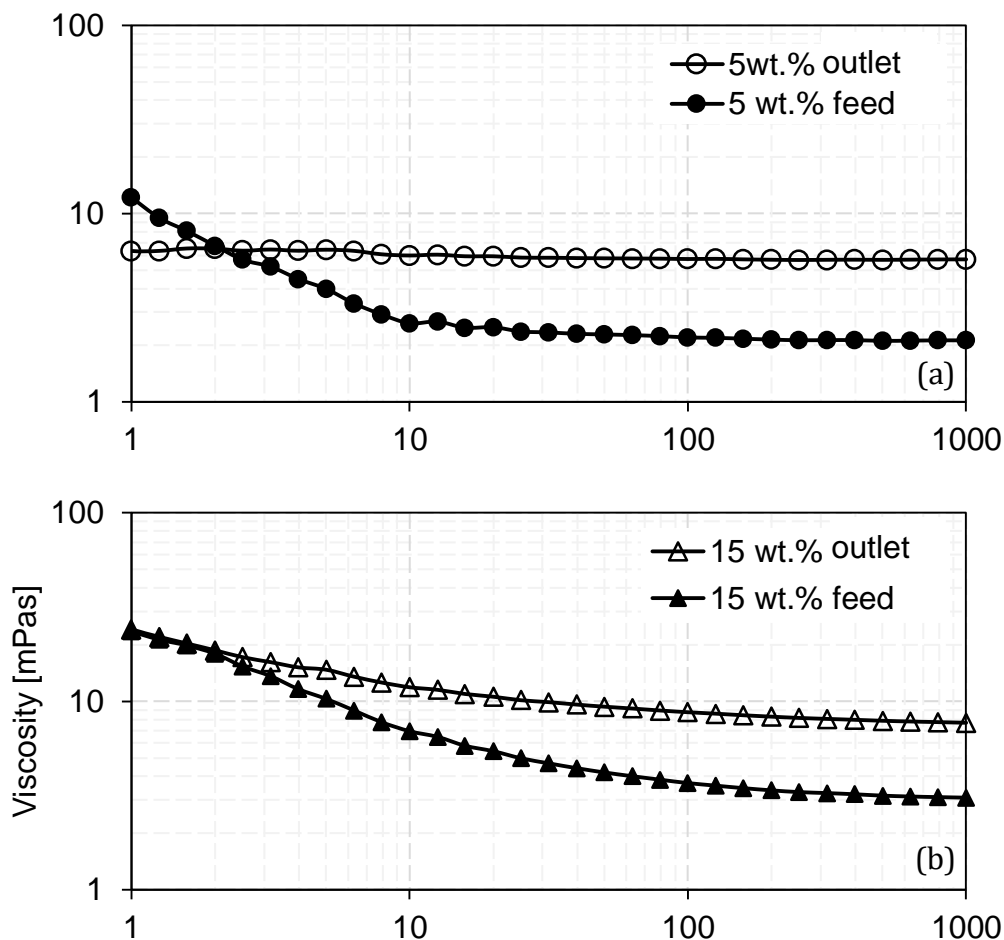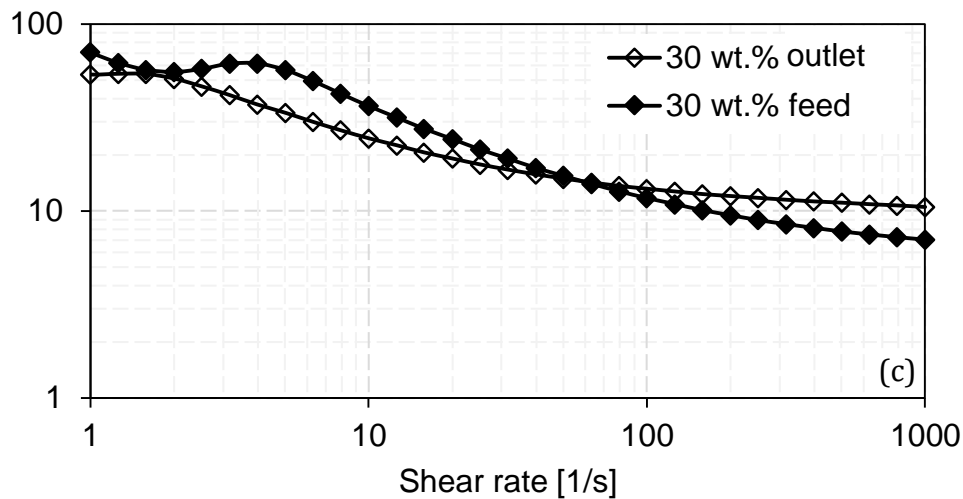
Figure 10. Viscosity over shear rate of the feed suspensions and the outlets after the precipitation experiments with 5 wt.% (a), 15 wt.% (b) and 30 wt.% (c) initial suspended solids.

The viscosity-shear rate curves were recorded to determine the empty pipe Reynolds numbers (Re) for different mass flow rates (200, 300 and 400 g/min) for the 8 mm setup. The mean shear rate of the pipe flows was calculated via Eq.1 (Figure 11a) and the related viscosities (Figure 11b) were obtained from the viscosity-shear rate curves (Figure 10). The 5 wt.% outlet suspension showed nearly Newtonian flow behavior, as the viscosity did not change over the investigated mass flow rates. In contrast, the 15 wt.% and 30 wt.% outlet suspensions revealed a non-Newtonian (shear-thinning) behavior at higher suspended solid volume fractions and anti-solvent content. Figure 11c depicts the Re of the outlet suspensions for different mass flow rates, indicating an increase of Re with higher mass flow rates and lower suspended solid volume fraction (lower viscosity).
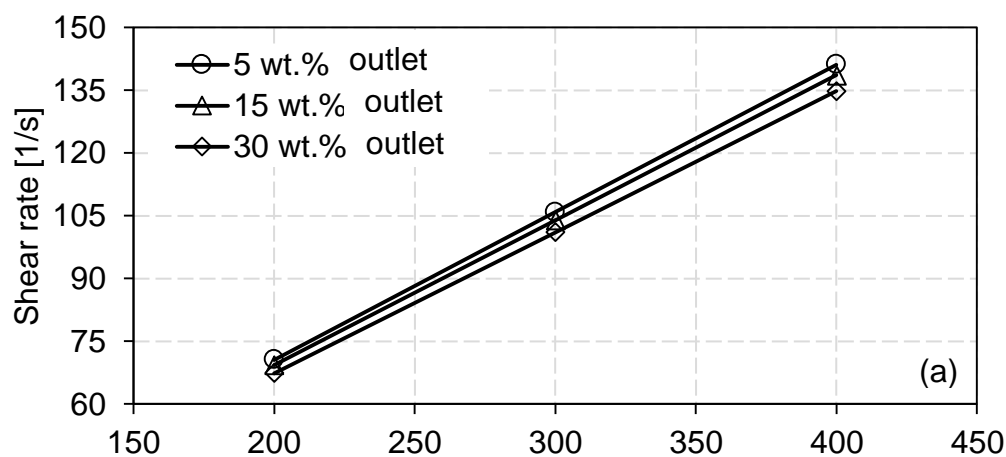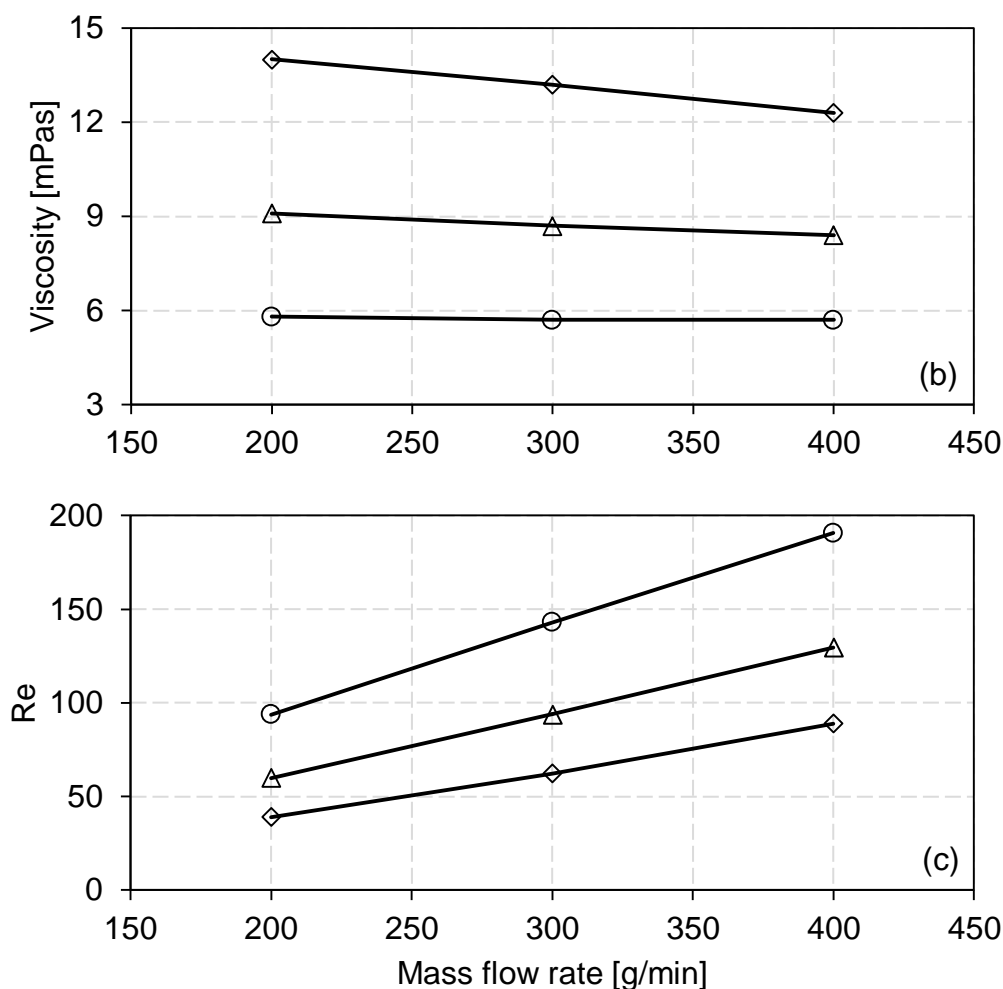
Figure 11. Shear rate, viscosity and Re in empty pipe over different outlet suspension mass flow rates (8 mm setup).

3.3.2 Fouling probability and stability of static mixers in precipitating environments

The applicability and robustness of SMs in crystallizing environments was investigated through long-term experiments of up to several hours. Figure 12depicts a typical pressure evolution in the system as a function of time for precipitation experiments of feed suspensions with 5 wt.%, 15 wt.% and 30 wt.% suspended lactose solids. In this case, feed and anti-solvent, each with a 100 g/min mass flow rate, were mixed co-axially in a pipe with 8 mm diameter, followed by a PSM. It can be clearly seen that a higher mass fraction of suspended solids in the feed rapidly increases the pressure within the first 30 min, leading to an early blockage of the SM. The different process times until blockage are a result of different amounts of suspended and dissolved solids present in the SM. The 5 wt.% feed suspension had a lower mass flow rate of suspended solids (5 g/min) compared with the 15 wt.% (15 g/min) or 30 wt.% (30 g/min) feed suspensions. The mass

flow rate of dissolved solids varied between 18 g/min (5 wt.% feed suspension) and 13.2 g/min (30 wt.% feed suspension). After addition of the anti-solvent isopropanol, the solubility of lactose was shifted and dissolved components precipitated. Thus, new solid was generated before and within the SM. As shown in Table 5, the mass flow rate of suspended solids in the 5 wt.% feed suspension increased from 5 g/min to 20.7 g/min (15.7 g/min new precipitated mass flow rate) and for the 30 wt.% feed suspension from 30 g/min to 41.8 g/min (11.8 g/min). Even though the new precipitated mass was smaller for the 30 wt.% feed suspension, the process time until equipment fouling with total blockage occurred was shorter compared with the 5 wt.% feed suspension. The main driver in the case of equipment fouling apparently is the total mass flow rate of suspended solids in the SM. Due to precipitation of dissolved solids, the probability of agglomerate formation and material adherence on the surface of the SM is higher for higher concentration of solids. Therefore, the foulant material buildup on the elements of the SM is faster, resulting in shorter process times. The longest process time achieved was for a feed with 5 wt.% suspended solids (53 min).

Table 5. Suspended solid mass flow rate in feed ($\dot{m}_{s,f}$), crystallized solid mass flow rate in outlet ($\dot{m}_{c,p}$), suspended solid mass flow rate in outlet ($\dot{m}_{s,p}$) and dissolved solid mass flow rate in outlet ($\dot{m}_{d,p}$). $X_{c/s}$ is the ratio of crystallized mass in outlet to suspended mass in feed. Total mass flow rate of 200 g/min.

$\dot{m}_{s,f}$ [g/min]	$\dot{m}_{c,p}$ [g/min]	$\dot{m}_{s,p}$ [g/min]	$\dot{m}_{d,p}$ [g/min]	$X_{c/s}$ [kg/kg]
5	15.7	20.7	2.3	3.14
15	14.2	29.2	1.9	0.95
30	11.8	41.8	1.4	0.39

However, the amount of processed material (suspended and dissolved solids) in the SM before blockage was higher for more concentrated suspensions. As depicted in Table 6, the amount of processed material on dry basis increased from 1.24 kg (5 wt.% feed) to 1.77 kg (30 wt.% feed). In general, more processed material (suspended and dissolved solids) before blockage results in higher process efficiency. Thus, our experiments show that pre-concentration of the feed suspension in a precipitating environment can be an important process step to achieve higher material throughputs.
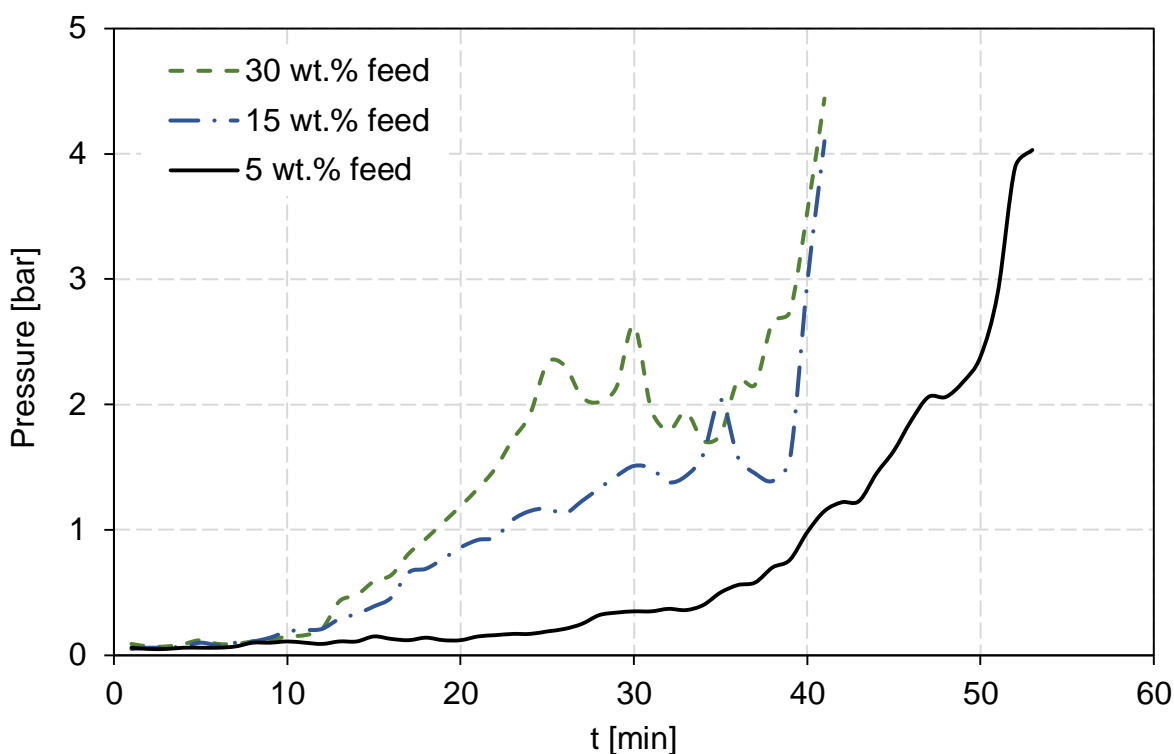
Figure 12. Pressure vs. time of precipitation experiments for different feed suspensions. 200 g/min total mass flow rate. Co-axial mixing of feed and anti-solvent into an outlet pipe with d = 8 mm and a subsequent PSM.

The precipitation experiments of a 15 wt.% feed suspension was repeated with the same settings as before, but with placing the setup in an US bath. In this case, the mixing point of anti-solvent and feed and the SM were irradiated by US. Figure 13demonstrates the influence of US on the process robustness. As can be seen, with US irradiation, the total process time was extended three times from 41 min to 123 min. Furthermore, the amount of processed material increased from 1.27 kg to 3.82 kg (Table 6), drastically increasing the process efficiency by two thirds. The first increase of the process pressure occurred at 50 min versus 8 min without US. Precipitated material did not adhere strongly on the surface of the SM compared with no US. Nevertheless, after some time, the foulant material on the elements of the SM steadily increased until the pressure increased rapidly. The first pressure peak was observed at 79 min, resulting in partial removal (flushing) of adhered material to the SM. After a few minutes, precipitated material started to build up again on the SM. The pressure increased slightly until 96 min, followed by a significant pressure increase until the SM was blocked after 123 min.
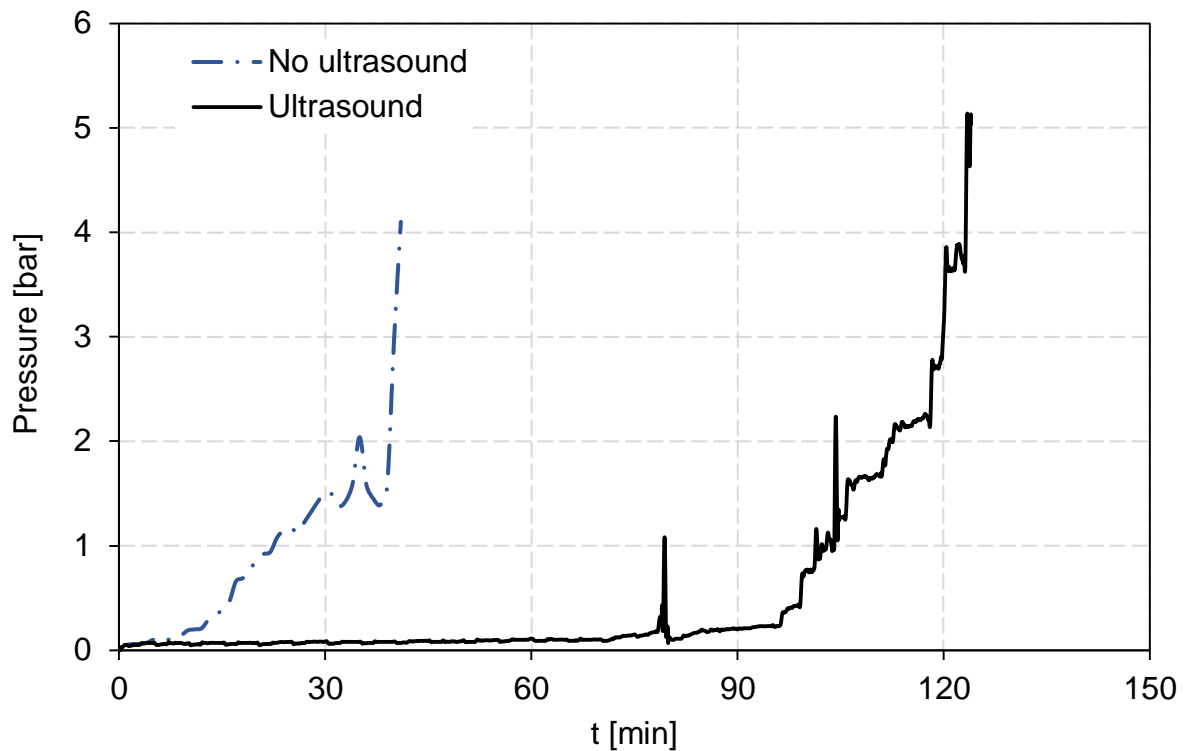
Figure 13. Pressure vs. time of precipitation experiments for a 15 wt.% feed suspension without and with US input. 200 g/min total mass flow rate. Co-axial mixing of feed and anti-solvent into an outlet pipe with d = 8 mm and a subsequent PSM.

In addition to an increase of the total process time, US had no negative influence on the particle size. Figure 14 shows the PSD for a 15 wt.% feed suspension with and without US irradiation. The PSD with and without US irradiation show that there is no significant change of the particle size due to US.
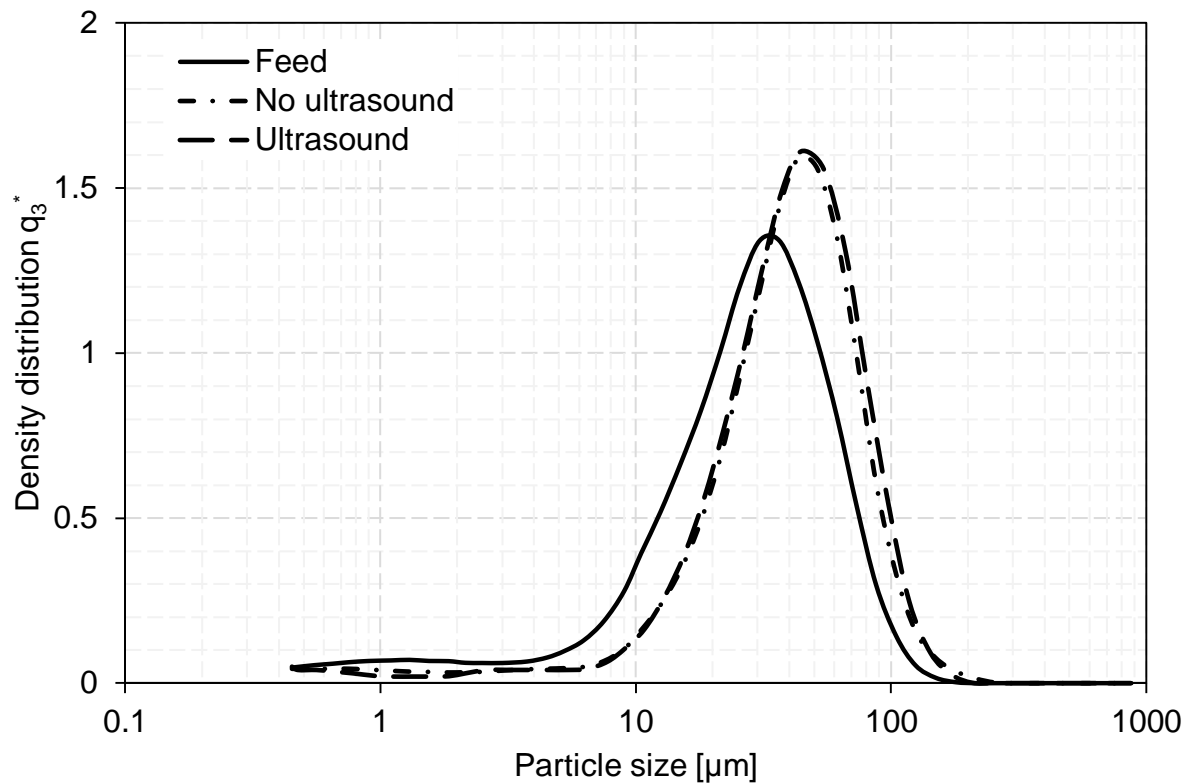
Figure 14. Density PSD q_3^* of the feed and outlet suspensions (with and without US input) after precipitation experiments with 15 wt.% suspended solids in the initial feed suspension.

The previous experiments were carried out by co-axial contact of feed suspension and anti-solvent. First precipitation of dissolved material occurred in the co-axial mixing region. In this region, the feed suspension (inner zone) is surrounded by anti-solvent (outer zone), thus minimizing the contact of solid material with walls from the pipe during precipitation. The first contact of precipitated material with the wall is delayed until the flow reaches the SM. Then mixing occurs in the SM, in which higher Re and flow velocities are predominant because of a reduced free area by the elements of the SM [43]. Switching from co-axial mixing to mixing in the T-piece results in local mixing of feed suspension and anti-solvent. Therefore, most of the precipitation probably occurs in the T-piece. In addition, the flow velocity of the feed suspension at the mixing point was reduced from 322 mm/s (d_i = 2.4 mm) for co-axial mixing to 30 mm/s (d_i = 8 mm) for T-piece mixing. At the mixing point, higher flow velocities and focusing the mixing zone centrally in the pipe are beneficial to avoid buildup of precipitated material.

Figure 15 depicts pressure curves of precipitation experiments for co-axial and T-piece mixing of a 15 wt.% feed suspension with anti-solvent, followed by a SM including

US irradiation. In the case of T-piece mixing, the free surface in the T-piece was quickly reduced by precipitated material, resulting in a faster increase of the pressure compared with co-axial mixing. Parts of the foulant material in the T-piece were flushed out, yet larger agglomerates accumulated before the SM. Total blockage of the system occurred after 79 min due to foulant material in the T-piece and before the SM. The amount of processed material on dry basis decreased from 3.82 kg for co-axial mixing to 2.45 kg for T-piece mixing (Table 6).
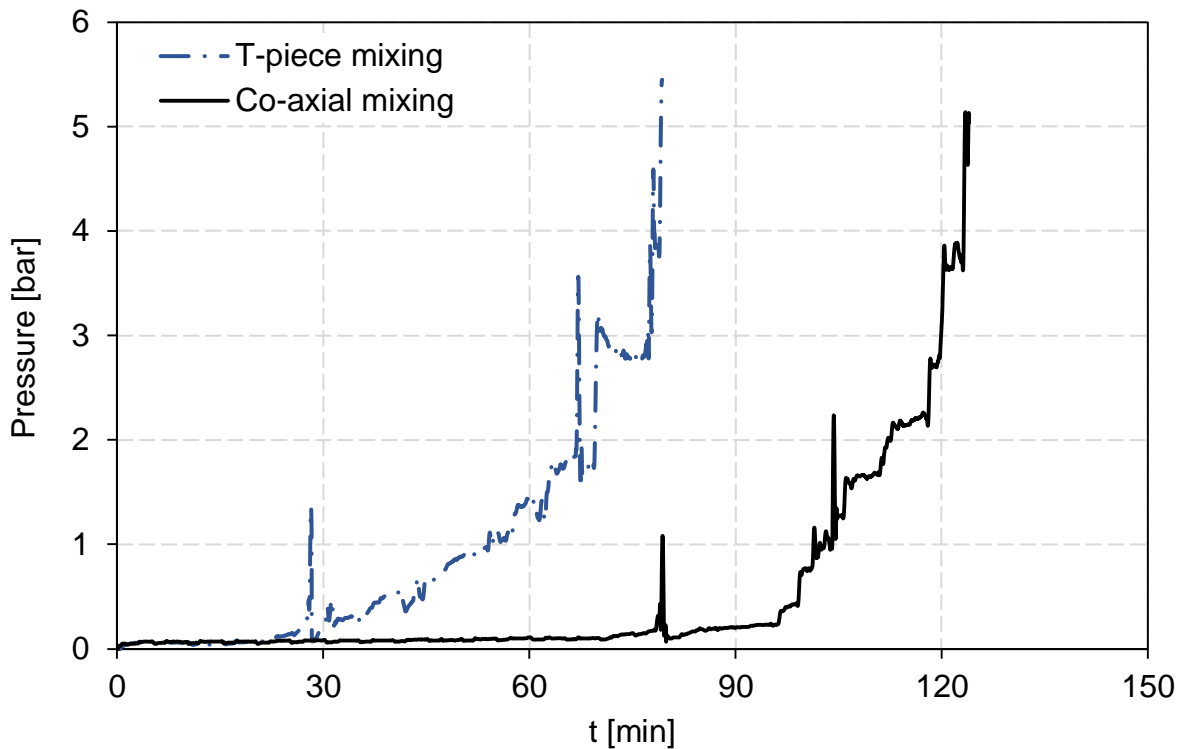
Figure 15. Pressure vs. time of precipitation experiments for a 15 wt.% feed suspension with 200 g/min total mass flow rate. T-piece (perpendicular) or co-axial mixing of feed and anti-solvent into an outlet pipe with d = 8 mm and a subsequent PSM.

All of the previous experiments were carried out by using a plastic PTFE SM with unknown surface roughness. To minimize foulant material on the elements of the static, a metal SM with a surface roughness of Ra < 0.8 µm was used. Figure 16 depicts pressure curves for co-axial mixing of a 15 wt.% feed suspension with the metal mixer. It can be seen, that the pressure buildup was the same for the plastic and metal SM within the first 60 min. Later, more and higher pressure peaks were observed for the metal SM, but the pressure level was lower besides the peaks. This indicates an easier removal of adhered material on the smooth metal surface, resulting in a total process time of 155 min until blockage of the SM.

Furthermore, after the end of the process, the MSM was easier to clean in comparison with the PSM. The effect of US input to remove foulant material is probably higher for the MSM, because the US input is more attenuated in plastic then in metal [44]. The amount of processed material on dry basis increased from 3.82 kg for the PSM to 4.82 kg for the MSM (Table 6).
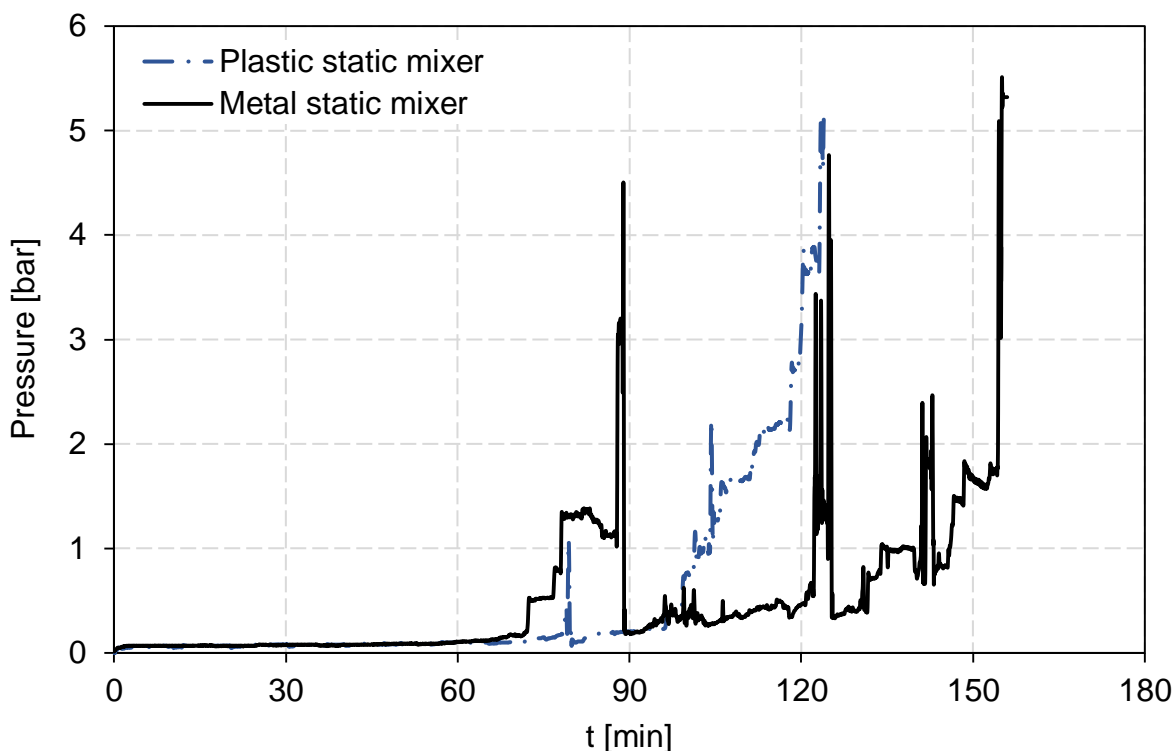
Figure 16. Pressure vs. time of precipitation experiments for a 15 wt.% feed suspension with 200 g/min total mass flow rate. Co-axial mixing of feed and anti-solvent into an outlet pipe with d = 8 mm and a subsequent plastic or metal SM.

The influence of the total mass flow on the process time was investigated in the next experiments. Precipitation experiments were carried out for a 15 wt.% feed suspension with US irradiation and co-axial mixing of feed and anti-solvent in a 1:1 ratio. The total mass flow rate was varied between 200 g/min and 400 g/min, as depicted in Figure 17. The base pressure drop increased from 0.06 bar for 200 g/min to 0.09 bar for 300 g/min, to 0.12 bar for 400 g/min. Reynolds number Re increased from 60 to 130. Surprisingly, the experiment with 300 g/min total mass flow rate showed no pressure peaks, indicating removal of foulant material on the elements of the SM, before blockage occurred after 163 min. The experiment with 400 g/min showed some pressure peaks and flushing of the SM, resulting in a low average pressure level. Due to higher throughput, the total process

time was extended from 155 min (4.82 kg processed material on dry basis, Table 6) for a total mass flow rate of 200 g/min to 287 min (17.83 kg) for a total mass flow rate of 400 g/min.
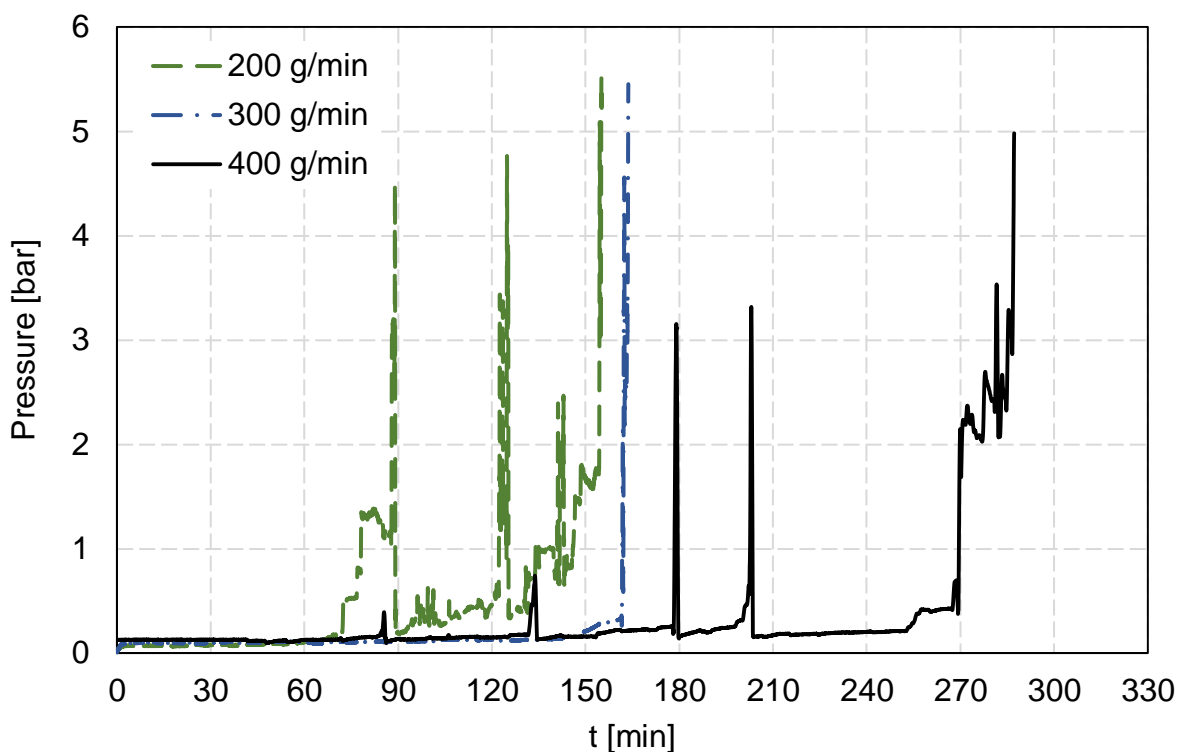
Figure 17. Pressure vs. time of precipitation experiments for a 15 wt.% feed suspension and variation of total mass flow rate between 200 g/min and 400 g/min. Co-axial mixing of feed and anti-solvent into an outlet pipe with d = 8 mm and a subsequent MSM.

Another way of increasing the flow velocity in the system (respectively Re) is to reduce the cross sectional area. Thus, a 6 mm inner diameter of the pipe and a 5.9 mm outer diameter of the SM was used. Precipitation experiments were carried out for a 15 wt.% feed suspension with 400 g/min total mass flow rate, co-axial mixing of feed and anti-solvent with a SM with 6 mm or 8 mm, and US irradiation. Reducing the dimensions of the setup from 8 mm to 6 mm increased the pressure drop over the SM from 0.12 bar to 0.15 bar (Figure 18). Only slight pressure increases were observed for the 6 mm setup before blockage occurred. The visual appearance of the SM after the experiment is depicted in Figure 19. To record this picture, the SM was disassembled from the setup and carefully cleaned with anti-solvent to avoid dissolution of foulant material. It can be clearly seen that the whole SM was covered with precipitated material (no metal surface visible anymore). The metal surface of the SM was only visible in areas where the SM touches the inner wall

of the PFA pipe. Interestingly, the foulant material was only formed on the mixing elements itself, but not on the pipe wall. Similar covering of the SM was also observed in the other precipitation experiments. In this experiment, the blockage was probably caused by a break-off of larger agglomerates from foulant material, which were further transported in flow direction, finally clogging the free residual cross section of the SM. The total process time was extended from 287 min (17.83 kg processed material on dry basis) to 332 min (20.63 kg).
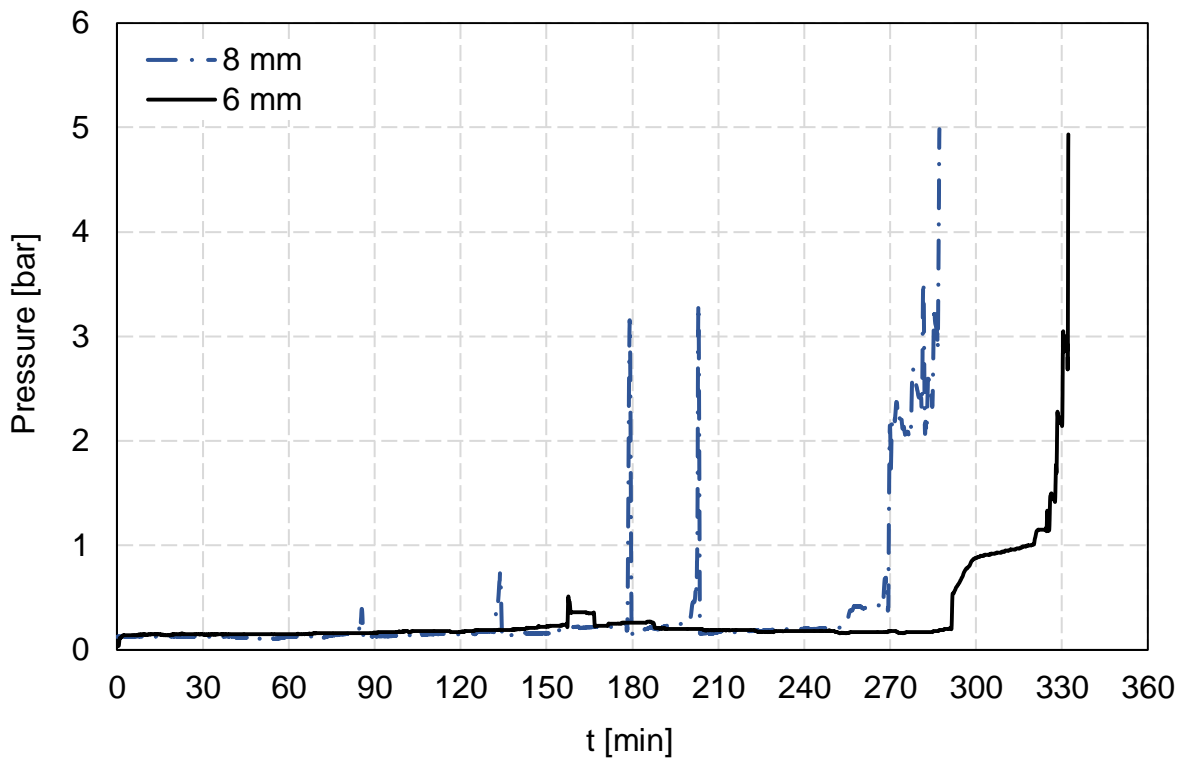
Figure 18. Pressure vs. time of precipitation experiments for a 15 wt.% feed suspension and a total mass flow rate of 400 g/min. Co-axial mixing of feed and anti-solvent into an outlet pipe with d = 8 mm or d = 6 mm and a subsequent MSM.

Figure 19. Foulant material on the elements of the 5.9 mm SM after the end of the precipitation experiment.

Table 6. Process time (t), processed material on dry basis (m_d) and Re empty pipe for different suspended solid mass fraction in feed ($w_{s,f}$), total mass flow rate of outlet ($\dot{m}_p$) and setup configurations of precipitation experiments.

$w_{s,f}$	$\dot{m}_p$	Setup configuration	t	m_d	Re
[wt.%]	[g/min]		[min]	[kg]	[-]
5	200	Co-axial, 8 mm PSM, No US	54	1.24	94
15	200	Co-axial, 8 mm PSM, No US	41	1.27	60
30	200	Co-axial, 8 mm PSM, No US	41	1.77	39
15	200	T-piece, 8 mm PSM, US	79	2.45	60
15	200	Co-axial, 8 mm PSM, US	123	3.82	60
15	200	Co-axial, 8 mm MSM, US	155	4.82	60
15	300	Co-axial, 8 mm MSM, US	164	7.64	94
15	400	Co-axial, 8 mm MSM, US	287	17.83	130
15	400	Co-axial, 6 mm MSM, US	332	20.63	182

A common characteristic of the investigated mixing process is the occurrence of slight or severe pressure spikes before a total blockage of the SM occurred. This can be explained by foulant material, which was gradually built up on the elements of the SM and reduced the cross-sectional area. Therefore, the total flow velocity and accordingly the Re increased until the forces were high enough to break off larger agglomerates of foulant material. The foulant agglomerates were then flushed towards the outlet of the equipment, resulting in sudden pressure spikes due to the fast reduction of the free cross section and subsequently "free-flushing" of the SM pipe. The break off of foulant material in larger fragments is attributable to the brittle material characteristics of crystalline lactose. Therefore, the process pressure curve shows pressure spikes when foulant agglomerates are flushed out, until a break off of a large fragment clogs the free cross-sectional area in the SM pipe resulting in total blockage of the setup.

The total process time in a precipitating environment is influenced by multiple factors, such as co-axial or perpendicular mixing, amount of processed solids, ultrasonication, material of SM and the flow behavior, amongst others. In a study by Hobbs et al., it was shown that the Reynolds number Re (investigated from 0.15-1000) has influence on the velocity fields and the mixing performance of SMs [45]. For Re = 100, zones with low flow velocity occurred close to the mixing elements and this effect was even more pronounced at Re = 1000. In addition, segregated zones were observed by a Poincaré plot for Re = 100

in the middle of the flow in each quadrant of the mixing element. These zones are segregated from the remainder of the flow, and are therefore, potential dead zones of the SM. At Re = 10 and Re = 1000 the segregated zones are not present anymore resulting in globally chaotic flow. Similar observations were made in our experimental investigations by the visible flow behavior through the translucent pipes. Equipment fouling by buildup of precipitated solid material started close to the walls of the mixing elements and also in the previously described segregated zones in the middle of the flow field. The performed experiments were done within a Re range of 39-182, which is close to 100. Possible, such segregated zones play an important role in the formation of agglomerates, leading to equipment fouling and finally blockage. For higher Re numbers (e.g., 6mm mixer) the process time was significantly extended. Thus, increasing the flow velocity either by smaller equipment size or higher mass flow rates had a positive impact on the process time. Another way to enable longer continuous processes in precipitating environments is to use several SMs in parallel arrangement. By doing this, the process could be switched from one SM to another if the pressure gradient exceeds a threshold. The previously used SM can be cleaned in between with the related solvent (in this case water) to remove foulant material, which takes approx. 10 min from our experience. This cleaning time as well as the process time depends on the processed materials and conditions (e.g. fouling rate on equipment surfaces), and has to be adjusted accordingly.

3.4   Conclusions

In this work, the performance of a SM in precipitating environments was investigated with respect to process stability and material properties. A wide range of suspension feed concentrations were considered to evaluate the rate of particle growth during different precipitation scenarios. The rate of particle growth was mainly determined by the amount of suspended solids in the feed suspension, rather than by the dissolved solids. Higher amounts of suspended solids in the feed led to a lower precipitation rate and therefore smaller increase of the outlet particle size. Furthermore, the amount of processed material on a dry basis was higher for concentrated suspensions, and therefore, the process output was increased.

In addition, the long-term stability of SMs in precipitating environments was analyzed. US irradiation increased the total process time by reducing the adhesion of foulant material to the elements of the SM. In this case, the attachment phase, as well as the fouling and aging phase, were delayed before blockage of the SM occurred. Comparing the experiments

with and without US indicates that the particle size of the outlet suspension was not affected by US. The longest process time of more than 5 h was achieved via co-axial mixing of feed and anti-solvent in the 6 mm setup with US irradiation. Smaller dimensions resulted in higher flow velocities (higher Re) in the SM, leading to a slower material fouling rate.

Therefore, it is suggested that mixing processes with SMs in precipitating environments are performed with higher concentrated suspensions (suspended solids equal or higher than 30 wt.%) with higher flow rates in adequate diameters to assure high Re-numbers via co-axial mixing and US irradiation. However, continuous processes in such precipitating environments are limited in terms of time. Further extension of the process time could be realized by parallel arrangement of SMs (redundant SMs), in which the process is switched from one SM to another after a pressure threshold is triggered through foulant material buildup in the SM. In the meantime, the previously-used SM could be flushed with a solvent to remove the foulant material. The number of SMs in parallel would be determined by the time needed for cleaning of the SM versus the process time until a switch is necessary.

References

[1]   A. Ghanem, T. Lemenand, D. Della Valle, and H. Peerhossaini, "Static mixers: Mechanisms, applications, and characterization methods - A review," Chem. Eng. Res. Des., vol. 92, no. 2, pp. 205–228, 2014.

[2]   M. Bayat, M. R. Rahimpour, M. Taheri, M. Pashaei, and S. Sharifzadeh, "A comparative study of two different configurations for exothermic-endothermic heat exchanger reactor," Chem. Eng. Process. Process Intensif., vol. 52, pp. 63–73, 2012.

[3]   S. Ferrouillat, P. Tochon, C. Garnier, and H. Peerhossaini, "Intensification of heat-transfer and mixing in multifunctional heat exchangers by artificially generated streamwise vorticity," Appl. Therm. Eng., vol. 26, no. 16, pp. 1820–1829, 2006.

[4]   R. Thakur, C. Vial, K. Nigam, E. B. Nauman, and G. Djelveh, "Static Mixers in the Process Industries—A Review," Chem. Eng. Res. Des., vol. 81, no. 7, pp. 787–826, 2003.

[5]   Z. Anxionnaz, M. Cabassud, C. Gourdon, and P. Tochon, "Heat exchanger/reactors (HEX reactors): Concepts, technologies: State-of-the-art," Chem. Eng. Process. Process Intensif., vol. 47, no. 12, pp. 2029–2050, 2008.

[6]   M.-C. Fournier, L. Falk, and J. Villermaux, "A new parallel competing reaction system for assessing micromixing efficiency—Experimental approach," Pergamon Chem. Eng. Sci., vol. 51, no. 22, pp. 5053–5064, 1996.

[7]   J. Baldyga and J. R. Bourne, Turbulent Mixing and Chemical Reactions. Wiley, 1999.

[8]   C. Castelain, A. Mokrani, P. Legentilhomme, and H. Peerhossaini, "Residence time distribution in twisted pipe flows: helically coiled system and chaotic system," Exp. Fluids, vol. 22, no. 5, pp. 359–368, 1997.

[9]   J. Aubin, D. F. Fletcher, and C. Xuereb, "Design of micromixers using CFD modelling," Chem. Eng. Sci., vol. 60, no. 8–9 SPEC. ISS., pp. 2503–2516, 2005.

[10]   I. M. Sokolov and A. Blumen, "Distribution of striation thicknesses in reacting lamellar systems," Phys. Rev. A, vol. 43, no. 12, pp. 6545–6549, 1991.

[11]   A. Ghanem, T. Lemenand, D. Della Valle, and H. Peerhossaini, "Transport Phenomena in Passively Manipulated Chaotic Flows: Split-and-Recombine Reactors," in Volume 1B, Symposia: Fluid Machinery; Fluid Power; Fluid-Structure Interaction and Flow-Induced Noise in Industrial Applications; Flow Applications in Aerospace; Flow Manipulation and Active Control: Theory, Experiments and Implementation; Fundamental Iss, 2013, p. V01BT15A002.

[12]   J. Branebjerg, B. Fabius, and P. Gravesen, "Application of Miniature Analyzers: from Microfluidic Components to μTAS," in Micro Total Analysis Systems: Proceedings of the $μ$TAS '94 Workshop, held at MESA Research Institute, University of Twente, The Netherlands, 21--22 November 1994, A. den Berg and P. Bergveld, Eds. Dordrecht: Springer Netherlands, 1995, pp. 141–151.

[13]   N. Kockmann, T. Kiefer, M. Engler, and P. Woias, "Silicon microstructures for high throughput mixing devices," Microfluid. Nanofluidics, vol. 2, no. 4, pp. 327–335, 2006.

[14]   J. B. Salmon, A. Ajdań, P. Tabeling, L. Servant, D. Talaga, and M. Joanicot, "In situ Raman imaging of interdiffusion in a microchannel," Appl. Phys. Lett., vol. 86, no. 9, pp. 1–3, 2005.

[15]   Y. Men, V. Hessel, P. Löb, H. Löwe, B. Werner, and T. Baier, "Determination of the Segregation Index to Sense the Mixing Quality of Pilot- and Production-Scale Microstructured Mixers," Chem. Eng. Res. Des., vol. 85, no. 5, pp. 605–611, 2007.

[16] T. R. Bott, Fouling of heat exchangers. Amsterdam: Elsevier B.V., 1995.

[17] R. Sheikholeslami, "Composite fouling of heat transfer equipment in aqueous media – A review," Heat Transf. Eng., vol. 21, no. 3, pp. 34–42, 2000.

[18] H. Müller-Steinhagen, "Cooling-Water Fouling in Heat Exchangers," Adv. Heat Transf., vol. 33, no. C, pp. 415–496, 1999.

[19] J. Mitrovic, Heat Exchangers - Basics Design Applications. InTech, 2012.

[20] L. F. Melo, T. R. Bott, and C. A. Bernardo, Fouling Science and Technology. Dordrecht: Springer Netherlands, 1988.

[21] H. Müller-Steinhagen, F. Reif, N. Epstein, and A. P. Watkinson, "Influence of operating conditions on particulate fouling," Can. J. Chem. Eng., vol. 66, no. 1, pp. 42–50, 1988.

[22] M. M. Awad, "Fouling of Heat Transfer Surfaces," in Heat Transfer - Theoretical Analysis, Experimental Investigations and Industrial Systems, vol. 10, no. 1, A. Belmiloudi, Ed. InTech, 2011, pp. 505–542.

[23] N. Epstein, "Elements of particle deposition onto nonporous solid surfaces parallel to suspension flows," Exp. Therm. Fluid Sci., vol. 14, no. 4, pp. 323–334, 1997.

[24] C. A. Bennett, "A Theory Describing Sedimentation Particulate Fouling Thresholds Inside Heat Exchanger Tubes," Heat Transf. Eng., vol. 37, no. 5, pp. 468–474, 2016.

[25] T. R. Bott, "Aspects of crystallization fouling," Exp. Therm. Fluid Sci., vol. 14, no. 4, pp. 356–360, 1997.

[26] D. I. Wilson and A. Paul Watkinson, "A Study of Autoxidation Reaction Fouling in Heat Exchangers," Can. J. Chem. Eng., vol. 74, no. 2, pp. 236–246, 1996.

[27] G. Dickakian and S. Seay, "Asphaltene precipitation primary crude exchanger fouling mechanism," Oil Gas J., vol. 86, 1988.

[28] J. Yang, M. G. J. Serratos, D. S. Fari-Arole, E. A. Müller, and O. K. Matar, "Crude Oil Fouling: Fluid Dynamics, Reactions and Phase Change," Procedia IUTAM, vol. 15, pp. 186–193, 2015.

[29] M. Hochstrasser, D. Jussen, and P. Riedlberger, "Towards process intensification: Remediation of fouling in continuous microscale synthesis of phosphated TiO2," Chem. Eng. Process. Process Intensif., vol. 121, no. January, pp. 15–23, 2017.

[30] M. Schoenitz, L. Grundemann, W. Augustin, and S. Scholl, "Fouling in microstructured devices: A review," Chem. Commun., vol. 51, no. 39, pp. 8213–8228, 2015.

[31] J. A. Barish and J. M. Goddard, "Anti-fouling surface modified stainless steel for food processing," Food Bioprod. Process., vol. 91, no. 4, pp. 352–361, 2013.

[32] Y. Dong, W. K. Ng, J. Hu, S. Shen, and R. B. H. Tan, "A continuous and highly effective static mixing process for antisolvent precipitation of nanoparticles of poorly water-soluble drugs," Int. J. Pharm., vol. 386, no. 1–2, pp. 256–261, 2010.

[33] J. Hu, W. K. Ng, Y. Dong, S. Shen, and R. B. H. Tan, "Continuous and scalable process for water-redispersible nanoformulation of poorly aqueous soluble APIs by antisolvent precipitation and spray-drying," Int. J. Pharm., vol. 404, no. 1–2, pp. 198–204, 2011.

[34] M. Zlokarnik, Rührtechnik: Theorie und Praxis. 1999.

[35] J. J. B. Machado, J. A. Coutinho, and E. A. Macedo, "Solid–liquid equilibrium of α-lactose in ethanol/water," Fluid Phase Equilib., vol. 173, no. 1, pp. 121–134, 2000.

[36] J. A. Hourigan, E. V. Lifran, L. T. T. Vu, Y. Listiohadi, and R. W. Sleigh, "Lactose: Chemistry, Processing, and Utilization," in Advances in Dairy Ingredients, Oxford, UK: Wiley-Blackwell, 2013, pp. 21–41.

[37]   R. W. Hartel and A. V Shastry, "Sugar crystallization in food products," Crit. Rev. Food Sci. Nutr., vol. 30, no. 1, pp. 49–112, 1991.

[38]   E. J. McDONALD and a L. Turcotte, "Density and refractive indices of lactose solutions," J. Res. Natl. Bur. Stand. (1934)., vol. 41, no. 1, pp. 63–68, 1948.

[39]   M. Kreimer et al., "Mechanical strength of microspheres produced by drying of acoustically levitated suspension droplets," Powder Technol., 2017.

[40]   S. Mueller, E. W. Llewellin, and H. M. Mader, "The rheology of suspensions of solid particles," Proc. R. Soc. A Math. Phys. Eng. Sci., vol. 466, no. 2116, pp. 1201–1228, 2010.

[41]   W. M. Haynes, T. J. Bruno, and D. R. Lide, CRC handbook of chemistry and physics. Boca Raton, FL: CRC Press, 2015.

[42]   B. J. Konijn, O. B. J. Sanderink, and N. P. Kruyt, "Experimental study of the viscosity of suspensions: Effect of solid fraction, particle size and suspending liquid," Powder Technol., vol. 266, pp. 61–69, 2014.

[43]   M. Gavrilescu and R. Z. Tudose, "Intensification of transfer processes in biotechnology and chemical engineering using static mixers," Acta Biotechnol., vol. 15, pp. 3–26, 1995.

[44]   Y. Zhang, "Measuring Acoustic Attenuation of Polymer Materials Using Drop Ball Test," Embry-Riddle Aeronautical University, 2013.

[45]   D. M. Hobbs and F. J. Muzzio, "Reynolds number effects on laminar mixing in the Kenics static mixer," Chem. Eng. J., vol. 70, no. 2, pp. 93–104, 1998.
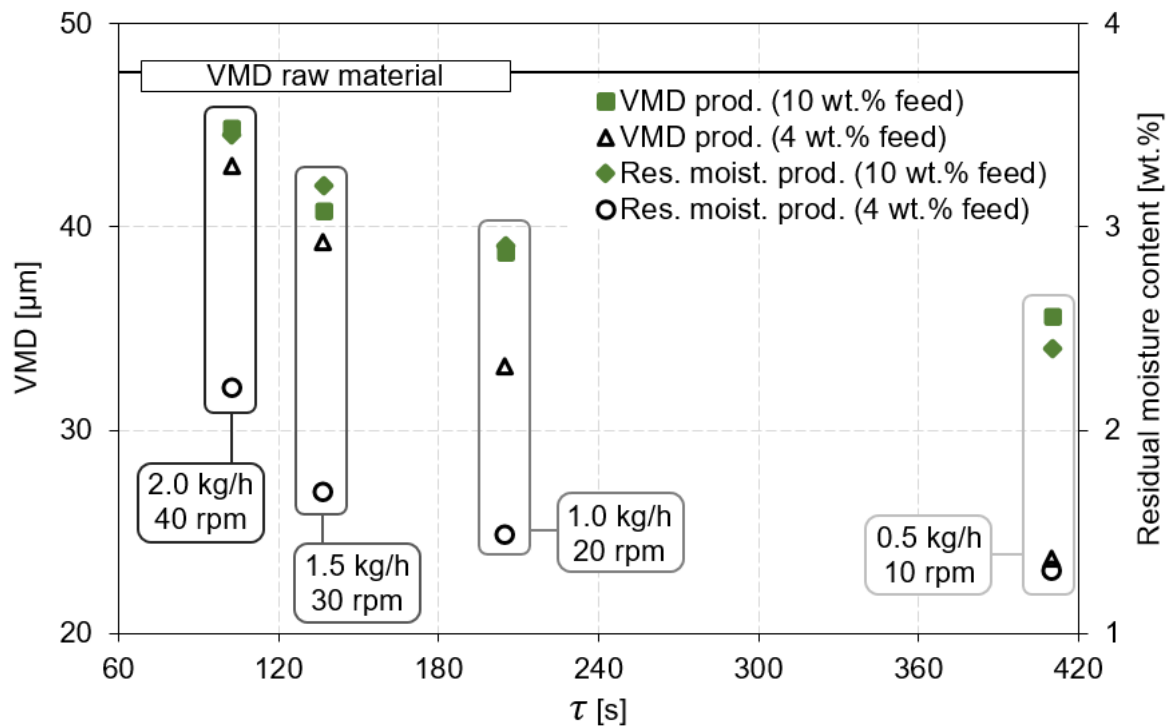
4. Continuous Drying of Pharmaceutical Powders Using a Twin-Screw Extruder

Manuel Kreimer[1], Isabella Aigner[1], Daniel Lepek[123], Johannes Khinast[1,3,]

TOC graphic

Continuous Drying of Pharmaceutical Powders Using a Twin-Screw Extruder

Manuel Kreimer[1], Isabella Aigner[1], Daniel Lepek[123], Johannes Khinast[1,3,]

[1] Research Center Pharmaceutical Engineering (RCPE) GmbH, 8010 Graz, Austria

[2] Department of Chemical Engineering, The Cooper Union, New York, New York 10003, United States

[3] Institute for Process and Particle Engineering, Graz University of Technology, 8010 Graz, Austria

*Corresponding author: Johannes Khinast

Tel. number: 0043 316 873 30400

E-mail address: khinast@tugraz.at

Abstract

Continuous manufacturing of pharmaceuticals offers such benefits as production flexibility, reduced drug product costs, and improved product quality. Moving toward continuous manufacturing requires suitable small-scale equipment, either by development of new equipment or optimization of existing equipment. In primary manufacturing, particle properties are often altered during crystallization and have to be restored during subsequent processing. Drying a crystallized product is one of the most challenging steps, especially since attrition and agglomeration can occur. To that end, we investigated the drying behavior of a crystalline model compound with moisture levels of up to 10 wt.% in a corotating twin-screw extruder. The feed mass flows on a piece of small-scale equipment used for pharmaceutical production varied between 0.5 and 2.0 kg/h. Experiments were conducted to evaluate the drying performance in various process settings. Because of a very narrow and consistent residence time distribution, extrusion drying has the potential for pharmaceutical compound drying. In our study, we successfully accomplished drying of a crystalline product with very little agglomeration and/or attrition in some process settings while preserving a crystal size similar to the raw material. The reduction in particle size occurred as a result of long residence times (low extruder screw speed) and a decrease in the residual moisture of the product. The aim of our work was to show the

potential of extruder drying as a novel continuous manufacturing process for pharmaceuticals and to enable further process development.

Nomenclature

C	concentration of the tracer
d_{50}	median diameter [µm]
E	density exit-age distribution
F	cumulative exit-age distribution
SMD	sauter mean diameter [µm]
t_x	time until x % of the tracer is removed [s]
VMD	volume mean diameter [µm]
τ	mean residence time [s]
R_{MS}	ratio of feed mass flow to screw speed [kg]

Abbreviations

API	active pharmaceutical ingredient
BCS	biopharmaceutics classification system
Lab	L for lightness, a and b for the color components (green-red and blue-yellow, respectively)
PSD	particle size distribution
RGB	red-green-blue
RTD	residence time distribution
SLR	single-lens reflex

4.1 Introduction

In pharmaceutical production, most of the unit operations are still performed via batch manufacturing. Batch manufacturing is widely used throughout industry and is accepted by the regulatory bodies. However, recent efforts by regulators and industry focus on well-controlled continuous manufacturing operations that yield consistent quality of the products.[1] Continuous production offers major benefits, including faster process development, straightforward scale-up, a smaller ecological footprint, and a better product quality via online monitoring and real-time testing.[2] Having recognized the potential of continuous production, some regulatory authorities now actively support the implementation of new production processes.[3] Furthermore, continuous manufacturing equipment can be used in formulation development, clinical trials, and fully automated continuous production.[4] Moreover, expiring patents of blockbusters and competition with generic companies prompt the pharmaceutical industry to increase their production efficiency.[5,6] Scale-up issues between small- and large-scale production can be prevented because the same equipment is used for formulation development and production. Larger quantities of the final production process are easily obtained by using longer process times.[6]

A simple approach for a shift toward a continuous production line is transforming batch processes into continuous ones unit by unit. Such transformations are especially easy if the specific step is continuous by nature, e.g., roller compaction, tableting, spray drying, and twin-screw wet granulation and extrusion.[7] In such production processes, the material is fed continuously and the finished product is removed continuously as well.[8,9] More advanced continuous processes, however, integrate several unit steps into one, i.e., during hot-melt extrusion.

An integrated continuous manufacturing plant contains numerous operations, beginning with active pharmaceutical ingredient (API) synthesis, purification, crystallization, and drying in primary manufacturing (dry powder as an intermediate product) and continuing with feeding, blending, tableting / capsule filling, optional coating and packaging in secondary manufacturing[10] (e.g., such an end-to-end continuous manufacturing approach to tablet production was proposed by Mascia et al.[11]).

In primary manufacturing, a transfer from the liquid state (e.g., wet powder, filter cake, paste, or slurries) to a solid dry powder is an especially crucial step. Since thermal drying is an energy-consuming process, as much of the liquid phase as possible is removed via mechanical drying,[12] e.g., filtration.[13,14] After mechanical removal of a large fraction of the

liquid phase, further thermal drying steps are required. Typically, tray or filter-bed systems, spray drying, spin-flash drying, or paddle drying is employed to achieve a desired moisture level in the product.[15] However, most technology currently available is operated in batch mode.

In a thermal dryer, the heat transfer is achieved either via convection (i.e., gas to liquid heat transfer during flow) or conduction (i.e., transfer of energy to the wet material through a hot surface).[16] Each of the drying modes can be used separately, with conductive drying being more environmentally friendly due to a higher thermal efficiency.[17] Various modern dryers use combined convective and conductive drying, providing better heat and mass transfer than dryers with only one mode of heat transfer.

API drying prior to solid-dosage-form production is a critical step in primary manufacturing since the particle morphology (e.g., particle size and shape distribution, etc.) achieved by crystallization should be carefully maintained.[18] This, however, is a significant challenge, as is well-known by practitioners in the field. In general, drying is a complex process, and uncontrolled drying can lead to an unsuitable particle morphology [19] or the formation of an unspecified polymorph state.[20] During drying, several phenomena, such as agglomerate formation by interparticle bonding forces, attrition, (re)crystallization and redissolution, may occur simultaneously. While agglomeration produces larger particles, attrition can lead to the formation of smaller fractions of fines. Both effects are undesirable in pharmaceutical manufacturing: small particles have poor flowability, which may affect blending or the tableting stage, and larger particles may result in low dissolution rates, which may influence the drug's bioavailability profile.[21] A reduction in the particle size during the process occurs via particle collisions (with each other or with equipment surfaces) due to shearing [17,22-25] or through induced stresses generated by pressure or temperature changes inside the machine. [26-28] Besides particle size reduction caused by the drying process, attrition is also affected by the particle properties such as size, shape, and hardness. The attrition rate is a strong function of the particle shape.[29,30] It has been reported that cubic particles have a higher resistance to attrition than needle-shaped ones.[22]

However, agglomerates are formed when wet particles stick together as a result of interparticle forces (e.g., liquid or solid bridges, van der Waals forces, viscous forces).[31] The most important interparticle force during drying is due to liquid bridges, which hold adjacent particles together.[17,32] As drying progresses, the liquid bridge evaporates, and the particles move closer to each other. Concurrently, the liquid force increases, resulting in a

higher probability of agglomerate formation.[31] In addition, liquid bridges may contain dissolved components, which precipitate during drying, forming strong solid bridges and agglomerates.[33,34] Such agglomeration effects are desired in twin-screw granulators, where fine powders are transformed into coarser granules.[35] Process parameters such as the liquid-to-solid ratio, method of binder addition, screw elements, screw speed and material feed rate greatly influence the final granule properties.[36-38]

In a dryer, the final particle size distribution (PSD) is influenced by the shear movement since agglomeration and/or attrition are present throughout the entire drying process.[21,27,39-41] The shear a single particle or granule experiences during drying can vary significantly from substance to substance and across the equipment scales and drying phases.[42] Thus, it is difficult to predict and control the performance of specific drying configuration in terms of impact on the PSD and shape. For example, dried material may be more susceptible to breakage due to mechanical forces caused by particle-particle and particle-equipment attrition, while a liquid layer in wetter materials may serve as a lubricant, preventing attrition.[21,41] Thus, overdrying may result in unintentional milling. However, more shear and thus more attrition, may occur in wetter materials during drying as a result of restricted mobility and therefore greater drive power required for agitation compared with drier materials.[42] Which of these effects dominates during drying depends on the material and the drying equipment used. To establish the performance of a drying process, experimental investigations to determine the influence of drying on the particle properties are required.

Drying of pharmaceuticals is still mainly conducted via batch processing.[9,21,27,39-41] An example of a semicontinuous drying method is fluidized bed drying, with six small batch fluidized bed compartments linked together.[2,43] Nevertheless, establishing a stable fluidized bed for fine cohesive particles is challenging since such materials do not fluidize.[44-46] As a result, there is a lack of continuous drying equipment on the market designed for drying of small-particle-size pharmaceuticals.

Previously, twin-screw granulators (e.g., the Consigma system by GEA) have been introduced for the continuous production of granules.[35-38] However, in this work we investigated small-scale continuous drying based on extrusion. In this case, the applicability of continuous extrusion drying was assessed in regard to drying while avoiding particle size changes. The drying capacity of the extruder and the material properties were evaluated by measuring the residual moisture content and the particle size. Correlations were established between the process settings, moisture content of the

feed, and dried powder particle properties. Furthermore, the drying process was characterized by measuring the residence time.

4.2   Materials and Methods

4.2.1   Materials

Naproxen was obtained from Bin Bo Biological (Shandong, China). It is a BCS Class II substance with a d_{50} of 47 µm and a PSD as shown in Figure 1. Actual light microscopy images of particles are shown in Figure 2. As can be seen, the particles are rather cubic with some larger ones having irregular shapes. The bulk density of the raw material is 0.475 g·cm^{-3}. The drug substance was mixed in various ratios with water of analytical grade produced via an Ultrapure Water System from TKA (Niederelbert, Germany). To ensure uniform dispersion and enable good water wettability of naproxen, 8 g of sodium pyrophosphate tetrabasic (Sigma-Aldrich, MO, USA) per liter of water was predissolved.[15] The starting material was prepared in a UMC 5 mixer (Stephan Machinery, Hameln, Germany) by mixing naproxen and water at 75% power for 1 min. Two moisture levels were prepared, i.e., 10 wt.% (90 wt.% solid feed concentration) and 4 wt.% (96 wt.% solid feed concentration). No change in the PSD was observed prior to and after mixing (results not shown). Since naproxen is poorly soluble in water (15.9 mg/L at 25 °C), the dissolved components were neglected.[47]
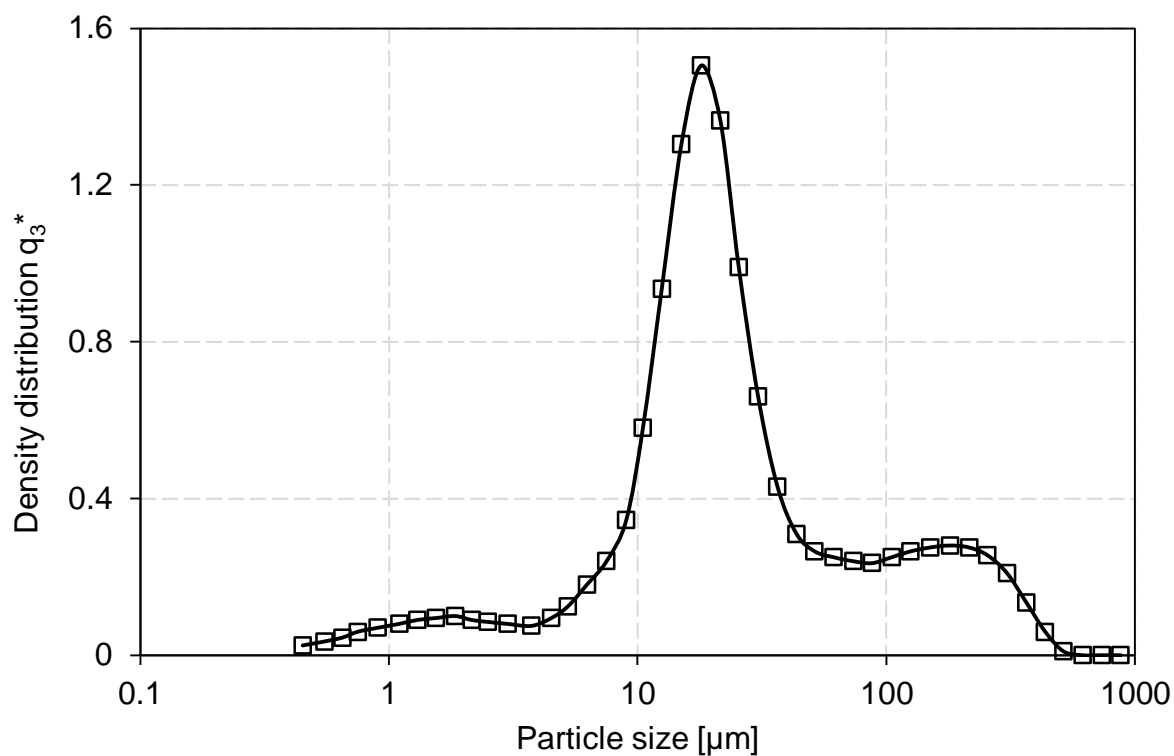
Figure 1. PSD of naproxen raw material.
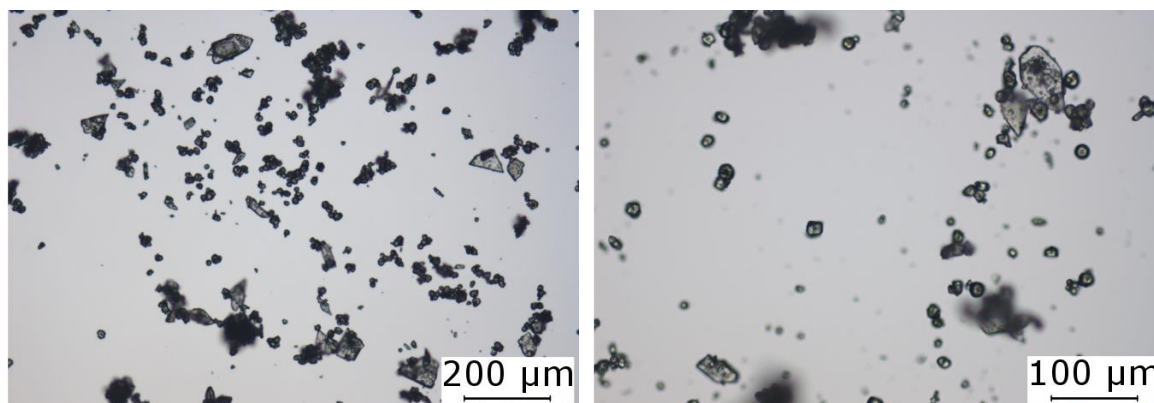
Figure 2. Light microscopy images of naproxen raw material.

4.2.2 Process Equipment and Settings

The process equipment consisted of a K-Tron K-CL-SFS-KT20 feeder (Coperion, Stuttgart, Germany), a Micro 27 twin-screw extruder (Leistritz, Nürnberg, Germany), a conveying belt, a D5200 digital SLR camera (Nikon, Tokyo, Japan), a product container, and a ML6002T scale (Mettler Toledo, Columbus, OH, USA), as depicted in the schematic process flow sheet in Figure 3. The extruder process setup is shown in Figure 4.
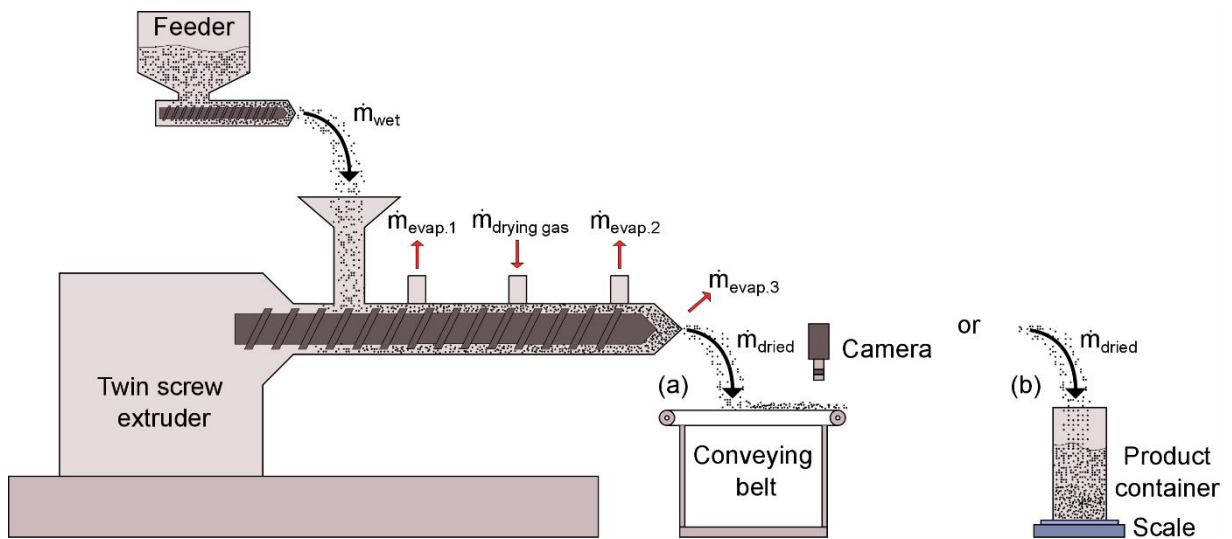
Figure 3. Process flow sheet of extrusion drying for (a) RTD and (b) dried product mass flow measurements.
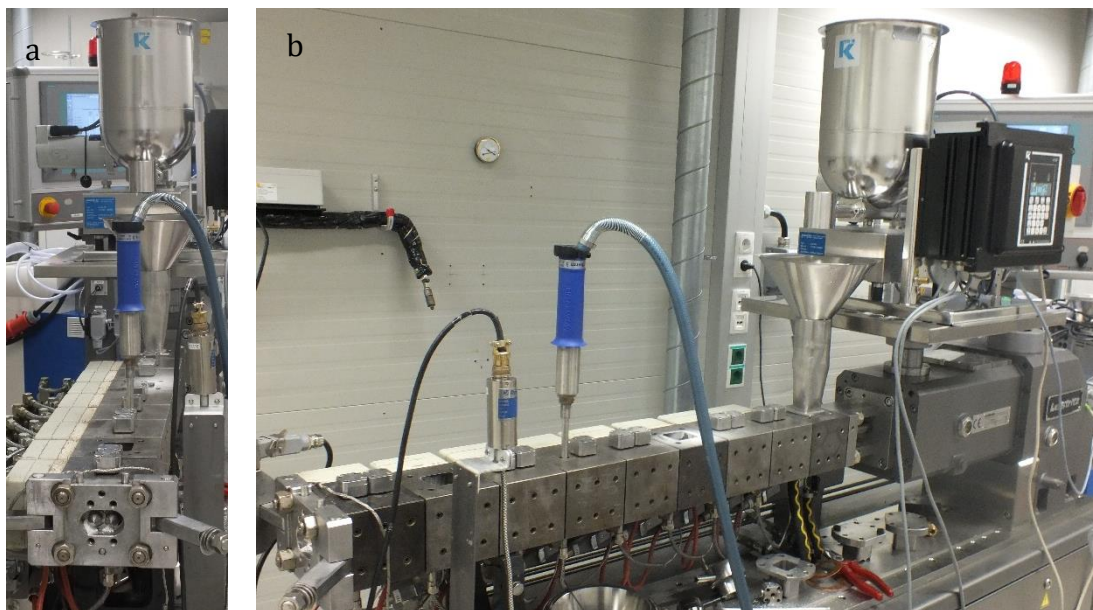
Figure 4. (a) Front and (b) side views of the extruder process setup.

The Leistritz Micro 27 extruder is a hot-melt extruder with two self-cleaning intermeshing 27 mm screws (L/D = 36) and a shear gap of 0.1 mm. The housing consists of nine individually heated blocks. The temperatures were set at 50 °C in the inlet zone (housing block 1) and 100 °C in the subsequent zones (housing blocks 2-9). The screw and housing configurations are presented in Figure 5. The feed material entered the extruder in zone 1

(housing block 1) and was transported along the screws toward the outlet. Drying air was introduced in zone 6 at a temperature of 25 °C and a volumetric flow rate of 0.5 Nm³/h. Zones 4 and 8 were left open to release the moisture-carrying air. The drying air was also released at the end (zone 9). Because of those open zones, a low drying air flow rate was specifically chosen to avoid blowing out of fines, as observed in pretrials (results not shown). Different drying conditions were created throughout the process: countercurrent drying between zones 4 and 6 and cocurrent drying between zones 6 and 8. In zones 3 to 9, the extruder had high-pitch conveying elements only partly filled with material to enable efficient drying air circulation and to minimize mechanical energy input on the particles.[48] The combination of co- and countercurrent drying was specifically chosen to enable low outlet drying air flow, thereby avoiding blowing out of fines. To avoid back flow of drying air from the vented zone into the inlet zone, left-pitch kneading elements were installed on the extruder screw in zone 2. They ensured complete filling of the preceding element with moist powder, effectively insulating the inlet zone from the subsequent vented zones.
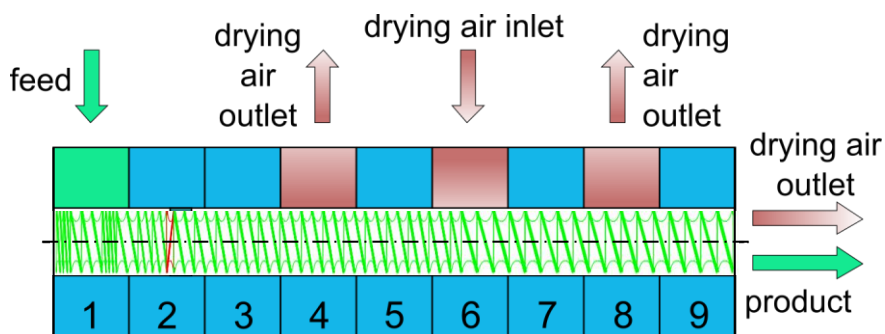
Figure 5. Sectioned view of housing blocks and extruder screw with material and drying air flow.

The wetted material was fed into the extruder and dried along the screw via a mixture of convective and conductive drying. The dried material was transported either on a conveying belt to record the residence time distribution (RTD) (Figure 3) or filled into a product container placed on a scale to measure the dried product mass flow (Figure 3). Recording the dried product mass flow immediately after it was placed on the conveying belt would result in inaccurate mass flow measurements due to slight material losses along the conveying operation. To that end, two separate experiments were performed, one for the RTD and one for the mass flow measurements.

A detailed experimental plan is provided in Table 1. The influence of process parameters on the processability and product properties was investigated by altering the initial moisture content in the feed, the feed rate and the extruder screw speed. The extruder screw speed and feed rate were varied while keeping R_{MS} (Eq. 1) constant at 0.83 g.

$$R_{MS} = \frac{Feed\ mass\ flow}{Screw\ speed} \qquad (1)$$

For each experiment, the processing time was 45 min, and a total of three samples was collected. The first sample was obtained after 30 min to ensure sampling during steady-state operation, and the next ones were obtained at 34 and 40 min.

Table 1. Material and Experimental Settings of Extrusion Drying Experiments

| moisture content in feed [wt.%]	solid feed concentration [wt.%]	ρ_{feed} [g·cm^{-3}]	naproxen feed rate [kg/h]	water feed rate [kg/h]	total set feed rate [kg/h]	extruder screw speed [rpm]
4	96	0.485	0.48	0.02	0.5	10
4	96	0.485	0.96	0.04	1.0	20
4	96	0.485	1.44	0.06	1.5	30
4	96	0.485	1.92	0.08	2.0	40
10	90	0.501	0.45	0.05	0.5	10
10	90	0.501	0.9	0.1	1.0	20
10	90	0.501	1.35	0.15	1.5	30
10	90	0.501	1.8	0.2	2.0	40

4.2.3 Material and Process Characterization

The raw materials, products and process were characterized in detail by measuring the PSD, residual moisture content and RTD. The volume-based density PSD, q_3^*, was assessed via laser diffraction using a Helos KR analyzer (Sympatec GmbH, Clausthal-Zellerfeld, Germany). Measurements were performed in wet-dispersed mode to uniformly disperse particles in the measuring liquid (water), thus enabling single-particle size measurements. To evaluate the drying performance, the residual moisture content was analyzed via MLS 50 3HA250 infrared moisture analyzer (Kern, Balingen, Germany). The drying temperature of the analyzer was constant at 130 °C. The residual moisture content was

determined after 240 s of weight consistency smaller than 1 mg based on a total samples mass of 2.5 g. The values for the residual moisture content are shown in wt.% based on the total mass. Each sample was analyzed in triplicate in terms of particle size and residual moisture, resulting in nine samples (three different times) for each process setting.

The RTD of the extruder was determined by adding a tracer at the extruder inlet and recording the powder flow with a camera at the outlet on a conveying belt. The setup for the conveying belt and light source is shown in Figure 6. The tracer material, iron (III) oxide (Sigma-Aldrich), was added through an impulse injection (30 mg) at the extruder inlet. Fe_2O_3 provided excellent coloring of naproxen due to its fine inorganic particles (particle size < 5 μm) at low concentrations. A change in the color from pure-white naproxen to reddish-colored naproxen and back to white again was recorded with the camera. Before data acquisition at 25 frames/s, a white balance was established manually by placing a white sheet of paper under measurement conditions to remove the influence of illumination.[49] Particular attention was paid to bright and homogeneous illumination of the recorded video sequence in order to prevent such undesired effects as a change in lightness (e.g., by a change in the ambient daylight). The material that remained on the conveyer belt was collected after data acquisition with a rotating brush and a vacuum cleaner to remove the remains of the powder adhering to the belt during previous rotations.
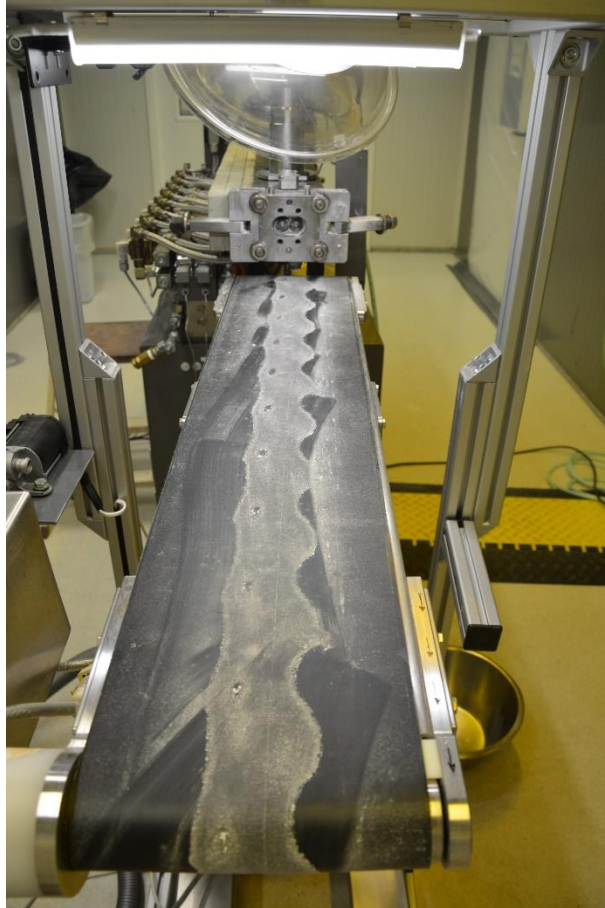
Figure 6. Setup of RTD measurements with the conveying belt and light source (camera not shown). The residual powder on the conveying belt after cleaning of the belt with a brush and a vacuum cleaner is visible.

Evaluation of the acquired data was performed using MATLAB. A specific region in the center of the powder layer on the conveying belt was selected (Figure 7). The recorded data from the camera in red-green-blue (RGB) color space was transformed into the *Lab* color space. In this way, variation in the brightness of the material due to its tracer content was reduced, and the lightness (L) was separated from the color values (*a* and *b*).[50] The red color of the tracer, represented by the *a* value in the *Lab* space was used for further data processing. Nonlinearity between the color value and the concentration was neglected since the tracer concentration varied only within a small range, suggesting a nearly linear relationship.[51]
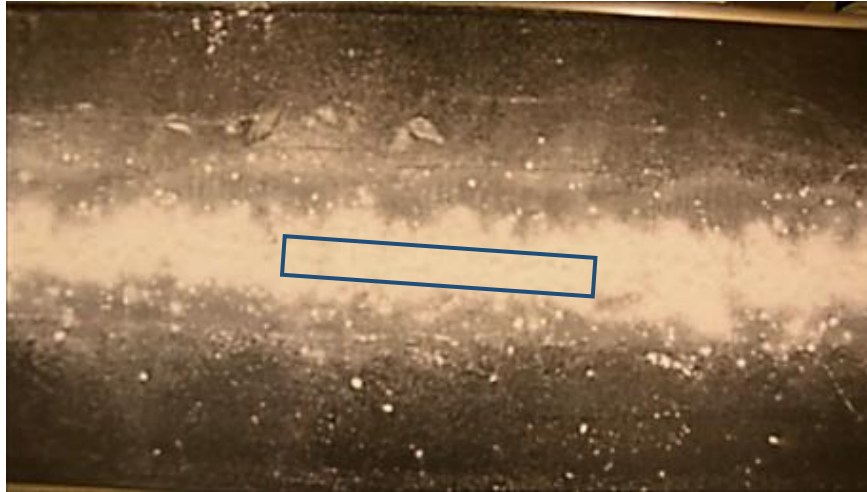
Figure 7. Image of the video sequence of RTD measurements. The rectangular selection (5 mm x 40 mm) shows the specific region of interest for the RTD evaluation in the main powder flow.

The RTD was determined by calculating the exit-age distribution $E(t)$, as shown in Eq. 2. $C(t)$ is the time-dependent concentration of the tracer at the outlet of the extruder on the conveying belt. Since the RTD is a probability density function, the condition $\int_0^\infty E(t)dt = 1$ has to be fulfilled. In addition to the RTD curve, other parameters of the exit-age distribution (τ, t_5, t_{50}, t_{95}) were established. τ is the mean residence time, which is calculated via Eq.3. t_x is calculated via Eq. 4 and is the time until 5%, 50% or 95% of the tracer are removed from the extruder after the impulse injection and are thus characteristics of the washout function.

$$E(t) = \frac{C(t)}{\int_0^\infty C(t)dt} \tag{2}$$

$$\tau = \int_0^\infty tE(t)dt \tag{3}$$

$$\int_0^{t_x} E(t)dt = \frac{x}{100} \tag{4}$$

Further evaluation of the process was carried out by calculating the power consumption of the extruder via Eq.5.

$$Power\ input = 2\pi \times torque \times screw\ speed \tag{5}$$

In addition, the powder temperature was measured at the outlet of the extruder with Testo 845 infrared thermometer (Testo, Lenzkirch, Germany).

4.3 Results and Discussion

4.3.1 Extrusion Process Data

On the basis of the analysis of the process data, a detailed evaluation of the connection between the input parameters (the feed flow) and the process responses (the torque) was performed. The set feed rate was varied between 0.5 and 2.0 kg/h. Depending on the feed rate, the screw speed was increased to a higher throughput to avoid material accumulation at the inlet zone and overfilling of the extruder (Figure 8a). A slightly lower throughput of dried powder occurred for the feed with 10 wt.% moisture content since less solid material was fed on the basis of the constant mass flow rate of the wetted powder. The associated evaporation rate is depicted in Figure 8b. Higher dried product mass flow (Figure 8c) and higher screw speed led to a higher torque of the extruder screw. The feed material with 4 wt.% moisture content was more powderlike with good flowability of particles, whereas the feed material with 10 wt.% moisture content was more of a pastelike substance. Therefore, a higher moisture content in the material is responsible for a higher torque of the extruder screw. Similar results for a higher torque at increased moisture content were obtained by am Ende et al.[52]
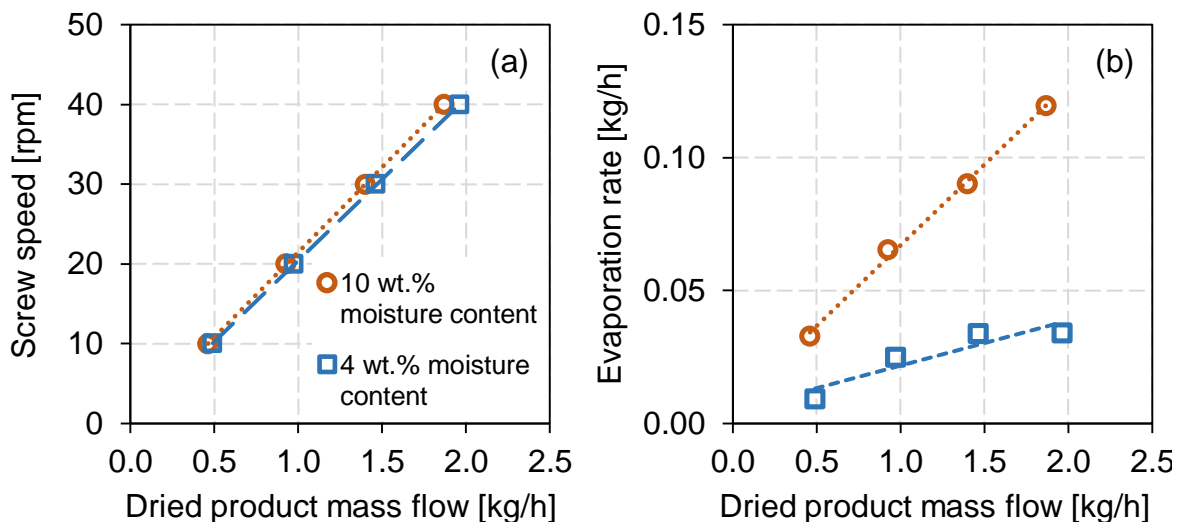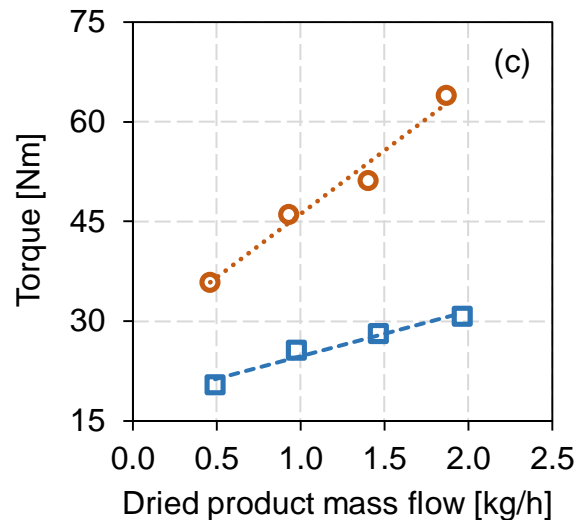
Figure 8. Process data of the extruder-drying experiments for (a) extruder screw speed, (b) evaporation rate, and (c) extruder screw torque as functions of the throughput of dried powder. The circle and square symbols show the results for the feed materials with 10 and 4 wt.% moisture content, respectively.

The results of the drying experiments, including feed composition, process settings, and dried product properties are reported in Table 2. The residual moisture content of both feed compositions increased at higher feed rates and extruder screw speeds. Dried products with a feed moisture content of 4 wt.% had a residual moisture content of 1.3 wt.% at the lower product mass flow of 0.49 kg/h (dried), whereas a higher product mass flow of 1.96 kg/h (dried) resulted in a residual moisture content of 2.2 wt%. The same trend was observed for a higher feed moisture content of 10 wt.%, leading to a residual moisture content between 2.4 wt.% and 3.8 wt.%.

Table 2. Effect of Process Settings on the Product's Residual Moisture Content and the Moisture Removal Extent for an Air Flow Rate of 0.5 Nm³/h

moisture content feed [wt.%]	solid feed concentration [wt.%]	extruder screw speed [rpm]	dried product mass flow [kg/h]	residual moisture content [wt.%]	moisture removal [%]
4	96	10	0.49	1.3	67.3
4	96	20	0.97	1.5	62.9
4	96	30	1.47	1.7	57.5
4	96	40	1.96	2.2	44.8

| 10 | 90 | 10 | 0.46 | 2.4 | 76.0 |
10	90	20	0.93	2.9	70.9
10	90	30	1.40	3.2	68.0
10	90	40	1.88	3.5	65.5

The residual moisture content of the dried products increased at higher throughputs as a result of shorter residence times in the extruder related to the higher screw speed, which was selected to keep the fill ratio of the extruder approximately constant. For a constant screw, speed overfilling of the inlet zone would have occurred. As can be seen in Table 2, the associated extent of moisture removal decreased with the throughput. Clearly, the extent of moisture removal was higher at higher feed moisture levels. The highest moisture removal extent of 76.0 % was obtained for a feed moisture content of 10 wt.% at the lowest dried product mass flow (0.46 kg/h). The lowest moisture removal extent of 44.8 % was obtained for a feed moisture content of 4 wt.% at the highest dried product mass flow (1.96 kg/h). The powder temperature measured at the extruder's outlet was in the range of 84-99 °C, which was well below the melting temperature of naproxen (155 °C).[53] Further reduction of the residual moisture content could result in higher powder temperatures, which might impact the physical and chemical stability.

Nevertheless, the physical and chemical particle properties of a crystalline material should not be significantly influenced by the drying temperature as long as the powder temperature is well below the melting temperature and few dissolved solids are present.[33] The closer drying is performed to the melting temperature, the higher is the probability of particles sticking together resulting in agglomeration. The same is true for dissolved solids: the more dissolved components are present during drying, the higher is the probability of bridge formation between single particles due to precipitated material. Such bridge formation effects are desired in twin-screw granulation, and the granule size increases with higher binder content (or dissolved solids).[48] Usually, the solubility of solids in liquids increases with the temperature, thereby increasing the probability of bridge formation at higher drying temperatures. In the case of naproxen in water, the solubility is still very low at elevated temperatures,[54,55] and therefore, dissolved components were neglected.

4.3.2 Evaluation of RTD

Figure 9 depicts the results of the RTD measurements for a feed material with 4 wt.% moisture content at a feed rate of 2 kg/h and a screw speed of 40 rpm. After the impulse

injection of the Fe_2O_3 tracer, the first colored material was transported from the inlet toward the outlet of the extruder after ∼ 68 s. The highest color intensity was reached after ∼ 85 s and the last portion of colored material left the extruder after ∼ 230 s. The mean residence time τ was 102.2 s. The cumulative RTD is shown in Figure 10. t_5 was reached after 76 s, 8 s after the first colored material left the extruder. t_{50} and t_{95} were reached after 93 and 165 s, respectively, showing fast transport of the material through the extruder with a narrow RTD.
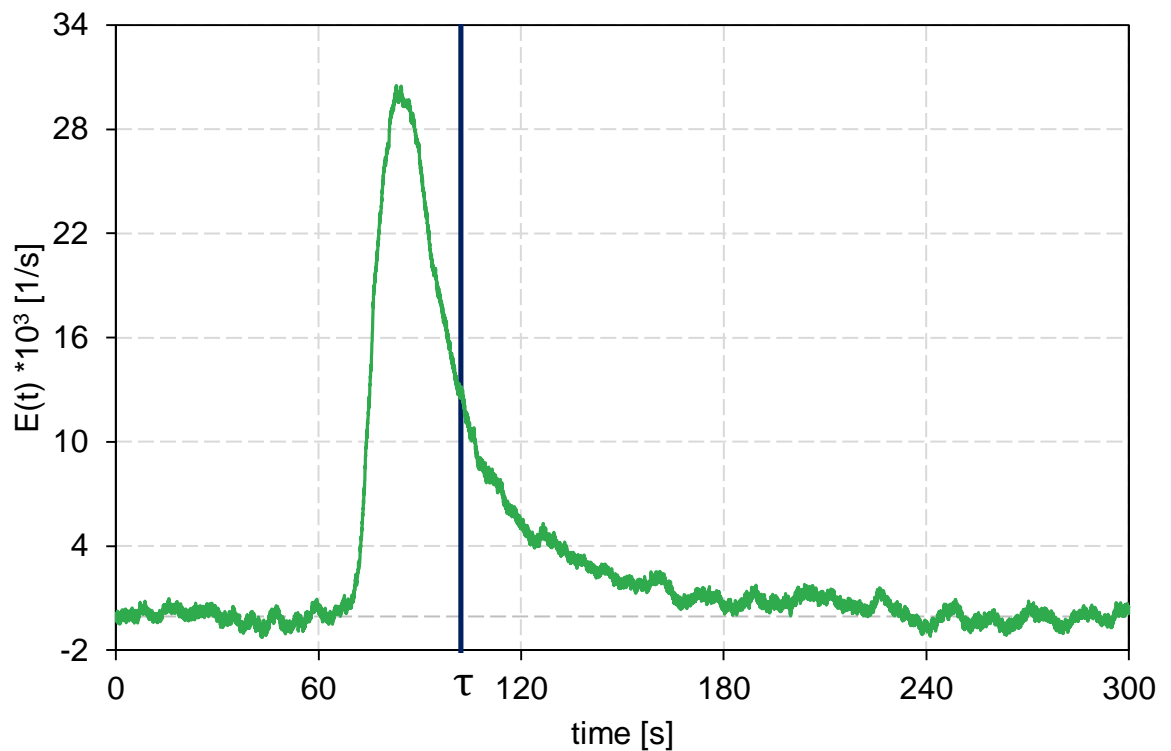
Figure 9. Density RTD and mean residence time τ for the drying test run using a feed material with 4 wt.% moisture content at a feed rate of 2 kg/h and a screw speed of 40 rpm.
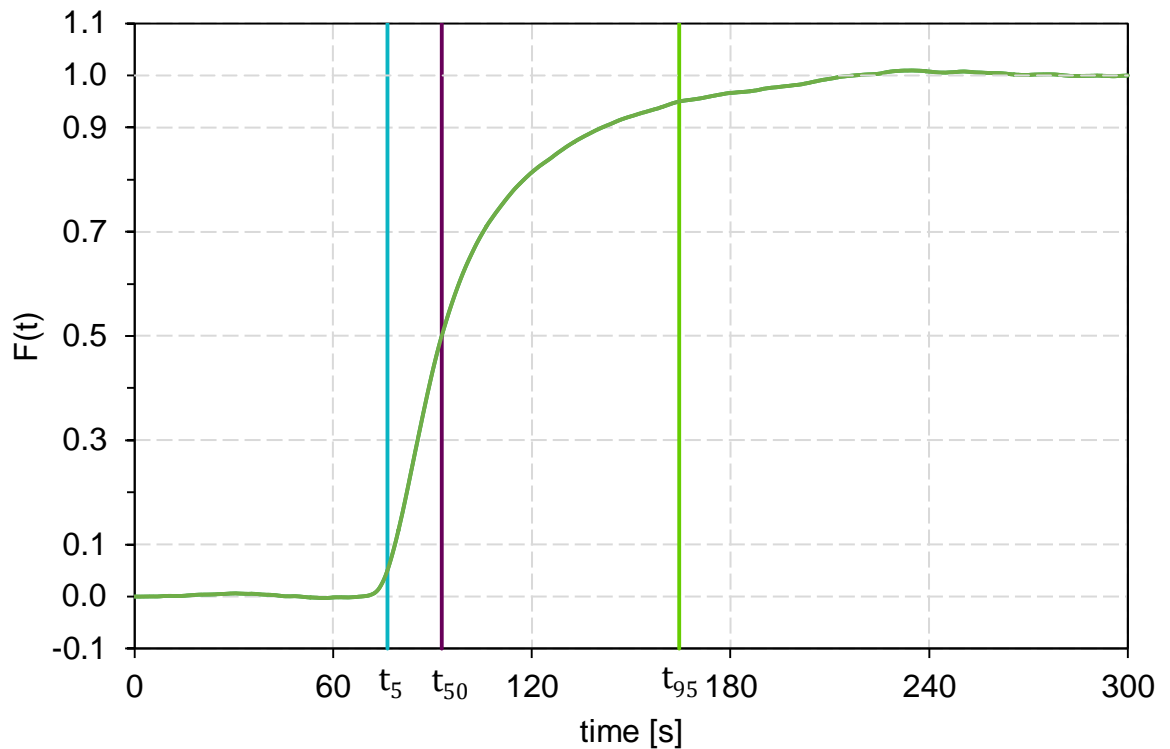
Figure 10. Cumulative RTD and t_5, t_{50}, t_{95} for the drying test run using a feed material with 4 wt.% moisture content at a feed rate of 2 kg/h and an extruder screw speed of 40 rpm.

Mean residence time τ was measured only at a set feed rate of 2 kg/h and an extruder screw speed of 40 rpm for the feed material with 4 wt.% moisture content. The fill level for this configuration was calculated to be 30.3 %. In partly filled extruders there is a linear relationship between the extruder screw speed and the residence time,[56] based on which residence times can be calculated. When the extruder screw speed was reduced from 40 to 10 rpm, the mean residence time τ increased by a factor of 4 (from 102.5 to 410 s), as the residence time is determined by the axial velocity of the screw surface. Thus, a constant ratio between the set feed rate and extruder screw speed guarantees a constant fill level in the extruder. The fill level fluctuated depending on the material composition and was 30.3 % for the feed with 4 wt.% moisture content and 29.4 % for the feed with 10 wt.% moisture content. A slightly lower fill level for the feed with 10 wt.% moisture content was obtained due to the higher material bulk density of 0.501 g/cm³ (compared to 0.485 g/cm³ for the feed with 4 wt.% moisture content).

4.3.3 Analysis of Dried Product PSD

Light microscopy images of the dried products for various feed moisture contents and process settings are shown in Figure 11. Similar sizes and shapes of the dried particles were obtained for the feed materials with moisture contents of 4 wt.% (Figure 11a,b) and 10 wt.% (Figure 11c,d). No apparent visual differences were observed in the dried particles at a low throughput and extruder screw speed (Figure 11a,c) or at a high throughput and extruder screw speed (Figure 11b,d). Furthermore, the raw (Figure 2) and dried (Figure 11) materials appeared to be very similar in shape and size. Since the resolution of light microscopy images was too low to detect differences in the particle size, they were measured for the feed material and the dried product via laser diffraction.
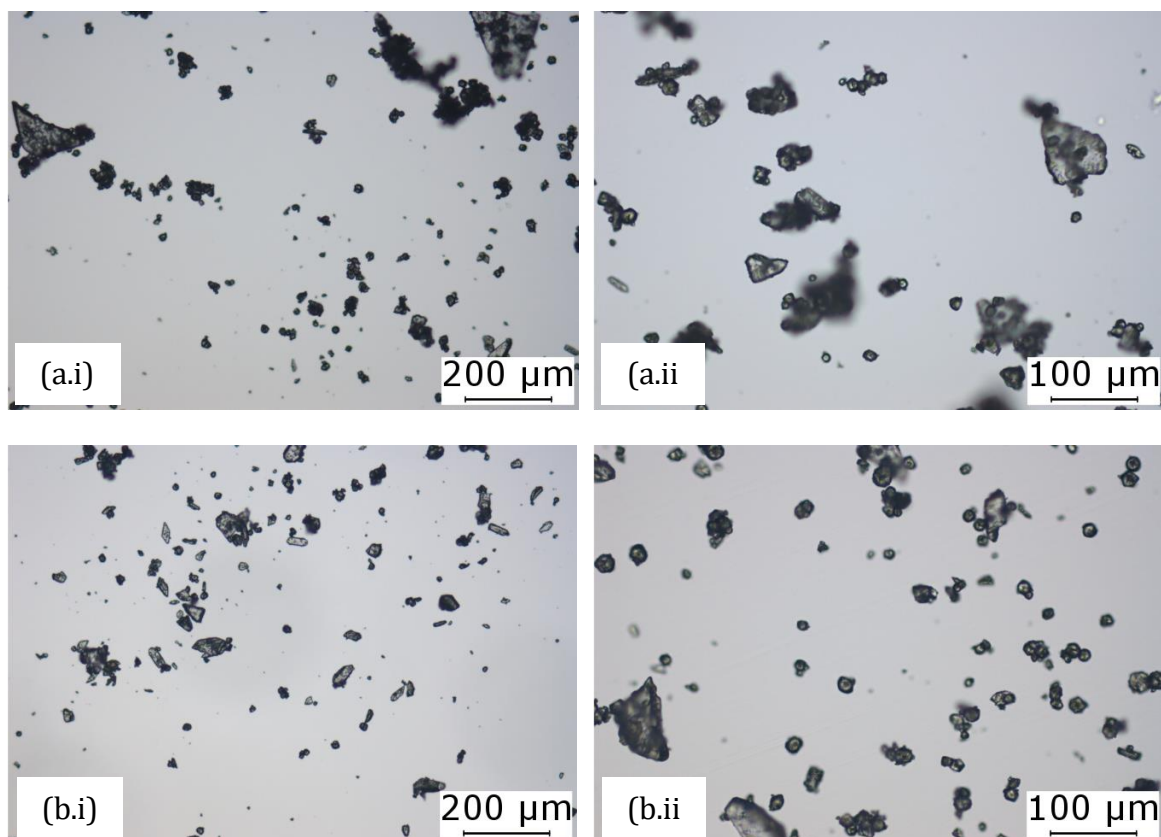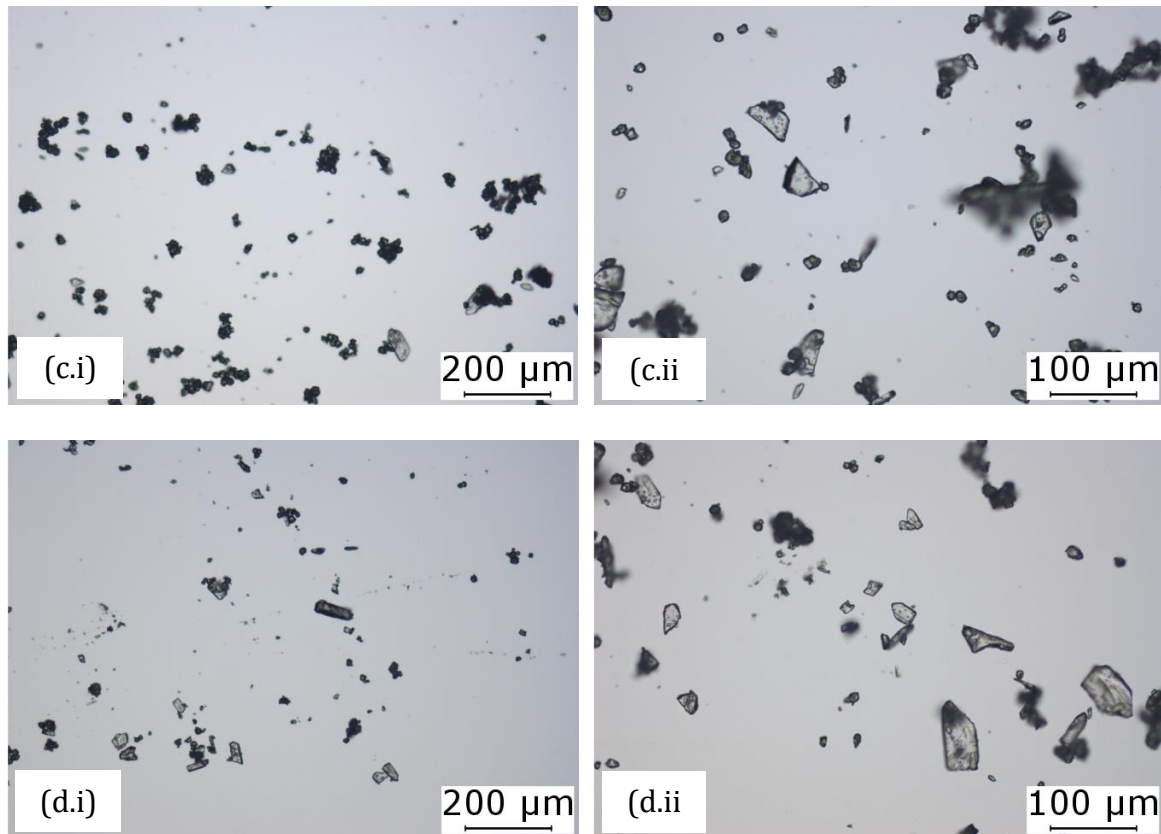
Figure 11. Light microscope images of dried material with various feed moisture content and dried in various process settings: (a) 4 wt.% water, feed rate of 0.5 kg/h, 10 rpm, (b) 4 wt.% water, feed rate of 2.0 kg/h, 40 rpm, (c) 10 wt.% water, feed rate of 0.5 kg/h, 10 rpm, (d) 10 wt.% water, feed rate of 2.0 kg/h, 40 rpm. Particles (i) at lower magnification and (ii) at higher magnification.

The PSDs (q_3^*) for feeds with 4 and 10 wt.% moisture content are shown in Figures 12 and 13. As can be seen, during drying of the feed with 4 wt.% moisture content at a feed flow rate of 0.5 kg/h feed flow rate and an extruder screw speed of 10 rpm, larger particles were crushed or reduced in size, especially those larger than 100 μm, as shown in Figure 12 Drying of the same material at an increased feed flow rate (2.0 kg/h) and extruder screw speed (40 rpm) led to a smaller degree of particle attrition during drying. Obviously, the reduction in particle size is connected to the residence time, which is 4 times longer in the case of the 0.5 kg/h feed flow rate. Similar phenomena were also reported for other unit operations.[57] Am Ende et al.[52] also described a decrease in the particle size at increased agitator revolutions. The particle size decrease during drying may mostly be attributable to a small shear gap between the extruder's screw and housing.

The PSDs (q_3^*) in Figure 13 for drying of the feed with 10 wt.% moisture content showed results similar to those obtained for the feed with 4 wt.% moisture content. Lower feed flows and extruder screw speeds resulted in a greater particle size reduction. Nevertheless, the decrease in the particle size was lower for the feed material with 10 wt.% moisture content than that with 4 wt.% moisture content. Possibly the higher water content lubricated the particles, effectively reducing the particle attrition via particle-particle and particle-wall collisions.[21,41]
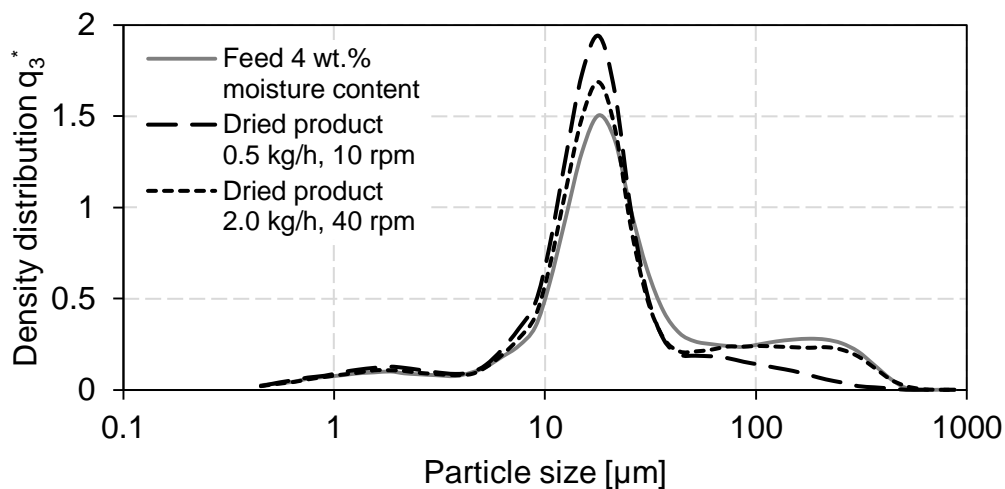
Figure 12. PSD density distributions q_3^* of the feed material with 4 wt.% moisture content and dried products for various process settings.
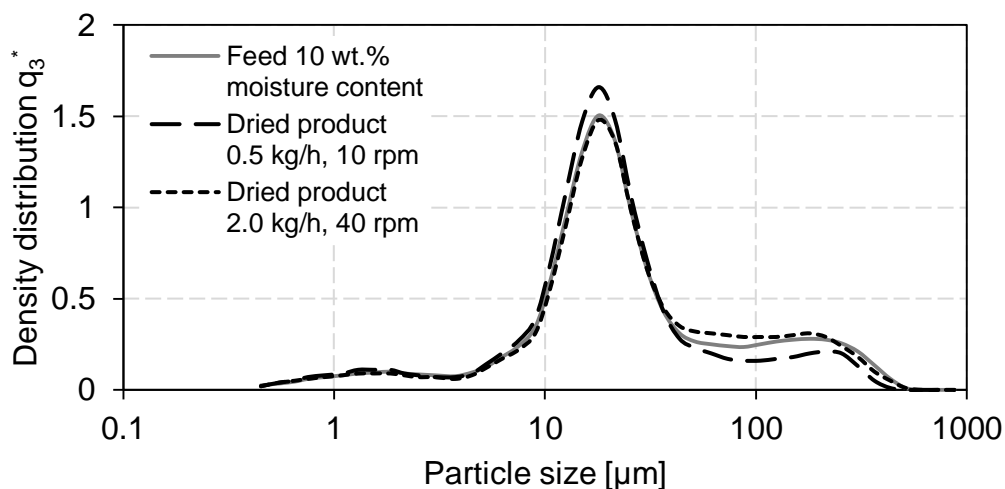

Figure 13. PSD density distributions q_3^* of the feed material with 10 wt.% moisture content and dried products for various process settings.

Evaluating the Sauter mean diameter (SMD), the volume mean diameter (VMD), and d_{50} provided additional information about the effect of the drying process on the particle size. Figure 14 depicts the results for drying of the feed materials with 4 wt.% and 10 wt.% moisture content. The most significant changes in the particle size occurred in the feed material with 4 wt.% moisture content at the lowest feed flow rate (0.5 kg/h) and extruder screw speed (10 rpm). Increasing the feed flow rate and the extruder screw speed reduced the particle attrition during drying. Similar values for the feed and dried product were obtained for the SMD and d_{50} at the highest feed flow rate (2.0 kg/h) and extruder screw speed (40 rpm). Therefore, the drying process for these settings had a negligible influence on the d_{50} and the surface of the particles. However, the VMD decreased slightly, indicating a small change in the particle volume. At low feed flow rates (0.5 kg/h) and low extruder screw speeds (10 rpm), the VMD decreased from 47.6 μm for the feed material to 23.6 μm for the dried product.

Similar trends (i.e., reduced particle size at a lower feed rate and extruder screw speed) were observed for drying of the feed material with 10 wt.% moisture content. In this case, the decrease in the particle size was in general not as high as for the feed material with 4 wt.% moisture content (possibly because of lubrication effects). Low attrition rates were obtained at a feed flow rate of 2.0 kg/h and an extruder screw speed of 40 rpm since no change in the SMD and d_{50} was observed. The VMD decreased slightly (47.6 μm for the feed material and 43.0 μm for the dried product).
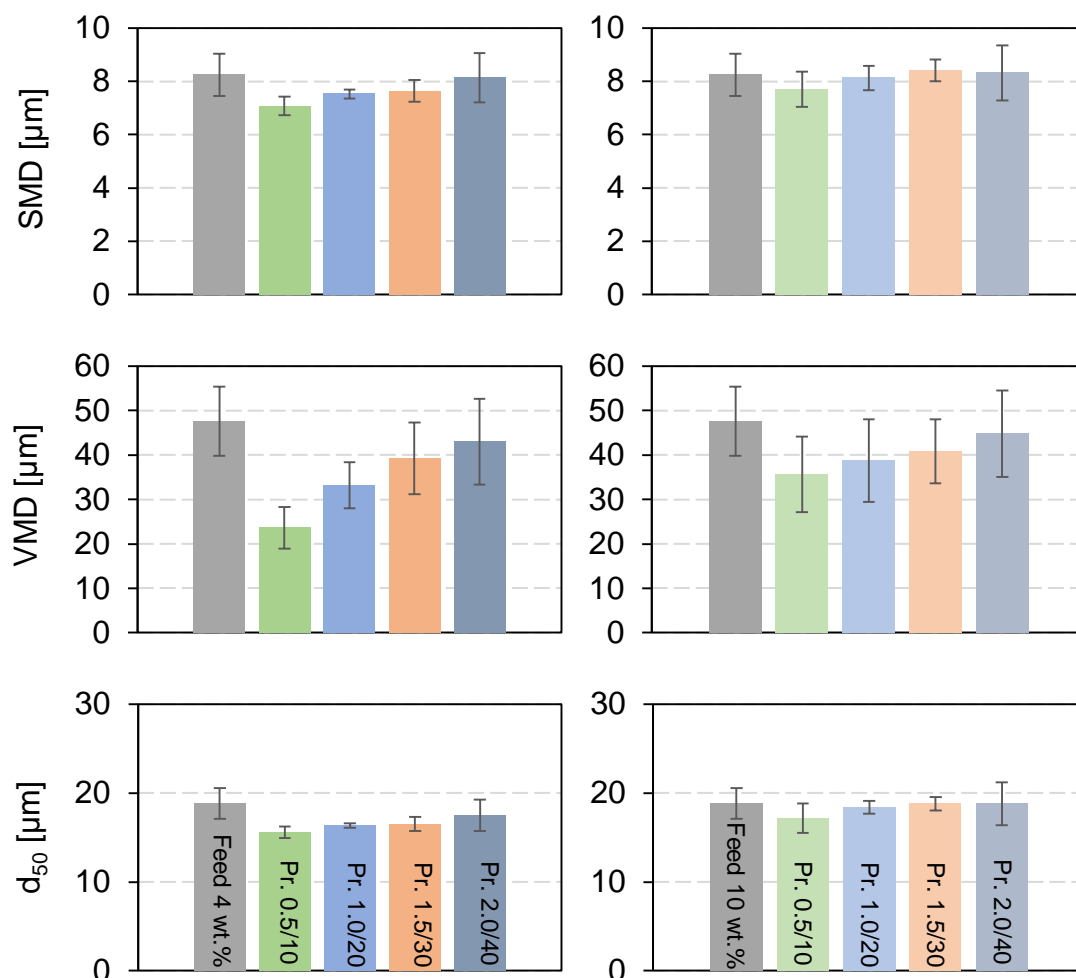
Figure 14. (top) SMD, (middle) VMD, and (bottom) d_{50} of the feed material with (left) 4 wt.% and (right) 10 wt.% moisture content and their corresponding dried products. Pr. *x/y* refers to a dried product with a feed flow rate of *x* kg/h and a screw speed of *y* rpm.

4.3.4 Combined Material and Process Data Analysis

Evaluating the relationship between process settings (feed mass flow rate, feed moisture content, and extruder screw speed), process responses (torque and residence time), and particle properties (residual moisture content, particle size) provided a better understanding of the predominant drying mechanisms. These correlations are depicted in Figure 15 for drying of naproxen with moisture contents of 10 and 4 wt.% in the feed material. The particle size was strongly influenced by the residence time in the extruder (Figure 15a). A longer residence time leads to a greater decrease in the particle size. The longer the material stays in the extruder and the drier it becomes, the more particle-particle and particle-wall collisions occur. Figure 15c shows that the VMD decreased with a lower residual moisture content in the dried product. Similarly, Lekhal et al.[21,41] reported

that most of the attrition occurred at a low moisture content. At a higher moisture content, the particles are surrounded by a liquid film, and particle-particle and particle-wall collisions are lubricated. Since the liquid acts as a lubricant, only a small fraction of the particles undergo attrition. As the drying progresses, particle-particle and particle-wall collisions are more frequent since the liquid film between the particles evaporates, resulting in higher attrition.

The power input (Eq. 5) has the opposite effect on the particles: interestingly, the lowest particle attrition occurred at the highest power input (Figure 15b). This can be explained by the higher power consumption that the extruder requires to convey materials with a higher moisture content. These materials are pastelike substances with poor flowability, whereas drier materials are powderlike and have better flowability. Thus, more power is necessary to convey materials with a higher moisture content, as shown in Figure 15e. Furthermore, the power consumption is higher at shorter residence times because higher torques provide a faster transportation of the material through the extruder (Figure 15d). This is in contrast to conventional wisdom that higher power input leads to increased particle attrition.

Reducing the residence time in the extruder affected the extent of moisture removal. Longer residence times in the dryer led to higher extents of moisture removal and vice versa (Figure 15f).
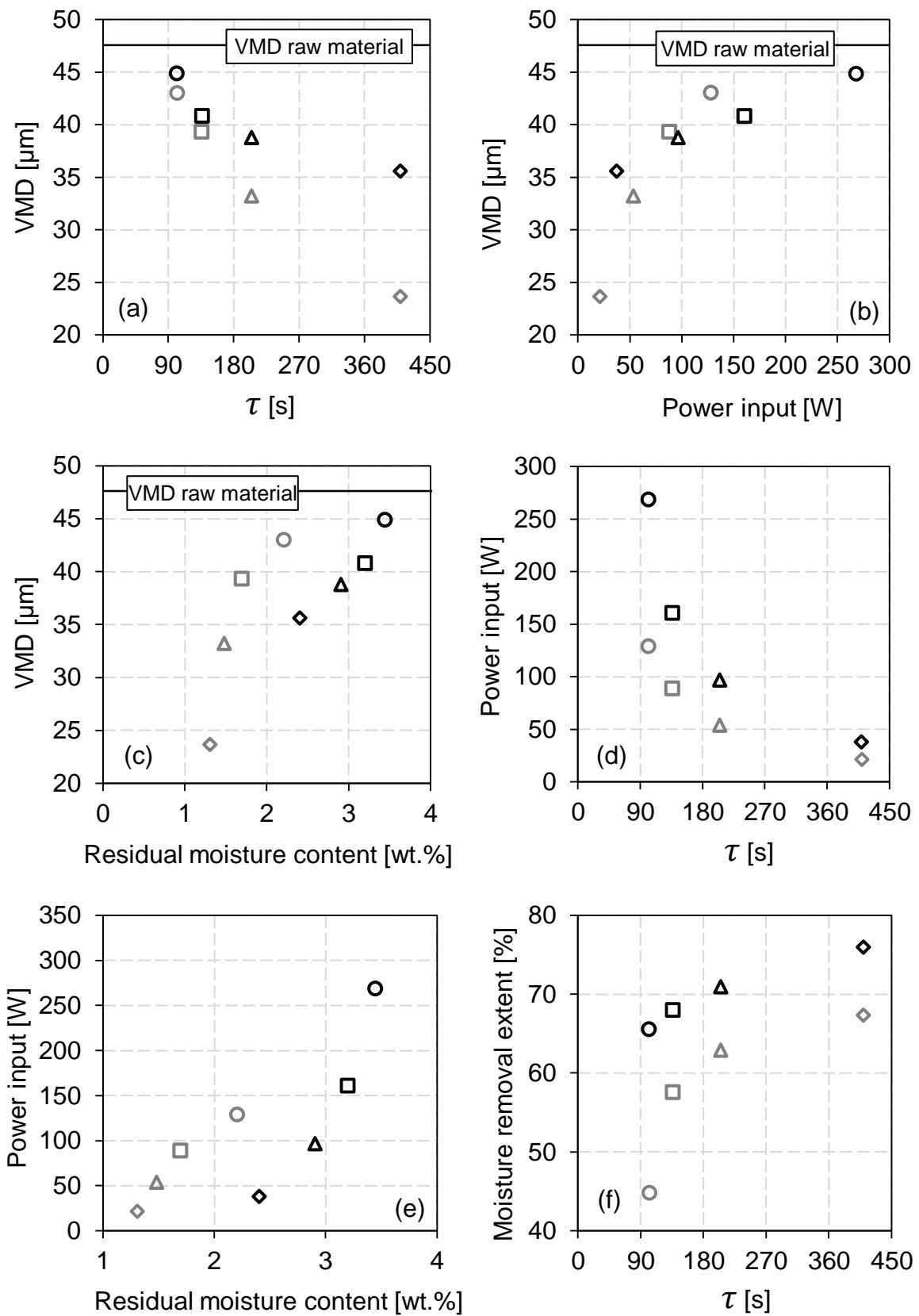
Figure 15. (a-c) Material and process data relating VMD to (a) mean residence time (τ), (b) power input, and (c) residual moisture content. (d),e) Influence of power input on

(d) τ and (e) residual moisture content. (f) Moisture removal extent as a function of . Black and gray symbols indicate the results for the data series for the feed materials with 10 and 4 wt.% moisture content, respectively. Circle symbols indicate a feed rate of 2.0 kg/h and an extruder screw speed of 40 rpm, square symbols 1.5 kg/h and 30 rpm, triangle symbols 1.0 kg/h and 20 rpm, and diamond symbols 0.5 kg/h and 10 rpm.

Drying is a highly dynamic process, and various factors can have an impact on the material properties. In the case of continuous extrusion drying, uniform product quality can be achieved with a short and consistent residence time in the extruder. In that regard, a big advantage that a twin-screw extruder offers is the prevention of stagnant areas inside the extruder, resulting in narrow RTDs.[58] The residence time in the extruder can be adjusted using the screw speed: slower screw speeds result in longer residence times and vice versa. However, a longer residence time leads to a greater decrease in the final particle size. In addition to the influence of the residence time on the final particle size, the main change in the final particle size is caused by the material composition and therefore the state of direness. The drier the material is at the beginning or becomes during drying, the more particle-particle and particle-wall collisions occur. Thus, the particle size decreases, resulting in more attrited fine particles. An important consideration is that in the case of extrusion drying (and most likely any mechanical drying operation), shear forces are permanently present throughout the entire drying process. Therefore, the design of the extruder screw has to be optimized to minimize the particle size reduction via attrition and the formation of agglomerates.

4.4 Conclusions

Although continuous drying technologies are available on the market, handling low material flow rates remains challenging. In that regard, we investigated continuous drying of pharmaceuticals via extrusion at low material flow rates and developed a robust drying process with a narrow RTD. Extruder drying is a promising method for the production of pharmaceutical drug substances since dead zones inside the extruder are negligible compared with other drying technologies (e.g., fluidized beds). The drying temperature can be easily and accurately adjusted via the extruder housing and drying gas temperature. Substances can be dried without exceeding the glass transition temperature, with minimal particle size changes. Consistent product quality without major changes in the product particle size was achieved for the selected model substance with specific process settings.

Particle size reduction was mainly influenced by the residual moisture content rather than by the residence time in the extruder. The drier the material is at the beginning or becomes during drying, the more attrition occurred. Since extrusion is a continuous process by nature, it could easily be implemented in a continuous production line, providing a link between the primary and secondary continuous manufacturing of pharmaceuticals. Design optimizations can be implemented (e.g., by increasing the gas flow rate and temperature) since the existing extrusion equipment is typically used in processing hot melts. Thus, higher temperatures and lower final moisture levels can easily be obtained, but changes in particle size or stability issues must be considered. Reducing the shear input by varying the extruder's screw design (larger shear gap) may also improve the product quality in drying of pharmaceuticals.

Acknowledgement

References

(1)   Plumb, K. Continuous Processing in the Pharmaceutical Industry. Chem. Eng. Res. Des. 2005, 83, 730–738.

(2)   Vercruysse, J.; Delaet, U.; Van Assche, I.; Cappuyns, P.; Arata, F.; Caporicci, G.; De Beer, T.; Remon, J. P.; Vervaet, C. Stability and Repeatability of a Continuous Twin Screw Granulation and Drying System. Eur. J. Pharm. Biopharm. 2013, 85, 1031–1038.

(3)   Poechlauer, P.; Manley, J.; Broxterman, R.; Ridemark, M. Continuous Processing in the Manufacture of Active Pharmaceutical Ingredients and Finished Dosage Forms: An Industry Perspective. Org. Process Res. Dev. 2012, 16, 1586–1590.

(4)   Srai, J. S.; Badman, C.; Krumme, M.; Futran, M.; Johnston, C. Future Supply Chains Enabled by Continuous Processing-Opportunities and Challenges May 20-21, 2014 Continuous Manufacturing Symposium. J. Pharm. Sci. 2015, 104, 840–849.

(5)   FDA-Administration. Guidance for Industry - PAT - A Framework for Innovative Pharmaceutical Development, Manufacturing, and Quality Assurance; 2004.

(6)   Leuenberger, H. New Trends in the Production of Pharmaceutical Granules: Batch versus Continuous Processing. Eur. J. Pharm. Biopharm. 2001, 52, 289–296.

(7)   Teżyk, M.; Milanowski, B.; Ernst, A.; Lulek, J. Recent Progress in Continuous and Semi-Continuous Processing of Solid Oral Dosage Forms: A Review. Drug Dev. Ind. Pharm. 2016, 42, 1195–1214.

(8)   Remon, J. P.; Vervaet, C. Continuous Processing of Pharmaceuticals. In *Encyclopedia of Pharmaceutical Technology*; Swarbrick, J., Ed.; Taylor & Francis: New York, 2013; pp 743–749.

(9)   Leuenberger, H.; Betz, G.; Junker-Bürgin, P. Batch and Continuous Processing in the Production of Pharmaceutical Granules. Pharm. Dev. Technol. 2003, 8, 289–297.

(10)   Khinast, J.; Bresciani, M. Continuous Manufacturing: Definitions and Engineering Principles. In *Continuous Manufacturing of Pharmaceuticals*; John Wiley & Sons, Ltd: Chichester, UK, 2017; pp 1–31.

(11)   Mascia, S.; Heider, P. L.; Zhang, H.; Lakerveld, R.; Benyahia, B.; Barton, P. I.; Braatz, R. D.; Cooney, C. L.; Evans, J. M. B.; Jamison, T. F.; et al. End-to-End Continuous Manufacturing of Pharmaceuticals: Integrated Synthesis, Purification, and Final Dosage Formation. Angew. Chemie - Int. Ed. 2013, 52, 12359–12363.

(12)   Vaxelaire, J.; Bongiovanni, J. M.; Puiggali, J. R. Mechanical Dewatering and Thermal Drying of Residual Sludge. Environ. Technol. 1999, 20, 29–36.

(13)   Gursch, J.; Hohl, R.; Toschkoff, G.; Dujmovic, D.; Brozio, J.; Krumme, M.; Rasenack, N.; Khinast, J. Continuous Processing of Active Pharmaceutical Ingredients Suspensions via Dynamic Cross-Flow Filtration. J. Pharm. Sci. 2015, 104, 3481–3489.

(14)   Gursch, J.; Hohl, R.; Dujmovic, D.; Brozio, J.; Krumme, M.; Rasenack, N.; Khinast, J. Dynamic Cross-Flow Filtration: Enhanced Continuous Small-Scale Solid-Liquid Separation. Drug Dev. Ind. Pharm. 2016, 42, 977–984.

(15)   Gursch, J.; Hohl, R.; Armenante, M. E.; Dujmovic, D.; van der Wel, P.; Brozio, J.; Krumme, M.; Rasenack, N.; Khinast, J. Continuous Drying of Small Particles for Pharmaceutical Applications - An Evaluation of Selected Lab-Scale Systems. Org. Process Res. Dev. 2015, 19, 2055–2066.

(16)   Mujumdar, A. S. Handbook of Industrial Drying, Fourth Edition; Taylor & Francis, 2014.

(17) Keey, R. B. Drying of Loose and Particulate Materials; Hemisphere Publishing, 1992.

(18) Burgbacher, J.; Wiss, J. Industrial Applications of Online Monitoring of Drying Processes of Drug Substances Using NIR. Org. Process Res. Dev. 2008, 12, 235–242.

(19) Kukura, J.; Izzo, B.; Orella, C. Scale up of a Granulation Phenomenon: During the Drying of an Active Pharmaceutical Ingredient. Pharm. Technol. 2005, 29.

(20) Morris, K. R.; Nail, S. L.; Peck, G. E.; Byrn, S. R.; Griesser, U. J.; Stowell, J. G.; Hwang, S. J.; Park, K. Advances in Pharmaceutical Materials and Processing. Pharm. Sci. Technol. Today 1998, 1, 235–245.

(21) Lekhal, A.; Girard, K. P.; Brown, M. A.; Kiang, S.; Glasser, B. J.; Khinast, J. G. Impact of Agitated Drying on Crystal Morphology: KCl-Water System. Powder Technol. 2003, 132, 119–130.

(22) Bemrose, C. R.; Bridgwater, J. A Review of Attrition and Attrition Test Methods. Powder Technol. 1987, 49, 97–126.

(23) Neil, A. U.; Bridgwater, J. Attrition of Particulate Solids under Shear. Powder Technol. 1994, 80, 207–219.

(24) Bravi, M.; Di Cave, S.; Mazzarotta, B.; Verdone, N. Relating the Attrition Behaviour of Crystals in a Stirred Vessel to Their Mechanical Properties. Chem. Eng. J. 2003, 94, 223–229.

(25) Hare, C.; Ghadiri, M.; Dennehy, R. Prediction of Attrition in Agitated Particle Beds. Chem. Eng. Sci. 2011, 66, 4757–4770.

(26) Bika, D. G.; Gentzler, M.; Michaels, J. N. Mechanical Properties of Agglomerates. Powder Technol. 2001, 117, 98–112.

(27) MacLeod, C. S.; Muller, F. L. On the Fracture of Pharmaceutical Needle-Shaped Crystals during Pressure Filtration: Case Studies and Mechanistic Understanding. Org. Process Res. Dev. 2012, 16, 425–434.

(28) Kowalski, S. J.; Rajewska, K.; Rybicki, A. Destruction of Wet Materials by Drying. Chem. Eng. Sci. 2000, 55, 5755–5762.

(29) Gahn, C.; Krey, J.; Mersmann, a. The Effect of Impact Energy and the Shape of Crystals on Their Attrition Rate. J. Cryst. Growth 1996, 166, 1058–1063.

(30) Schæfer, T.; Mathiesen, C. Melt Pelletization in a High Shear Mixer. VII. Effects of Product Temperature. Int. J. Pharm. 1996, 134, 105–117.

(31) Seville, J. P. K.; Willett, C. D.; Knight, P. C. Interparticle Forces in Fluidisation: A Review. Powder Technol. 2000, 113, 261–268.

(32) Papadakis, S. E.; Bahu, R. E. The Sticky Issues of Drying. Dry. Technol. 1992, 10, 817–837.

(33) Kreimer, M.; Aigner, I.; Sacher, S.; Krumme, M.; Mannschott, T.; van der Wel, P.; Kaptein, A.; Schroettner, H.; Brenn, G.; Khinast, J. G. Mechanical Strength of Microspheres Produced by Drying of Acoustically Levitated Suspension Droplets. Powder Technol. 2018, 325, 247–260.

(34) Birch, M.; Marziano, I. Understanding and Avoidance of Agglomeration during Drying Processes: A Case Study. Org. Process Res. Dev. 2013, 17, 1359–1366.

(35) Seem, T. C.; Rowson, N. A.; Ingram, A.; Huang, Z.; Yu, S.; de Matas, M.; Gabbott, I.; Reynolds, G. K. Twin Screw Granulation - A Literature Review. Powder Technol. 2015, 276, 89–102.

(36) Djuric, D.; Kleinebudde, P. Impact of Screw Elements on Continuous Granulation with a Twin-Screw Extruder. J. Pharm. Sci. 2008, 97, 4934–4942.

(37)   Meier, R.; Moll, K. P.; Krumme, M.; Kleinebudde, P. Impact of Fill-Level in Twin-Screw Granulation on Critical Quality Attributes of Granules and Tablets. Eur. J. Pharm. Biopharm. 2017, 115, 102–112.

(38)   Meier, R.; Moll, K. P.; Krumme, M.; Kleinebudde, P. How Deformation Behavior Controls Product Performance After Twin Screw Granulation With High Drug Loads and Crospovidone as Disintegrant. J. Pharm. Sci. 2017, 106, 291–301.

(39)   Cypes, S. H.; Wenslow, R. M.; Thomas, S. M.; Chen, A. M.; Dorwart, J. G.; Corte, J. R.; Kaba, M. Drying an Organic Monohydrate: Crystal Form Instabilities and a Factory-Scale Drying Scheme to Ensure Monohydrate Preservation. Org. Process Res. Dev. 2004, 8, 576–582.

(40)   Kougoulos, E.; Chadwick, C. E.; Ticehurst, M. D. Impact of Agitated Drying on the Powder Properties of an Active Pharmaceutical Ingredient. Powder Technol. 2011, 210, 308–314.

(41)   Lekhal, A.; Girard, K. P.; Brown, M. A.; Kiang, S.; Khinast, J. G.; Glasser, B. J. The Effect of Agitated Drying on the Morphology of L-Threonine (Needle-like) Crystals. Int. J. Pharm. 2004, 270, 263–277.

(42)   Lamberto, D. J.; Cohen, B.; Marencic, J.; Miranda, C.; Petrova, R.; Sierra, L. Laboratory Methods for Assessing API Sensitivity to Mechanical Stress during Agitated Drying. Chem. Eng. Sci. 2011, 66, 3868–3875.

(43)   Kemp, I. C. Drying of Pharmaceuticals in Theory and Practice. Dry. Technol. 2017, 35, 918–924.

(44)   Geldart, D. The Effect of Particle Size and Size Distribution on the Behaviour of Gas-Fluidised Beds. Powder Technol. 1972, 6, 201–215.

(45)   Geldart, D. Types of Gas Fluidization. Powder Technol. 1973, 7, 285–292.

(46)   Visser, J. Van Der Waals and Other Cohesive Forces Affecting Powder Fluidization. Powder Technol. 1989, 58, 1–10.

(47)   Yalkowsky, S. H.; He, Y.; Jain, P. Handbook Of Aqueous Solubility Data, 2nd ed.; CRC Press: Boca Raton, FL, 2010.

(48)   Thompson, M. R.; Sun, J. Wet Granulation in a Twin-Screw Extruder: Implications of Screw Design. J. Pharm. Sci. 2010, 99, 2090–2103.

(49)   Kruisz, J.; Rehrl, J.; Sacher, S.; Aigner, I.; Horn, M.; Khinast, J. G. RTD Modeling of a Continuous Dry Granulation Process for Process Control and Materials Diversion. Int. J. Pharm. 2017, 528, 334–344.

(50)   Wang, X.; Hänsch, R.; Ma, L.; Hellwich, O. Comparison of Different Color Spaces for Image Segmentation Using Graph-Cut. In Computer Vision Theory and Applications (VISAPP); 2014; Vol. 1, pp 301–308.

(51)   Peng, J.; Huff, H. E.; Hsieh, F. An RTD Determiantion Method For Extrusion Cooking. J. Food Process. Preserv. 1994, 18, 263–277.

(52)   Am Ende, D.; Birch, M.; Brenek, S. J.; Maloney, M. T. Development and Application of Laboratory Tools to Predict Particle Properties upon Scale-up in Agitated Filter-Dryers. Org. Process Res. Dev. 2013, 17, 1345–1358.

(53)   Lide, D. R. CRC Handbook of Chemistry and Physics; CRC Press: Boca Raton, FL, 2007; pp 3–386.

(54)   Panahi-Azar, V.; Soltanpour, S.; Martinez, F.; Jouyban, A. Solubility of Naproxen in 2-Propanol+water Mixtures at Various Temperatures. J. Mol. Liq. 2015, 206, 110–113.

(55)   Pacheco, D. P.; Martínez, F. Thermodynamic Analysis of the Solubility of Naproxen in Ethanol + Water Cosolvent Mixtures. Phys. Chem. Liq. 2007, 45, 581–595.

(56)   Witschnigg, A. Characterization of Polymers in Terms of Inline Quality Control in Extrusion Processes Using near-Infrared Spectroscopy, Montanuniversität Leoben, 2014.

(57)   Chen, Z.; Grace, J. R.; Jim Lim, C. Limestone Particle Attrition and Size Distribution in a Small Circulating Fluidized Bed. Fuel 2008, 87, 1360–1371.

(58)   Radl, S.; Tritthart, T.; Khinast, J. G. A Novel Design for Hot-Melt Extrusion Pelletizers. Chem. Eng. Sci. 2010, 65, 1976-1988.

„Genius is one percent inspiration and
ninety-nine percent perspiration"

Thomas Edison (1847-1931)

5. Summary and Conclusion

Chapter 1 provides an overview of (1) the state of the art in CM, (2) challenges in continuous purification and drying in relation to process stability and preserving particle properties and (3) the motivation to work in this research field.

In Chapter 2, small scale droplet drying experiments were performed with a pharmaceutical model suspension by variation of suspended solids, dissolved solids and liquid components. The amount of dissolved solids was dependent on the liquid composition of water and organic solvent, according to the solubility. An acoustic levitator was used to freely levitate single droplets with different compositions, to observe the drying progression as similar present in spray dryers. The single droplet drying experiments revealed the influence of the suspension composition on the drying kinetics and the microsphere morphology. Higher water content and therefore more dissolved solids resulted in the formation of denser packed microspheres, where the main precipitation of dissolved solids occurred on the surface with crust formation. At the end of drying, the dried microspheres were extracted from the acoustic field and the agglomeration strength was measured through a compression strength test. These measurements revealed the formation of loosely agglomerated microspheres below a threshold of dissolved solids. Based on these results, suspensions after crystallization should be purified until the amount of dissolved solids is below this threshold. Afterwards, drying of the purified suspension should enable production of powders with similar particle size as obtained after crystallization.

Therefore Chapter 3 investigated the purification of the model substance through a continuous solvent exchange washing process with static mixer by addition of anti-solvent to the feed suspension. Different feed suspension compositions by variation of suspended and dissolved solids were processed and the applicability of static mixers in precipitating environments was assed. The main driver for particle size growth was given by the amount of suspended solids, rather than by the dissolved solids. Lower amount of suspended solids

in the feed resulted in a larger increase of the product particle size after solvent exchange washing due to precipitation of dissolved solids on suspended solids. Therefore, a filtration step is suggested to pre-concentrate the suspension before purification is done by solvent exchange washing. Thus, larger changes of the product particle size can be avoided, because dissolved solids are already removed before precipitation can occur by addition of anti-solvent. Furthermore, the long-term stability of the continuous solvent exchange washing process was analyzed for different setup configurations. Adhesion of precipitated material on the static mixer elements was reduced by US irradiation. In comparison to the setup configuration without US irradiation, the attachment, fouling and aging phase were prolonged before blockage of the static mixer occurred. In addition, the product particle size after washing was not affected by US irradiation. The most stable process of more than 5 h was established with the smaller pipe dimensions (6 mm) via co-axial mixing of feed and anti-solvent under US irradiation. Smaller pipe dimensions increased the flow velocities of the fluids (higher Re) in the static mixer, resulting in a slower material buildup on the elements of the static mixer. Fully continuous processing under precipitating environments can be established by parallel arrangement of several static mixers, in which the process is switched simultaneously from one static mixer to another if the pressure gradient in the systems exceeds a certain threshold.

In chapter 4, a feasibility study was done for continuous drying of a crystalline API via extrusion. Some continuous drying technologies are already available on the market, but there is lack of continuous drying equipment which can reliable handle and dry cohesive materials for low throughput ranges (low kg per hour range). It was shown that, extrusion drying is a promising continuous processing technology for the production of pharmaceutical substances, since narrow RTDs are achieved and dead zones are minimal in comparison to other drying technologies (e.g., fluidized bed). The drying temperature of a pharmaceutical substance can be easily regulated and adjusted through the extruder housing and drying gas temperature. This enables drying of heat-sensitive substances without exceeding the glass transition temperature and therefore prevents particles sticking together resulting in agglomerate formation. The selected model substance was dried without major changes in particle size for specific process settings. The particle size was mainly influenced by the dryness level of the substance: the drier the substance was at the beginning or became during drying, the more attrition occurred. The residence in the extruder had only a minor influence on the particle size. Implementation of extrusion drying can be done easily, since it is a continuous technology by nature. Furthermore, in a CM environment, extrusion drying provides the possibility of linking primary and

secondary manufacturing. The drying performance can be improved, because the used extruder usually processes hot melts. Changing or adapting the extruders screw design (larger shear gap) may also improve the product quality.

„Life is not easy for any of us. But what of that?
We must have perseverance and above all confidence
in ourselves. We must believe that we are gifted for
something and that this thing must be attained"

Marie Curie (1867-1934)

6. Outlook

Changing the manufacturing route of pharmaceuticals from batch to continuous is still a challenging endeavor, especially for an end-to-end CM approach. Many years or decades will pass by until a fully continuous production line will produce the first drug products, where production starts with synthesis and ends with the final product (e.g., capsule or tablet). In secondary manufacturing, continuous production lines already exist and some drug products have been released on the market. In contrast to this, continuous primary manufacturing from synthesis to an intermediate drug product (e.g. dry API) is underdeveloped. Implementation and integration of a fully CM environment relies on the innovation pace of production equipment. Constant and coherent progress in the development of continuous pharmaceutical manufacturing equipment is therefore a key driver to enable innovative continuous production of pharmaceuticals one day.

During this thesis, two continuous primary manufacturing methods were developed and investigated. Both of them, continuous purification by solvent exchange washing and continuous drying by extrusion, showed great potential for applications in continuous primary manufacturing. Limitations in continuous solvent exchange washing are still given from the precipitating environment, resulting in process times of only a few hours. Reduction of the fouling tendency and therefore extension of the process time might be realized by further process intensification through application of stronger external forces. Such external forces could be the/a creation of back and forth flow for more turbulences, periodically tensile and compression forces on the pipe or stronger ultrasound irradiation. In addition, inert coating materials could be applied on the static mixer elements, which reduce the adherence tendency of precipitated material. Another way to intensify the mixing process is to reduce the pipe diameters to even smaller dimensions, which increases the flow velocities and related Re numbers.

Continuous drying of a crystalline API via extrusion showed very stable process conditions, but further improvements are necessary in relation to dried powder properties. Preservation of the particle size from crystallization was not achieved (reduction of particle size in all process settings) and therefore design improvements of the extruder are necessary. The used extruder usually processes hot melts, where a narrow shear gap between screw and housing is desirable to introduce the necessary shear energy for melting up polymers. High shear energies are not favorable in a drying process, because this can lead to undesired particle size changes by agglomeration or, most likely, attrition. Extruder designs with larger shear gaps and extrusion elements specifically tailored for drying applications might avoid changes in the particle properties after drying. Furthermore, insertion and release zones for the drying gas have to be specially designed to achieve higher drying rates and to avoid blowing out of fines, as observed during the experiments. Realization of these suggested design improvements might transform extrusion drying into an important unit operation for linking primary and secondary manufacturing.

After improvement of the single unit operations, a continuous process line consisting of a purification cascade (solvent exchange washing and filtration) and extrusion drying can be set up. Continuous filtration equipment was developed in a previous study and can be implemented in the continuous purification cascade. Moreover, the implementation of a suitable process analytical technology (PAT) strategy is an important task to monitor material and process parameters during processing. On line measurement of volume flow rate, pressure progression and particle size of feed and product suspension in continuous purification as well as moisture content and particle size of the dried particles in extrusion drying should be investigated in future research work.

Another part of this thesis deals with small scale drying experiments of suspensions in an acoustic levitator and the evaluation of related mechanical properties of dried particles. The developed small scale process can be a very useful tool to determine process parameters for continuous purification of pharmaceuticals. As in the study shown, drying of primary particles can be achieved mainly if the amount of dissolved solids in the suspension is below a certain threshold. Loose particles are formed below this threshold and will eventually break by further processing. This method can be used for process and material design, to determine the necessary purification steps to avoid formation of strong agglomerates in the downstream process drying. Such investigations are especially valuable, if rare or expensive substances are handled. For example, before carrying out the

purification process, a tiny amount of material can be used to determine the maximum amount of dissolved solids in the suspension, where loose particles can be expected after drying and therefore crystal particle size can be preserved. This method will be used in the future for material and process screening before the continuous purification and drying process is done.

This work highlights a number of avenues that could be explored in order to enhance and progress with the interesting research field of continuous purification and drying in primary manufacturing of pharmaceutics.

7. Appendix

7.1 Curriculum vitae

Manuel Kreimer

Born on April 14th 1989, Graz, Austria

Austrian citizen

E-Mail: manuel.kreimer@rcpe.at

EDUCATION

Since 06/2015	**Doctoral Program in Technical Science**
	University of Technology, Graz, Austria
	Research Center Pharmaceutical Engineering GmbH
	Thesis: Continuous purification and drying of pharmaceuticals with regard to material properties and process stability
	Supervisor: Prof. Johannes G. Khinast
04/2014 – 10/2014	**Master Program Polymer Engineering and Science**
	Montan-University Leoben, Leoben, Austria
	Polymer Competence Center Leoben GmbH
	Thesis: Reversible crosslinking of epoxy based materials
	Supervisor: Prof. Wolfgang Kern
	Pass with distinction
10/2009 – 04/2014	**Bachelor Program Polymer Engineering and Science**
	Montan-University Leoben, Leoben, Austria
	Polymer Competence Center Leoben GmbH
	Thesis: Kovalente Bindung von funktionellen Beschichtungen an oberflächenfunktionalisierten Naturkautchuk-Latexfilmen

Supervisor: Prof. Wolfgang Kern

09/2003 – 06/2008	**Bachelor Program Polymer Engineering and Science**

Montan-University Leoben, Leoben, Austria

Polymer Competence Center Leoben GmbH

Thesis: Kovalente Bindung von funktionellen Beschichtungen an oberflächenfunktionalisierten Naturkautchuk-Latexfilmen

Supervisor: Prof. Wolfgang Kern

09/2003 – 06/2008	**Higher Technical College**

HTBLA Weiz, Weiz, Austria

Tyromotion GmbH

Thesis: Konstruktion und Bau eines Prüfstandes für ein Rehabilitationsgerät

Supervisor: DI Josef Löffler

PROFESSIONAL EXPERIENCE

Since 06/2015	**Research Center Pharmaceutical Engineering GmbH**
	Scientist (Area III, Process and Manufacturing Science)
08/2013	**Andritz Hydro GmbH**
	Internship: Training coordination department
06/2013 – 07/2013	**Elin Motoren GmbH**
	Internship: Engineering department for construction of wind generators
07/2012 – 08/2012	**ACC Austria GmbH**
	Internship: Department material characterization and development
08/2011 – 09/2011	**Rosendahl Maschinen GmbH**
	Internship: Commissioning department
07/2010 – 08/2010	**Elin Motoren GmbH**
	Internship: Electrical design of generators

05/2009 – 09/2009	**Maschinenring Almenland**
	Construction- and forestry worker
07/2007 – 08/2007	**Siemens Transformatoren**
	Internship: Design and calculation of transformers
07/2007 – 08/2007	**Tyromotion GmbH**
	Internship: Design and construction of therapeutic robots
06/2006 – 07/2006	**Mosdorfer GmbH**
	Internship: Hot-dip galvanizing of metal parts
07/2005 – 08/2005	**Mosdorfer GmbH**
	Internship: Hot-dip galvanizing of metal parts
07/2004	**Weitzer Parkett GmbH & CO KG**
	Internship: Laying of parquet and other wood floor coverings

7.2 Publications

Research Papers

M. Kreimer, M. Zettl, I. Aigner, M. Krumme, T. Mannschott, P. van der Wel, J. G. Khinast: Performance characterization of static mixers in precipitating environments. Org. Process Res. Dev. 2018, submitted July 2018.

M. Kreimer, I. Aigner, D. Lepek, J. G. Khinast: Continuous Drying of Pharmaceutical Powders Using a Twin-Screw Extruder. Org. Process Res. Dev. 2018, DOI: 10.1021/acs.oprd.8b00087

M. Kreimer, I. Aigner, S. Sacher, M. Krumme, T. Mannschott, P. van der Wel, A. Kaptein, H. Schroettner, G. Brenn, J. G. Khinast: Mechanical Strength of Microspheres Produced by Drying of Acoustically Levitated Suspension Droplets. Powder Technol. 2018, 325, 247–260.

Talks

M. Kreimer, I. Aigner, S. Sacher, M. Krumme, T. Mannschott, P. van der Wel, A. Kaptein, J. G. Khinast: Investigation of different continuous drying routes for pharmaceuticals – in: 8th World Congress on Particle Technology, Orlando, 2018.

M. Kreimer, I. Aigner, S. Sacher, M. Krumme, T. Mannschott, P. van der Wel, A. Kaptein, H. Schroettner, G. Brenn, J. G. Khinast: Investigation of Single-Droplet Drying Kinetics in an Acoustic Levitator, Microsphere Morphology and Mechanical Properties of Pharmaceutical Excipients – in: 8th World Congress on Particle Technology, Orlando, 2018.

M. Kreimer, I. Aigner, S. Sacher, M. Krumme, T. Mannschott, P. van der Wel, A. Kaptein, H. Schroettner, G. Brenn, J. G. Khinast: Investigation of Agglomeration Strength of Single Microspheres – in: ProcessNet, Düsseldorf, 2018.

M. Kreimer, I. Aigner, S. Sacher, M. Krumme, T. Mannschott, P. van der Wel, A. Kaptein, J. G. Khinast: Continuous Dryinig of Pharmaceuticals – in: AIChE Annual Meeting, Minneapolis, 2017.

M. Kreimer, I. Aigner, S. Sacher, M. Krumme, T. Mannschott, P. van der Wel, A. Kaptein, H. Schroettner, G. Brenn, J. G. Khinast: Investigation of Microsphere Strength for Spray Drying Applications by Means of Acoustic Levitation – in: AIChE Annual Meeting, Minneapolis, 2017.

M. Kreimer, I. Aigner, S. Sacher, M. Krumme, T. Mannschott, P. van der Wel, A. Kaptein, H. Schroettner, G. Brenn, J. G. Khinast: Mechanical properties of microspheres produced by drying of levitated suspension droplets – in: PSSRC, Graz, 2017.

M. Kreimer, I. Aigner, G. Koscher, D. Lepek, J. G. Khinast: Continuous Drying of Powders and Slurries in an Extruder without Changing Product Particle Size Distribution – in: AIChE Annual Meeting, San Francisco, 2016.

Posters

M. Kreimer, I. Aigner, J. G. Khinast: Continuous Secondary Drying of Powders via Extrusion – in: I2APM, Glasgow, 2016.

M. Kreimer, I. Aigner, S. Sacher, M. Krumme, T. Mannschott, P. van der Wel, A. Kaptein, J. G. Khinast: Continuous solvent exchange washing of pharmaceutical intermediates – in: AIChE Annual Meeting, Minneapolis, 2017.

M. Kreimer, I. Aigner, J. G. Khinast: Small-scale Continuous Drying of Powders via Extrusion avoiding Agglomeration or Attrition of the Final Product – in: Minisymposium Verfahrenstechnik, Innsbruck, 2017.

I. Aigner, M. Kreimer, S. Sacher, M. Krumme, T. Mannschott, P. van der Wel, J. G. Khinast: Development of a Continuous Process for Drying of an Actice Pharmaceutical Ingredient – in: World Meeting on Pharmaceutics, Biopharmaceutics and Pharmaceutical Technology, Granada, 2018.

Supervised Bachelor Students

Kristian Gavric (graduation June 2018)

Supervised Master Students

Craig Denny Hauser (graduation Jannuary 2018)

Rafael Halb (graduation July 2018)

„Your time is limited, so don't waste it living
someone else's life. Don't be trapped
by dogma - which is living with the
results of other people's thinking.

Don't let the noise of others opinions
drown out your own inner voice.
And most important, have the courage
to follow your heart and intuition.
They somehow already know what you
truly want become.
Everything else is secondary."

Steve Jobs (1955-2011)